NASA Contractor Report 178347

Six Component Robotic Force-Torque Sensor

A. R. Grahn, B. L. Hutchings, D. R. Johnston,
D. C. Parsons, and R. F. Wyatt

BONNEVILLE SCIENTIFIC, INC.

Salt Lake City, UT 84105

Contract NAS1-17997

August 1987

National Aeronautics and
Space Administration

Langley Research Center
Hampton, Virginia 23665-5225

TABLE OF CONTENTS

LIST OF TABLES

LIST OF FIGURES

LIST OF FIGURES (cont.)

INTRODUCTION

This document constitutes the final report for Phase II of the Six Component Robotic Force-Torque Sensor, Contract No. NAS1-17997 sponsored by the National Aeronautics and Space Administration under the Small Business Innovation Research (SBIR) Program. The objective of this two-year phase of the project was to design, fabricate, and evaluate a prototype force-torque sensor system.

The first part of this document provides background information taken from the Phase II proposal. The remainder covers the research methods and results, and conclusions.

BACKGROUND

Introduction

NASA has the responsibility of deploying, operating and maintaining a variety of space missions. Because of the expense and complexity of manned space flights, it is desirable to perform as many of the necessary program functions as possible by teleoperator control of space-based robotic systems. The Remote Orbital Servicing System (ROSS) is being evaluated for enabling an unmanned space vehicle to perform maintenance and repair duties. The robotic servicer kit portion of ROSS will differ from industrial robots in several respects. The primary requirement is that the entire system must be very flexible and adaptable. Industrial robots require a highly structured work environment where the position of objects is precisely known. In space, few objects will be of the same configuration. They may be light and fragile, and their exact positions will be unknown. Initially, ROSS will require direct human control, but it also must have on-board intelligence to make some decisions independently of the operator. This is mandatory to reduce operator fatique and avoid control problems due to propagation delays in communication links. For example, the robot should be able to control the force with which it is grasping an object and should be able to avoid collisions, etc. without teleoperator intervention.

Vision systems are the basic element of the required sensory modalities, but they cannot provide all the necessary information. Exact three-dimensional orientation and alignment are difficult to obtain from video cameras, and at times the robot itself or parts of the spacecraft may obscure vision. Therefore, multisensory inputs including tactile information and reaction forces and torques will also be necessary. In rigid-part contact operations, small errors in relative position or angular orientation can produce very large forces, preventing successful completion of the task and sometimes causing damage to the parts, fixtures or the robot. However, these same forces that tend to impede the task can be easily detected and measured with sensors. If the relationship between the forces and workpiece position errors is known, this force information can be effectively used for adaptive control.

With funding from a National Science Foundation SBIR grant, we have demonstrated the technical feasibility of a tactile sensor having high spatial resolution and normal force sensitivity. We will continue to refine this tactile sensor, but currently it lacks the ability to measure shear forces and torques. This document reports on an approach to the design of a small, light-weight six-component force-torque sensor that can operate in conjunction with the tactile sensor to give a complete, integrated sensory device that can be placed on the grasping surfaces of the end effector.

Both of these sensors are based upon ultrasonic pulse-echo ranging techniques. The tactile system images the surface of a compliant elastomeric pad used as the gripping surface, and the force-torque sensor measures the displacement of an array of targets constrained by an elastomeric pad that is deformed by reaction forces and torques.

Robotic Force-Torque Sensors

Most multi-dimensional force-torque sensors are equipped with strain gauges mounted on a somewhat complex mechanical structure. The design and positioning of the strain gauges are calculated so as to uncouple as much as possible the forces and the torques applied on the robotic gripper by having each sensing element, or each pair of them, measure one element of the stress tensor applied to the sensor. This mechanical uncoupling theoretically simplifies the transfer matrix between the forces measured by the sensing elements and the stress tensor.

An example of "uncoupled gauging" is the six-dimensional force-torque sensor of J.P.L. [Bejczy, 1980] having a maltese cross configuration with semi-conductor strain gauges mounted on the four deflection bars of the cross. There is one gauge on each side of each of the four deflection bars, giving a total of 16 gauges. The gauges on opposite sides of a deflection bar are wired together to provide a single reading reflecting the differences in strain levels on opposite sides of the bar. The dynamic range of this sensor is 0.5 to 300 Newtons.

A coupled gauged device has been developed by Gaillet and Reboulet [1983]. The design methodology of this sensor is based upon strong but known coupling between the different elements of the stress tensor. The sensor structure consists of two parallel disks joined by six articulated

rods each carrying a measurement device (of undisclosed type). The reaction forces on the articulations resulting from application of a force or torque on the upper plate are oriented in the direction of the rods and measured by their sensing elements. Overstressing of the sensing elements is avoided by the inclusion of a compliant member similar to that used in remote center compliance (RCC) devices. This sensor has a 15 gm force sensitivity in all directions over a 10 kg range.

A different approach to sensor design has been taken by Benjamin [1983] in the development of a five-axis tactile postion sensor. Three of the five measurement axes define the position of the target in the robot's X, Y, and Z axes while the other two measurements define the target plane's orientation with respect to the Z axis of the robot as measured in the X and Y planes. This device uses movable pins protruding perpendicularly from the bottom of the sensor. The peripherally placed pins move a total of 2.5 mm against a cantilevered spring having full-bridge strain gauges mounted on them near the support end. The central pin is free to move axially but constrained laterally. This pin mates with a rod with four flats ground on it with opposed flats instrumented with full bridge strain gauges so that the center probe is two independent cantilevered rods capable only of orthogonal deflection. The sensor is 58 mm in diameter, 40 mm high, weighing 600 gm with a range of ± 6.4, ± 0.0025 mm in the X, Y, and Z axes and ± 3.0, ± 0.01 degrees.

The Lord Corporation makes two devices for multi-axis force sensing. One device is an instrumented RCC containing three elastomer pads with three LED-dual photodiode pairs measuring the displacement of the RCC [Seltzer, 1982]. This is a null-seeking device with sensing in the X, Y, and θ_z dimensions with total displacements of about 2.5 mm. The second Lord sensor is a touch sensor array having 8 x 12 sensing elements on 2.5 mm centers. This device is 44 mm long by 29 mm wide and 16 mm thick. Besides giving the force distribution applied to the surface, it is also purported to measure the magnitude, direction, and location of the total loading vector resulting from pressing on an object. Little information is given on the performance of this device and the sensing technology is undisclosed. In fact, Lord Corporation personnel stated that they had yet to determine the sensing technology to be used.

The first four devices are bulky, heavy structures that can reduce robotic payload and interfere during assembly operations. Moreover, wrist-mounted sensors experience inertial loadings due to gripper mass and are prone to vibration sensitivity and mechanical resonance problems. These problems can be exacerbated by the use of flexible or "limber" manipulators. Little is known about the new Lord tactile sensor. However, previous models were expensive and complex with the individual sensing elements consisting of light-emitting diode and photo-detector pairs with a shutter mechanism modulating optical intensity with applied force. Although smaller than the previously mentioned devices, it is still about 50 times the volume of our ultrasonic six-component force-torque sensor. Our sensor is a small, low mass, rugged device with high overload capability that is mounted on the grasping surface of the end effector and compatible with Bonneville Scientific's high resolution tactile sensor arrays.

Ultrasonic Pulse-Echo Ranging

Our force-torque measuring technique is based upon using ultrasonic pulse-echo ranging to determine the position of ultrasonic reflectors attached to a metal or ceramic cover plate. The underside of the cover plate is bonded to an elastomeric pad whose bottom surface is anchored to a substrate attached to the end effector gripping surface. Loading of the pad, through its cover plate, produces small changes in reflector position. Reflector position is determined from the time it takes an ultrasonic pulse to traverse the path in the elastic pad and return to the transducer. From this time-interval measurement, knowledge of the speed of sound in the pad, and knowledge of the pad's spring constant (appropriate for the type of loading) the force and torque deforming the pad can be calculated.

Two basic principles are involved in pulse-echo distance measurement. First, the speed of sound, C, in the medium (e.g. elastic pad) is known so that the distance, d, can be determined from the two-way travel time, t, by $d = 1/2\ ct$. Second, the reflecting interface must reflect the ultrasonic pulse. How well an interface reflects is given by the reflection coefficient which is a function of the specific acoustic impedances of the two media on either side of the interface. For an elastic pad made

out of silicone rubber and a steel reflector surface the reflection coefficient is about 96%.

In order to accurately and consistently measure the small distance changes produced by the applied loading, the ultrasonic transducer must have high mechanical dampening to reduce ringing and increase bandwidth without the need for matching or mismatching layers, and have adequate sensitivity at the high frequencies necessary to resolve small distances. For these reasons as well as the advantages it offers in sensor fabrication and its low cost, polyvinylidene flouride (PVDF) was used for the transducer material.

Polyvinylidene Flouride (PVDF) Ultrasonic Transducers

Polyvinylidene Flouride (PVDF) is a thin-film polymer material that was originally manufactured for use as a protective packaging material. In 1969 [Sussner, 1979] Kawai in Japan demonstrated that stretched and poled films of PVDF are five to ten times more piezoelectric than crystalline quartz.

Under a recent National Science Foundation grant we have investigated the use of PVDF transducer arrays for accurately measuring small distances in elastomeric materials using pulse-echo ranging. The results of that study showed that 28μm thick PVDF will be highly suited for the force-torque sensors. Specific findings were that 8 mm square transducer elements, when excited with 5.0 v pulses, produced echo signals of 5 mv for a 9.5 mm silicone rubber path length. The echo signals were a single cycle of approximately sinusoidal shape 600 ns wide with no discernible ringing. Since the signals were large, bipolar pulses, detection can be achieved with relatively simple electronic circuits. For the same excitation voltage the echo amplitude is, theoretically, independent of transducer area. Practically, a size limit is reached due to amplifier input impedance loading the small, capacitive transducer.

Elastomeric Pad Characteristics

Acoustic and preliminary mechanical characterization of silicone and natural rubbers, covering a range of durometers has been carried out under the previously mentioned National Science Foundation grant. The

speed of sound in these materials is constant with elastomer compression (i.e., with the material free to expand laterally while being compressed) and the acoustic attenuation is acceptably small (e.g. 3.4dB/cm for silicone rubber at 2.0MHz). Static compression of a silicone rubber sample resulted in a linear force-compression relationship over the range of 5 to 600 gm and 50% compression of the pad. Deviations from linearity at both ends of the force range were likely due to inadequacies in the measuring apparatus.

Dynamic compression tests were made with an Instron material testing machine. Figure 1 shows the results of these tests for a silicone rubber sample and a natural rubber sample. During force application the compression varies linearly with force but during force removal the hysteresis is apparent, especially for the silicone rubber sample. This hysteresis will limit the accuracy of our sensor. We are currently working with two rubber fabrication companies to develop formulations with acceptable levels of hysteresis. No compression set was evident in any of the six rubber types tested.

Technical Approach

Phase I of this project was devoted to proving the feasibility of the proposed force-torque sensor concept. Although we are sensitive to the requirements for sensor operation in space (e.g. heat sinking, heat shielding, or the need for on-sensor heat production, along with the out-gassing characteristics of the polymers used for adhesives and elastomers, etc.) we used materials that were readily available and, when appropriate, easily shaped by conventional means. Basic experiments were conducted with simple sensor configurations to identify fundamental limitations of the technique that were not originally apparent. In Phase II complete, functional sensors will be constructed with materials suitable for space application, integrated with a dedicated microprocessor, and extensively evaluated.

Our force-torque sensing technique utilizes an ultrasonic transducer configuration that is a compromise between ease of fabrication and the degree of coupling between the different components of the applied stress tensor. We chose to maximize accuracy by 1) locating the transducers in a pattern that weakens coupling, and 2) using redundant

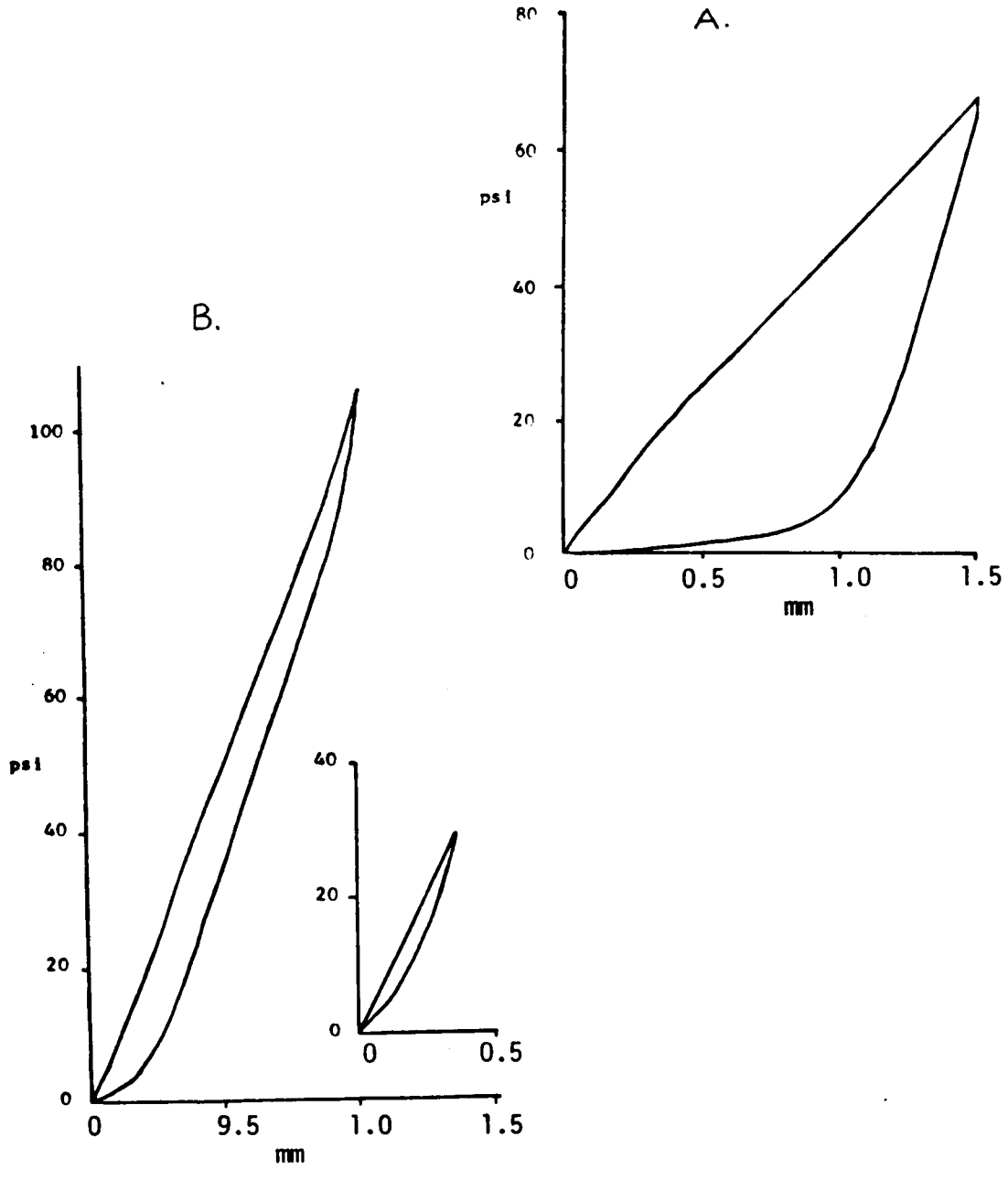

Figure 1. Dynamic compression and hysteresis characteristics of: A. Silicone rubber, RTV-700, compressed at 0.25 mm/min. B. Natural rubber, R-45, compressed at 1.0 mm/min., inset at identical conditions except smaller range.

transducers so that for some component measurements can be averaged to improve accuracy. The redundant transducers also simplify computation of the force-torque components. In Phase I we determined how well the method can resolve the individual components in the presence of others and determined what factors establish the overall accuracy of the technique.

Figure 2 shows the basic sensor design that was investigated and the principle of operation. Ultrasonic pulse-echo ranging is used to measure the position and orientation of the sensor cover plate whose movement is restrained by a ring of elastomeric material. The scheme shown uses nine transducer elements. Four of them, X_5, X_6, X_7, and X_8, are mounted on a planar substrate and measure the degree of compression of the elastomeric ring by sending ultrasonic pulses through the elastomer and receiving the echo from the bottom surface of the cover plate. The remaining five transducers X_1, X_2, X_3', X_3'', and X_4, are mounted on the four sides of a square post mounted in the center of the sensor assembly. These transducers measure the distance to vertical targets, T_1, T_2, T_3, and T_4 fixed to the cover plate. The interior cavity of the sensor contains a silicone gel or very-low-durometer silicone rubber to provide acoustic coupling between these trasducers and targets. Most of the sensor's compliance is controlled by the elastomeric ring characteristics.

The sensor is designed so that the maximum forces and torques to be measured (except F_z, the normal compression force) will produce changes in pad dimensions on the order of 10%. This means that to a first-order approximation changes in pad thickness due to shear can be neglected as well as target alignment changes due to rotation. The errors introduced by making these assumptions have been determined during Phase I. In Phase II compensation can be made for some of these effects by the use of appropriate processing algorithms.

Very small target displacements can be accurately measured by pulse-echo transit times. For example, if pulse-echo times are measured by counting the 10ns pulses from a 100 MHz clock, then for a silicone rubber pad the displacement resolution is 5 μm so that for a displacement of 1.0 mm, displacements could be resolved to one part in 200. Sampling of a voltage ramp when an echo is detected and conversion of that voltage into a digital word could give 2 ns time resolution so that 1.0 mm displace-

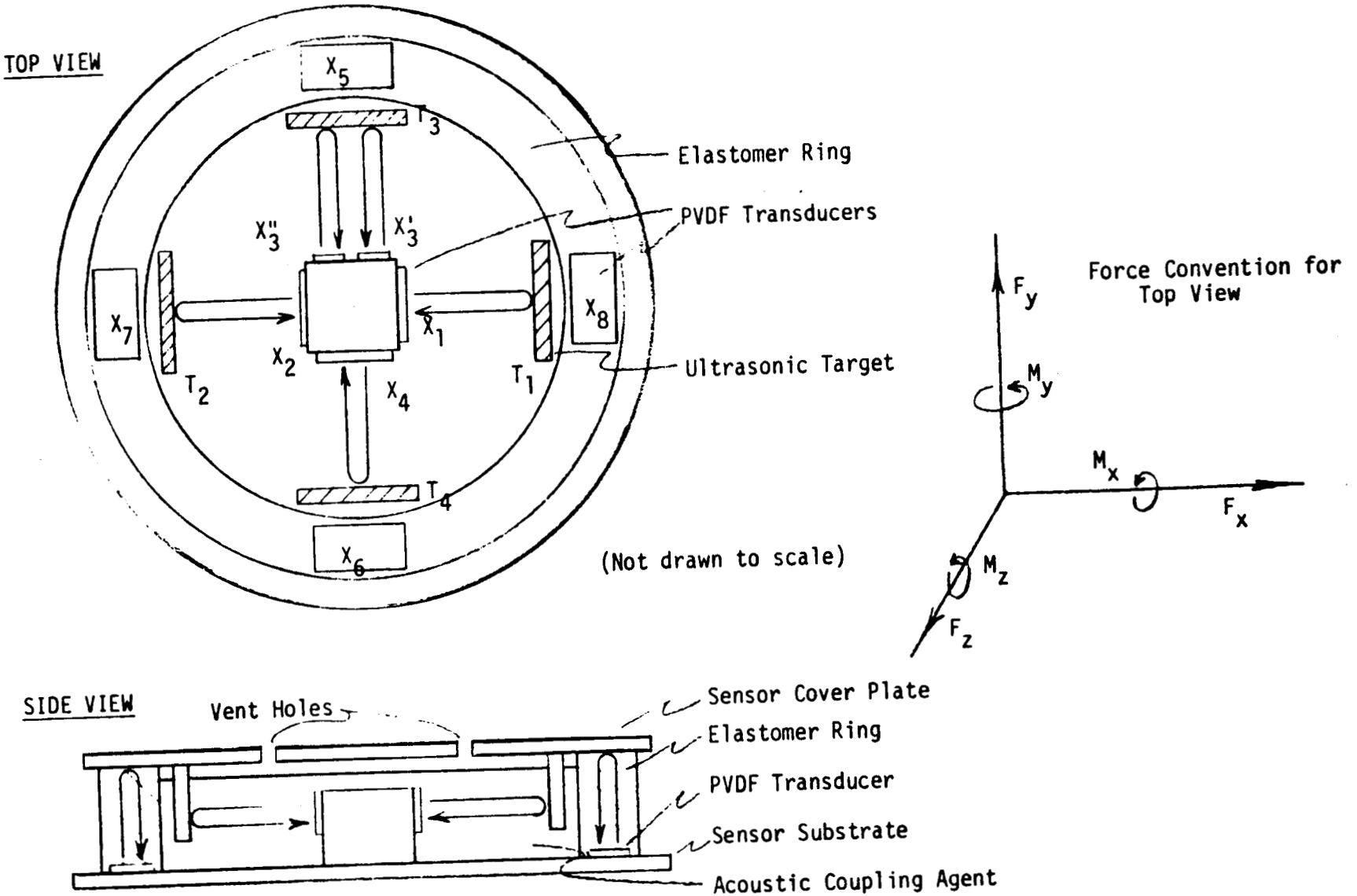

Figure 2. Basic Force-Torque Sensor Design

ments could be resolved to one part in 1000 if greater accuracy is required.

Table 1 gives all the contributions to the pulse transit time for each transducer. The change in transit time, t, is given by multiplying the tabulated coefficients in the desired transducer row by the force or torque components heading the columns, and then summing the factors. The minus sign indicates that a positive force or torque decreases the transit time. For example, the transit time change for transducer X_5 is $t_5 = cF_z + dM_x$. The force coefficients, a through f, are simply 2 ($k_i c$) where k_i is the elastomeric spring constant for the appropriate force or torque component (to be measured experimentally) while c is the speed of sound in th elastomer.

Transducers X_5 and X_6 measure elastomer thickness which changes primarily with normal force, F_z, and moment, M_x, which "rocks" the cover plate about the x-axis (see Figure 2). Similarly, X_7 and X_8 are primarily sensitive to F_z and M_y. Transducers X_1 and X_2 measure translation of the cover plate along the x-axis due to F_x (which produces shear in the elastomer) and rotation of the cover plate due to M_z, the moment or torque normal to the cover plate. Transducers X_3 and X_4 respond to the y-axis translation due to F_y and also to M_z. Because of symmetry, rotation of targets T_1 through T_4 due to M_z produce a decrease in pulse transit time regardless of the direction of rotation. Therefore, transducer X_3, is divided into two transducers X_3' and X_3'' as shown in Figure 2. For a positive M_z (producing a counter-clockwise rotation of the cover and vertical targets) target T_3 rotates so that it is closer to transducer X_3'' than X_3'. Consequently, the sign of the difference in transit time between transducers X_3'' and X_3' gives the direction of M_z.

Table 2 lists the solutions to the transit time equations of Table 1. The force and torque components are given in terms of the force-torque coefficients and transit time measurements. Each component is given by only two transit time measurements indicating relatively "loose" coupling. Both F_z amd M_z are given by two equations so that the results of the calculations could be averaged to improve accuracy.

If each transducer requires its own electrical leads, then nine leads (plus a common) have to be externalized. To reduce the number of leads

TABLE 1

t	F_x	F_y	F_z	M_x	M_y	$\lvert M_z \rvert$
X_1	a					-f
X_2	-a					-f
X_3		b				-f
X_4		-b				-f
X_5			-c	d		
X_6			-c	-d		
X_7			-c		e	
X_8			-c		-e	

TABLE 2

$F_x = (1/2a)(t_1 - t_2)$ $\qquad M_x = (1/2d)(t_5 - t_6)$

$F_y = (1/2b)(t_3 - t_4)$ $\qquad M_y = (1/2e)(t_7 - t_8)$

$F_z = (-1/2c)(t_5 + t_6)$ $\qquad |M_z| = (-1/2f)(t_1 + t_2)$

$F_z = (-1/2c)(t_7 + t_8)$ $\qquad |M_z| = (-1/2f)(t_3 + t_4)$

sign of $t_3' - t_3''$ gives direction of M_z (see text)

each horizontal transducer could be connected to one vertical transducer to reduce the number of leads to five. Echoes from each of the transducer-pairs would be identifiable by their separation in time if the respective ultrasonic pathlengths differ sufficiently (e.g. about 1.0 mm). If some sacrifice in sensor miniaturization can be tolerated, then its possible to adjust target distance such that all transudcers can be connected in parallel and each echo separated in time. Consequently, only a single shielded lead would exit the sensor.

During Phase I we investigated the transducer signal levels to determine if they were sufficiently high to allow the use of remotely located processing electronics. If they were too low, then during Phase II we would have to investigate the use of on-sensor hybrid electronics for transducer multiplexing and signal conditioning.

METHODS AND RESULTS

Introduction

The research objective of the Phase I study was to determine the feasibility of the proposed six-component robotic force-torque sensing technique by:

1. Determining the suitability of the proposed reflector scheme and the errors introduced by misalignment and rotation.
2. Determining the suitability of silicone rubber and natural rubber as a multidimensional, linear spring.
3. Evaluating sensor performance under different loadings and evaluate indicated design alterations to improve performance.

The research in Phase I was conducted in the three main areas listed above. The first step was devoted to determining the effects of ultrasonic reflector rotation and misalignment on the ultrasonic echo pulse. We determined the degree of misalignment that is permissible before echo zero-crossing time is significantly affected. In the second step we measured the elastic properties of silicone rubber in compression, tension, shear, and torsion and determined equivalent spring constants and their range of applicability. Finally, in the third step a simple prototype sensor was designed and constructed, based upon the results of the previous experiments and preliminarily evaluated to determine its capability as a force-torque sensor.

Reflector Alignment Experiments

The underside of the sensor cover plate serves as a reflector for the four substrate-mounted transducers (X_5, X_6, X_7, and X_8 in Figure 2) while perpendicular tabs attached to the bottom surface of the cover plate reflect the ultrasonic pulses from the post-mounted transducers (X_1, X_2, X_3, and X_4 in Figure 2). During translation of the cover plate (as occurs with any combination of applied forces - F_x, F_y, and F_z) reflector-transducer alignment is preserved. However, when one or more torques are applied the reflecting surfaces are rotated off of perpendicular alignment thereby affecting the ultrasonic echo pulse. The echo pulse is affected in two ways. First, echo amplitude is reduced because

not all of the ultrasonic energy is returned to the transducer when the reflector is no longer perpendicular. And second, the echo pulse becomes wider, containing more cycles, as misalignment increases because the portion of the reflector closer to the transducer reflects energy first while the portion of the reflector that has rotated away from the transducer is the last to reflect.

In this Phase I study we have investigated the feasibility of using zero-crossing detection of the echo signal to measure pulse transit time. Zero-crossing detection is attractive because it is easily implemented and relatively independent of echo amplitude. It is also practical because for aligned reflectors the echo consists of essentially one cycle of approximately sinusoidal shape. This is due to the inherent high dampening (i.e. broadband) properties of PVDF transducer film.

A series of experiments was conducted to measure the change in echo zero-crossing time with reflector rotation while the distance from the transducer surface to the center of rotation of the reflector remained constant. For these experiments the ultrasonic transducer consisted of a rectangular piece of 28μm thick PVDF (Kynar Piezo Film, Pennwalt Corp., King of Prussia, PA) 3.2 mm x 1.6 mm having tin-aluminum electroded surfaces about 80 nm thick. This was bonded with a cyanoacrylate adhesive to a 2.4 mm square brass tube having 0.4 mm wall thickness. The cyanoacrylate produces a strong bond having suitably small thickness so that its capacitance is small compared to the PVDF, thus allowing the brass tube to serve as a transducer lead. The hollow thin-walled tube provides an excellent acoustic backing for the transducer in that what little acoustic energy enters the brass wall from the back surface of the PVDF is almost immediately reflected back from the brass-air interface and is quickly attenuated. Consequently, no interferring echoes are produced by the backing. The remaining transducer lead consisted of a small length of # 38 AWG copper magnet wire bonded to the top PVDF surface with a conductive epoxy. A braided shield of a short length of 2.5 mm diameter coaxial cable was soldered to the brass tube and the center lead connected to the magnet wire to complete the transducer assembly.

Electrically, the transducer was connected to a 0-30 V, 200 ns pulser and video amplifier having a gain of 130. The output of the video amplifier was displayed on an oscilloscope for measurement of pulse transit time and echo amplitude and shape. Mechanically, the transducer

assembly was mounted in a fixture attached to a goniometer that was designed for x-ray diffraction studies. This device can accurately rotate an object through a precise range of angles and has a calibrated readout having 0.005^{o} (18 seconds of arc) resolution. A flat stainless steel reflector plate was fitted to the goniometer so that the axis of revolution lay on the surface of the plate and the transducer assembly adjusted to be centered 6 mm from the reflector surface and parallel to it (i.e. the ultrasonic radiation is perpendicular to the reflecting surface). The gap between transducer and reflector was filled with silicone rubber to conduct the ultrasonic pulse. This arrangement is shown in Figure 3.

Using this setup measurements of change in pulse transit time at different reflector angles were taken. These measurements were repeated with the transducer assembly misaligned with the reflector by about 6^{o} as shown in Figure 3. These measurements are shown plotted in Figure 4 and show that zero-crossing time of the echo pulse is constant within $\pm$ 5 ns over about a 5^{o} range of reflector rotation without misalignment and within $\pm$5 ns over about a 7^{o} range when the reflector offset is about 6^{o}. Consequently, zero-crossing detection can provide accurate distance measurements with reflectors misaligned by 5 to 7^{o}. It is anticipated that this amount of cover plate rotation is all that can be tolerated in a force-torque sensor without introducing significant robotic positioning error due to sensor compliance. The $\pm$5 ns time measurement tolerance corresponds to an uncertainty in distance of $\pm$2.5 μm and was chosen arbitrarily. Although a time resolution greater than this is possible, it is not likely to produce greater measurement accuracy due to other error sources.

Z-Axis Torque (M_z) Measuring Scheme

Our proposed methods for measuring the five force-torque components other than M_z are straight forward and involve simple trigonometric relationships between the ultrasonic distance measurement and the force or torque that produces the distance change. However, for measuring M_z our proposed scheme (Figure 2) involved vertically-mounted ultrasonic transducers that would measure the change in angular orientation of reflectors mounted to the sensor cover plate. In order to determine the direction of rotation a double or split transducer was used. With this

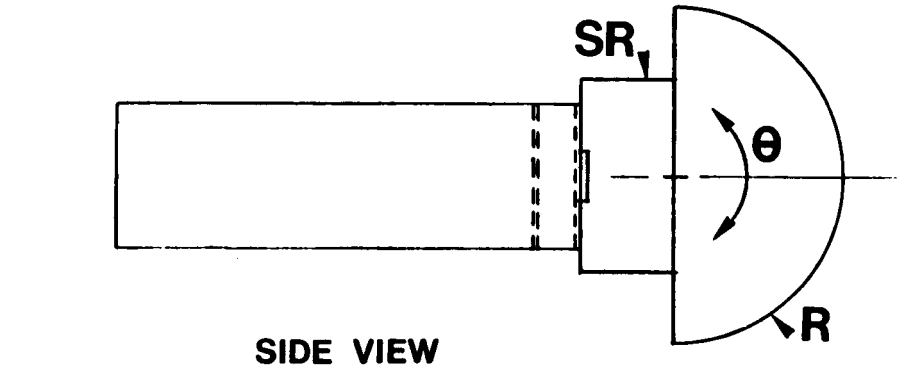

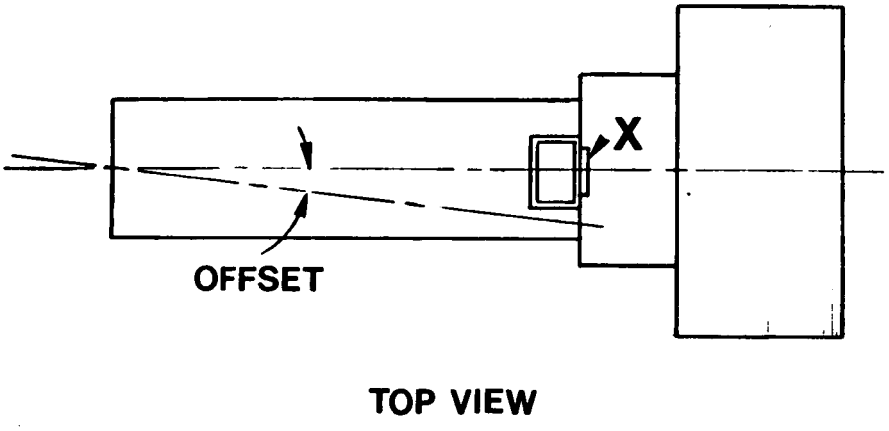

Figure 3. Reflector Alignment Detail. R, reflector which rotates through θ; SR, silicone rubber; x transducer mounted on a square brass tube set in supporting rod which may be offset at fixed angles.

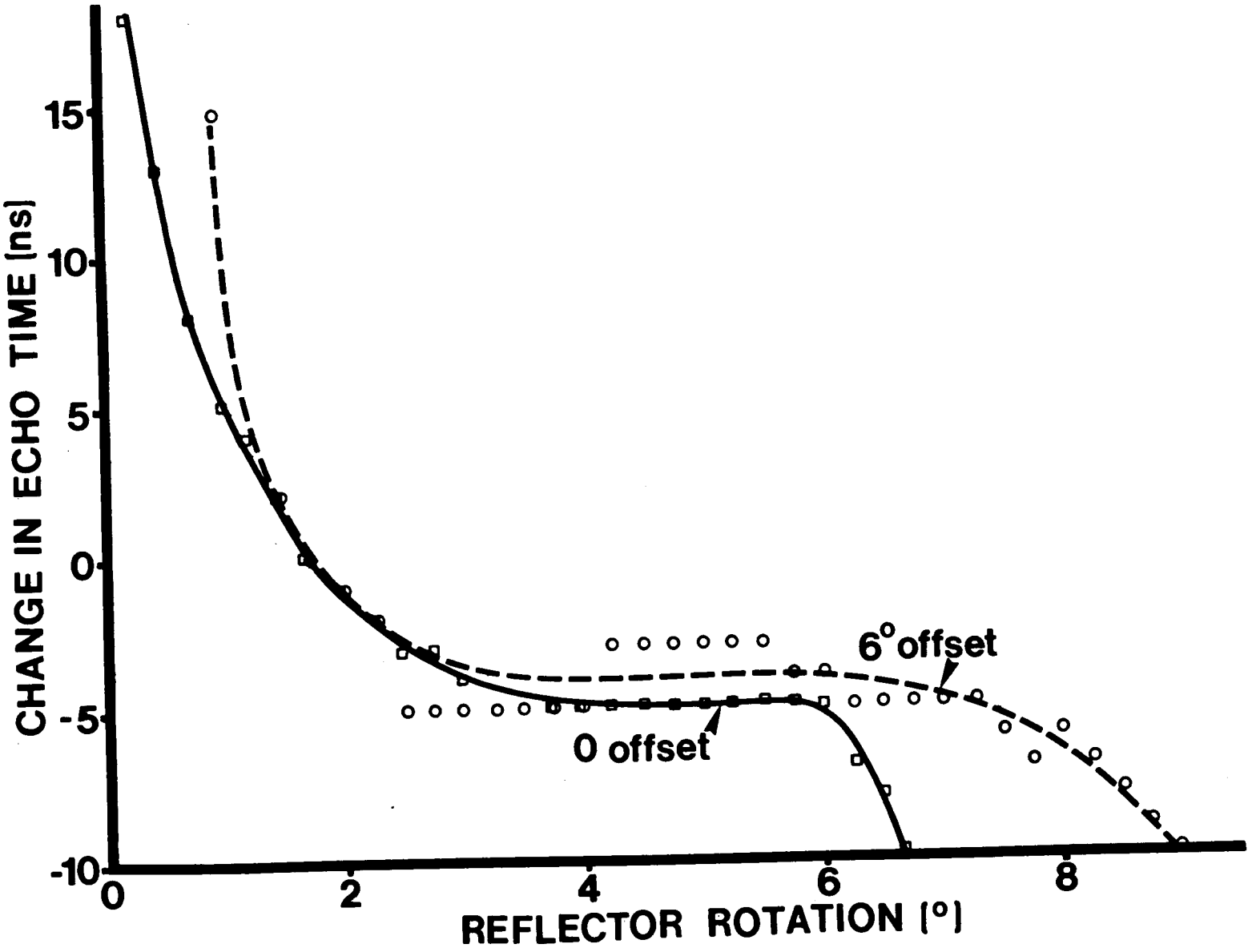

Figure 4. Reflector Alignment Versus Echo Time. The perpendicular incidence is at approximately 4^{0}.

technique there were questions concerning 1) the effects of reflector rotation on the echo signal, 2) the sensitivity of the method, and 3) the nonlinear relationship between the transit time measurements and rotation of the cover plate and, therefore, M_z.

The data presented previously in Figure 4 showed that the reflectors can be rotated by at least 5^0 before simple zero-crossing detection of the echo signal becomes inaccurate due to changes to echo waveform or amplitude. The remaining two questions were answered as well. However, first a mathematical analysis was conducted on the proposed transducer-reflector geometry which suggested simple changes could be made to improve performance and simplify construction. This modified scheme eliminates the need for the double transducer and offsets at least one pair of the four vertically-mounted transducers as shown in Figure 5. Referring to Figure 5, as the cover plate, and therefore, reflectors R_1 and R_2 rotate clockwise, reflector R_1 rotates away from transducer X_1 so that pulse transit time t_1 increases while R_2 moves closer to X_2 thereby decreasing t_2.

This scheme was tested using the dimensions given in Figure 5. These dimensions are the same as those used in the prototype transducer described later. Fixtures were made to implement this transducer-reflector configuration on the goniometer. Figure 6 shows the relationship between echo transit time and rotation of the cover plate. Negative angular rotation indicates movement of the reflector toward the transducer and therefore, a decrease or negative change in echo arrival time. At the vicinity of 0^0 rotation the slope of the straight line approximating this relationship is 0.02^0/ns.

The proposed method for calculating M_z involves measuring the change in the difference between the pulse transit times for a pair of transducers. Specifically, in Figure 5 this would be the change in the differential transit time, $t_2 - t_1$ rather than just t_1 or t_2 as has been plotted in Figure 6. The relationship between $t_2 - t_1$ and cover plate rotation can be derived from the data in Figure 6 by realizing that for a cover rotation of θ $t_2 - t_1$ is the change in echo time at θ minus the change at $-\theta$. For example, for $\theta = 5^0$ $t_2 - t_1 = 307$ ns - (-230 ns) = 537 ns. Similarly, for $\theta = -5^0$ $t_2 - t_1 = -230$ ns - 307 ns = -537 ns so that the curve is symmetrical about $\theta = 0^0$. This relationship is shown plotted in Figure 7 for positive angular rotation of the cover

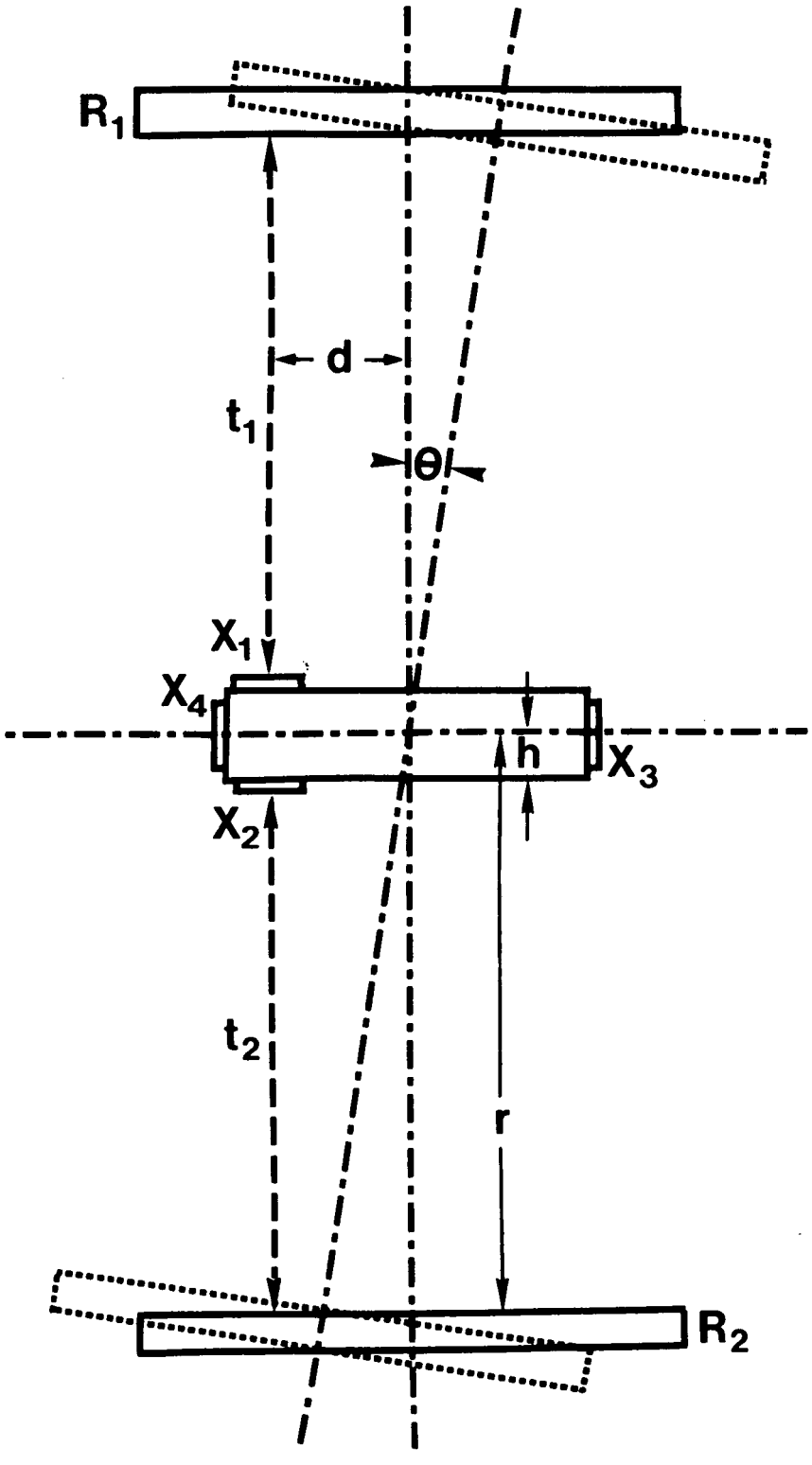

Figure 5. Modified Torque Measuring Scheme. X_1, X_2, X_3, X_4 = tranducers; R_1, R_2 = reflectors; t_1, t_2 = transit times.
For prototype sensor: r = 6.4 mm, d = 2.4 mm, h = 1.2 mm

$$t_1 = \frac{2}{c}(r \sec\theta + d \tan\theta - h) \qquad t_2 = \frac{2}{c}(r \sec\theta - d \tan\theta - h)$$

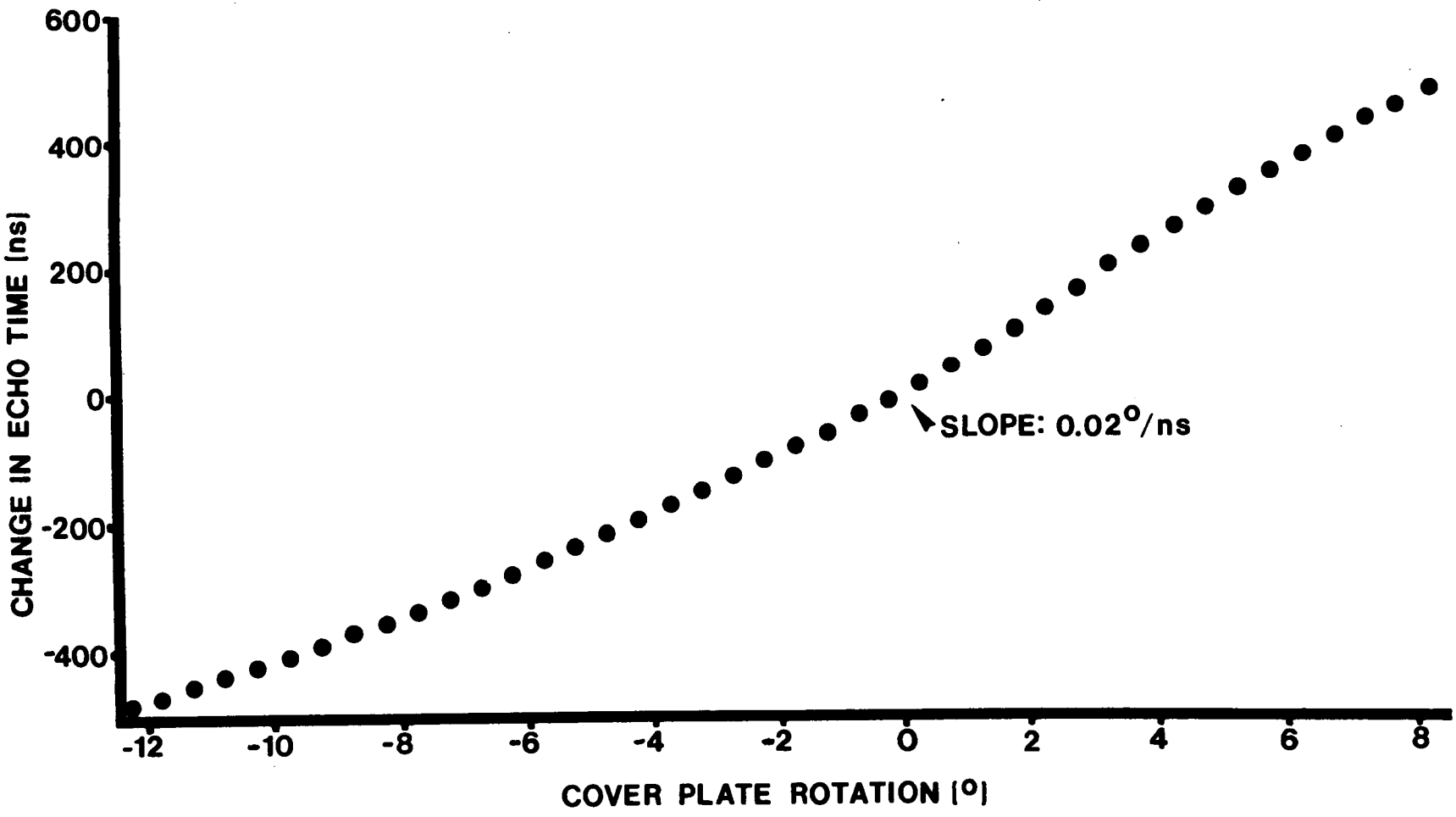

Figure 6. Echo Transit Time Verses Cover Plate Rotation, M_z.

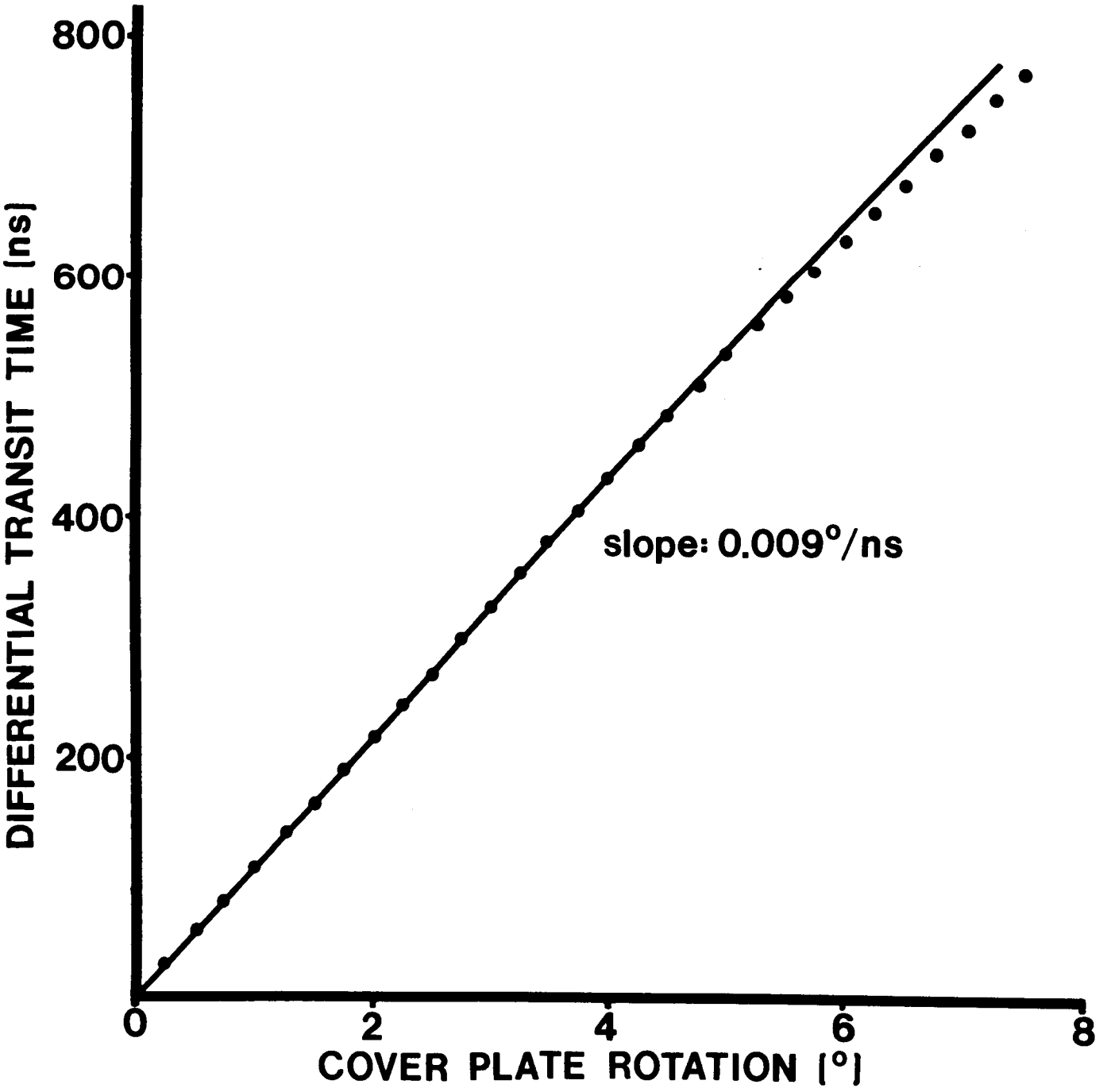

Figure 7. Cover Plate Rotation Versus $t_2 - t_1$.

plate. This curve is quite linear up to 5^{o}. Consequently, for the dimensions used the differential transit time measurement is linearly related to cover plate rotation over a $\pm 5^{o}$ range. The slope of the line in Figure 7 is $-0.009^{o}/ns$ so that for a ± 5 ns time resolution, the angular error is about $\pm 0.05^{o}$.

We conclude that even though the flat reflecting surfaces behave as specular reflectors, their performance is entirely adequate in the proposed force-torque sensor. Therefore, alternative reflector forms, such as spherical surfaces, were not investigated.

Coupling Agent Attenuation

The proposed force torque sensor contains a cavity between the four ultrasonic transducers mounted vertically on the centrally-located post and their respective reflectors attached to the cover plate. This cavity must contain a suitable acoustic coupling agent to carry the ultrasonic pulses. The agent must conduct the ultrasonic energy without excessive attenuation as well as not adversely affecting the mechanical properties of the sensor or its response. This latter consideration will be discussed later. The two coupling materials considered were silicone oil and silicone gel. Silicone oil would have less effect on sensor performance but would be harder to keep within the cavity, compared to the silicone gel.

Acoustic attenuation measurements were made on representative samples of a silicone oil and gel. A vertically-mounted ceramic ultrasonic transducer was used for these measurements. For reference purposes, a 6.4 mm thick pad of silicone rubber (RTV-615, General Electric Company, Waterford, New York) was coupled to the transducer surface with a thin layer of grease and the amplitude of the echo pulse produced at the silicone rubber-air interface recorded. This procedure was repeated with a 6.4 mm thick layer of a silicone gel (Dow Corning 3-6527 Silicone Dielectric Gel, Dow Corning Corp., Midland, Michigan) and with a well containing a 6.4 mm depth of a silicone oil (Dow Corning 200 Fluid, 5 cs viscosity, Dow Corning Corp., Midland Michigan). Both the silicone oil and gel had about the same attenuation which was about 0.6 times that of the silicone rubber. Consequently, either material would be a suitable coupling agent on the basis of low ultrasonic attenuation.

Static Elastomer Characterization

The success of the proposed sensing technique depends upon how well elastomers behave as multidimensional linear springs. Elastomer compression, tension, shear, and torsion characteristics were measured under static conditions for small displacements and rotations. Measurements were made on flat silicone rubber rings 25.4 mm O.D. x 12.7 mm I.D. x 6.4 mm thick. These rings were cast using RTV-615 silicone rubber that had previously been degassed and were cured overnight at 60°C. After removing from the mold, the flashing was trimmed off and the ring bonded (Dapcotac # 3300, Aircraft Products Co., Anaheim, California) between two aluminum plates. These plates were then attached to various fixtures instrumented with load cells for determining the different spring constants.

RTV-615 was chosen as a representative sample of silicone rubber for several reasons. First, it was easy to work with being clear and having a low viscosity in the liquid state so that cast rings were guaranteed to be free of macroscopic gas bubbles. Second, it is a medium durometer rubber having a shore A hardness of 40 points. And finally, it had been characterized by us before in compression and found to be quite linear under static conditions (but quite hysteretic under large deformation).

The compression-tension characteristics of the silicone rubber ring were measured with a special fixture instrumented with a $\pm$ 445 N range load cell (Model 100-0-CT-8L-FF-2.0-100#, Hardy Scales Co., Ogden, Utah) and mounted on a milling machine table. Movement of the table via its micrometer drive displaced the rubber ring by the same amount and the resultant force (load cell output) was displayed on a digital voltmeter having 1.0 μv resolution (Model 3460A, Hewlett Packard Co., Palo Alto, California). Figure 8 gives the results of one such experiment over a range of forces from about 50 N compression to 70 N tension. The relationship is linear with a slope of 145 N/mm. Consequently, the spring constant for F_z, the normal force applied to the sensor cover plate is 145 N/mm. This constant can be increased by using higher durometer elastomers, flatter rings, or wider rings; and conversely for lowering the spring constant.

The remaining two forces, F_x and F_y, are shear forces that laterally displace the top surface of the ring relative to the bottom

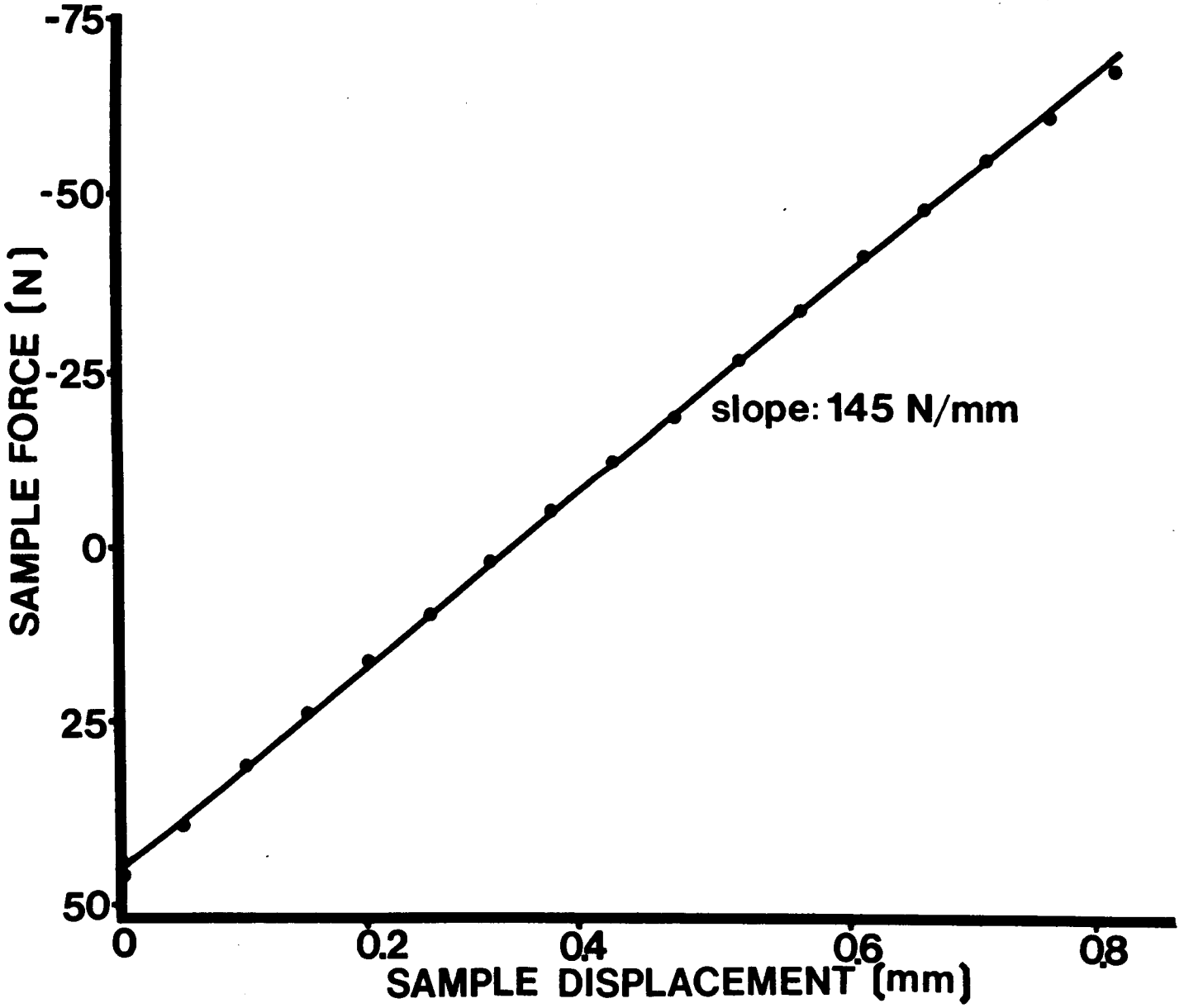

Figure 8. Compression-Tension Characteristics of a Silicone Rubber Ring: RTV-615, 25.4 mm O.D., 12.7 mm I.D., 6.4 mm thick.

surface. The spring constant relating this shear force to the deformation produced was determined with the same general set-up used for the compression-tension measurements except the forces were applied in shear. Figure 9 shows the results of one such test covering shear forces from + 22 N to - 40 N. The relationship is quite linear over the range tested except at the higher force range where the curve deviates from linearity likely due to partial failure of the bond between the rubber ring and the aluminum test plates. The slope of the line, and therefore, the shear spring constant, is 14.0 N/mm which is about one-tenth that for compression. Consequently, for this particular geometry the shear force sensitivity is about ten times greater than the compressive force sensitivity. This feature could be highly advantageous in many applications. For example, with the force-torque sensor mounted on the gripping surface of a robotic or manipulator finger, the compressive force, F_z, would give the gripping force which is usually moderately large. The shear forces, F_x and F_y could be used as a measure of impending slip or misalignment during a part insertion operation. In either case high F_x and F_y sensitivity would be beneficial in that corrective action could be taken sooner.

The two torque components M_x and M_y lie in the plane of the sensor cover plate so that during application of these components part of the elastomer ring is in compression and part is in tension. Consequently, one would expect the associated torque spring constant to be linear since the compression-tension characteristics were linear. The torque characteristics were measured using appropriate fixturing and the goniometer to produce highly accurate angular rotations and the 445 N load cell to give the resultant force. (The load cell and display instrumentation had a useful force resolution of $\pm$ 0.044 N.) Fixturing was simplified by the use of two silicone rubber rings bonded to a lever arm connected to the load cell. The resultant ring assembly was rigidly mounted in, and rotated by, the goniometer. The results for the <u>two</u> rings is given in Figure 10 for a range from + 1.7 N-m to - 2.1 N-m. Again the relationship is linear and the slope of the curve for <u>one</u> ring is 0.14 N-m/ ^{o}.

The remaining force-torque component is M_z, the torque that is perpendicular to the sensor cover plate. The spring constant associated with this component we have called the torsion spring constant since it

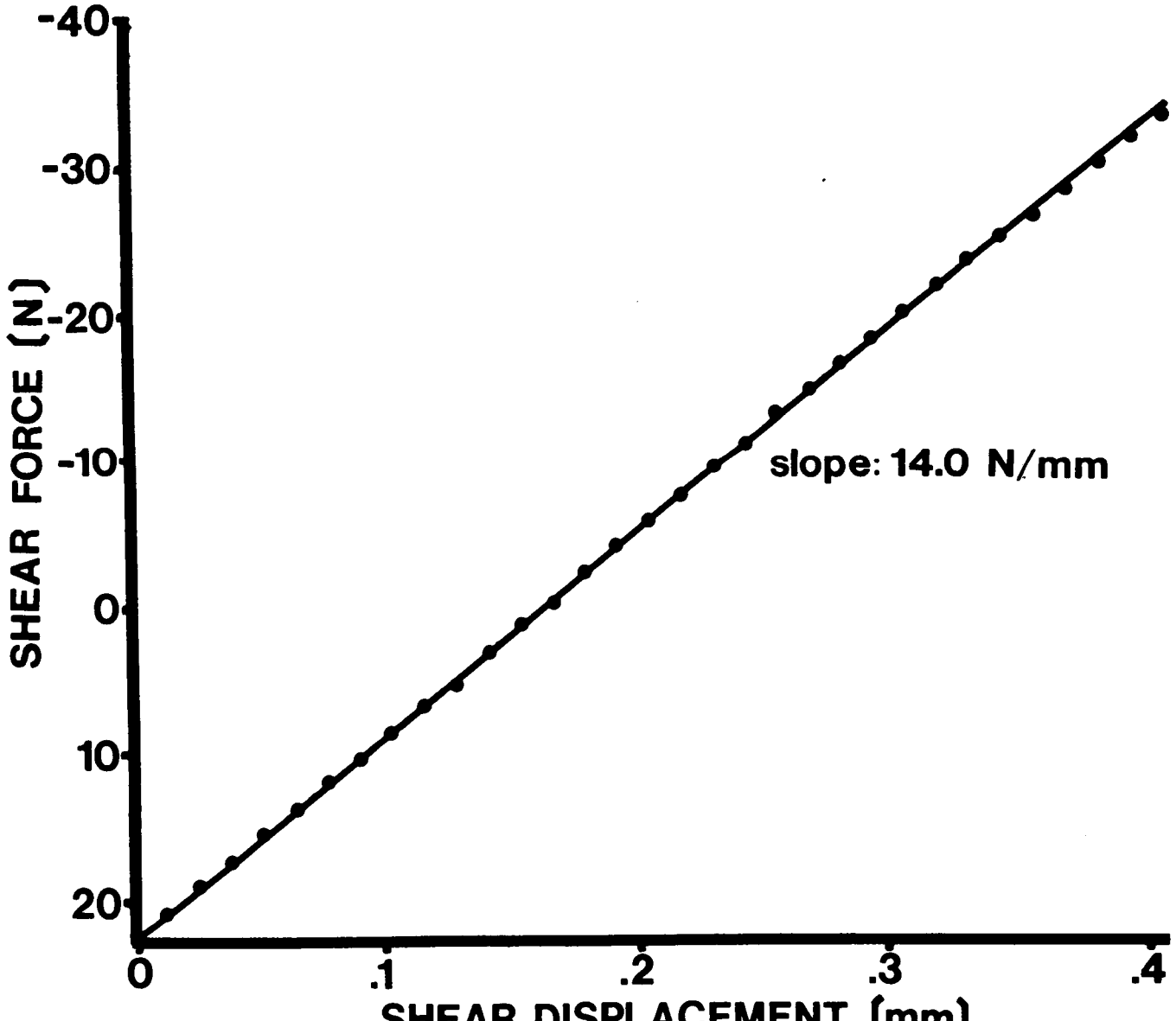

Figure 9. Shear Characteristics of a Silicone Rubber Ring: RTV-615, 25.4 mm O.D., 12.7 mm I.D., 6.4 mm thick.

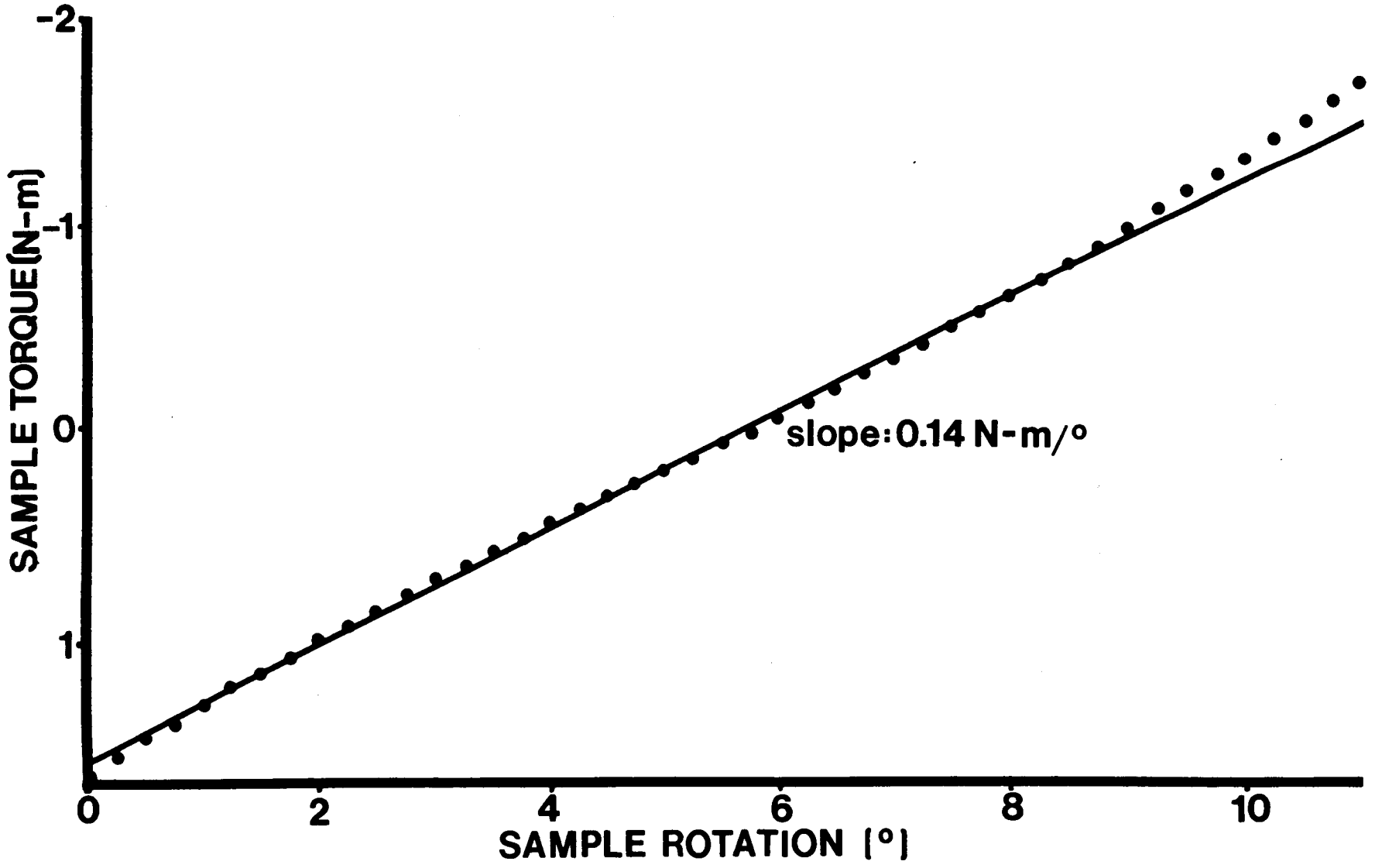

Figure 10. M_x - M_y Torque Characteristics of Two Silicone Rubber Rings. RTV-615, 25.4 mm O.D., 12.7 mm I.D., 6.4 mm thick.

tends to rotate or twist the ring. The torsional characteristics of the RTV-615 silicone rubber ring were measured with the goniometer used to rotate the ring and a ± 22 N range load cell (Model BA 5 lb., Alphatron, Inc., Andover, Massachusetts) to measure the resultant torque. These measurements are shown plotted in Figure 11. The relationship is again approximately linear over the measurement range of +0.056 N-m to - 0.092 N-m. The torsion spring constant is 0.010 N-m/^{o} which is about an order of magnitude less than the torque spring constant (for M_x and M_y) for the particular ring geometry used. This differential sensitivity can also be exploited.

Table 3 summarizes the findings in static elastomer characterization. The four spring constants are listed for RTV-615 silicone rubber along with the linear range of application and the force or torque resolution corresponding to a distance resolution of ± 2.5 μm (± 5 ns transit time) and angular resolution of ± 0.05^{o}.

Static natural rubber characterization was not undertaken in Phase I due to time limitations and previous findings that as a class, natural rubbers behave more linearly than silicone rubbers. The main potential advantage of natural rubber is its reduced hysteresis compared to silicone rubber. Limited dynamic testing of these two rubber families was conducted and the results will be presented later.

Force-Torque Component Interaction

A battery of tests were conducted to determine whether silicone rubber could be treated as a truly linear, isotropic material with the various force-torque components acting independently or whether there would be interaction. For example, would a moderate compressive force, F_z, change the slope of the shear characteristic so that the calibration factor for F_x and F_y (i.e. the shear spring constant) would be a function of F_z.

At first glance it would appear that there are 30 possible pairs of interactions since each of the six force-torque components could have any one of the remaining five components react with it. However, F_x and F_y along with M_x and M_y are analogous (i.e. they produce the same type

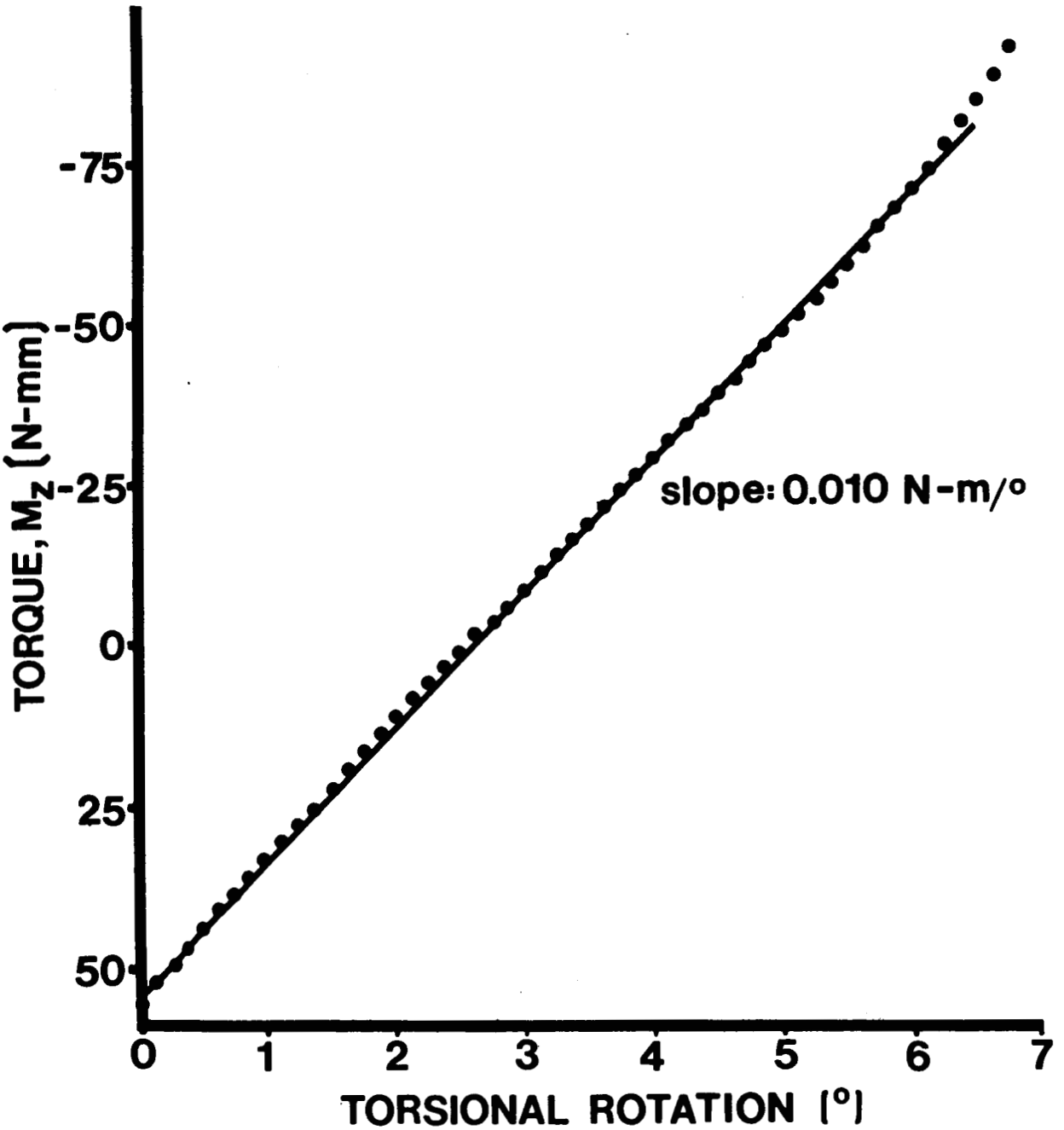

Figure 11. Torsional Characteristics of a Silicone Rubber Ring: RTV-615, 25.4 mm O.D., 12.7 mm I.D., 6.4 mm thick.

TABLE 3

RTV-615 SILICONE RUBBER ELASTIC PARAMETERS

Spring Constant	F/T Component	Value	Approximate Linear Range	Resolution
Compression	F_z	145 N/mm	>+50 to -70 N	± 0.36 N
Shear	F_x, F_y	14.0 N/mm	>+22 to -44 N	± 0.035 N
Comp./Tension	M_x, M_y	0.14 N-m/^{o}	+ 0.9 to - 0.9 N-m	± 0.007 N-m
Torsion	M_z	0.010 N-m/^{o}	+0.056 to -0.070 N-m	± 0.0005 N-m

of displacement in the rubber except their direction is 90^0 apart) so that only one of these forces and one of these torques needs to be considered. Consequently, the number of possible interactions is reduced to 4 x 3 or 12. But half of these are redundant in that it includes pairs like F_x, M_z and M_z, F_x which have the same effect. Therefore, we tested the six remaining interactions (F_x - F_z, M_z-F_z, M_y-F_z, M_y-M_z, F_x-M_z, and F_x-M_y).

These tests were difficult and time consuming. For each pair one component was measured over a range of linear or angular displacements: first without the second, potentially interfering component; then, the second component was applied in a series of steps using weights either applied directly to produce forces, or through lever arms to produce torques. It was extremely difficult in some tests to decouple the load cell from direct effects of the interfering component. This was especially true when the interfering component was changed. At such times it was sometimes necessary to uncouple the load cell and realign it to remove spurious loading signals. Since it was virtually impossible to do this exactly, the force or torque measurements were often offset slightly each time the interfering component was changed. However, this had little practical significance in that interference would show up as a change in slope of the characteristic (i.e. spring constant) and not the intercept.

The results of all six series of experiments were the same. There was no effect of the interfering component on the spring constant over the range tested. Typical results are shown in Figure 12 for the torsion characteristics in the presence of an orthogonal torque, and in Figure 13 for torsion in the presence of shear. Other curves had more offset than these. This result greatly simplifies operation of the proposed sensor because the material spring constants can be treated as indeed constant and independent.

Dynamic Elastomer Characterization

A number of samples, both silicone and natural rubber, was subjected to dynamic testing in order to determine the effects of the rate of force loading and unloading on hysteresis and the slope (or spring

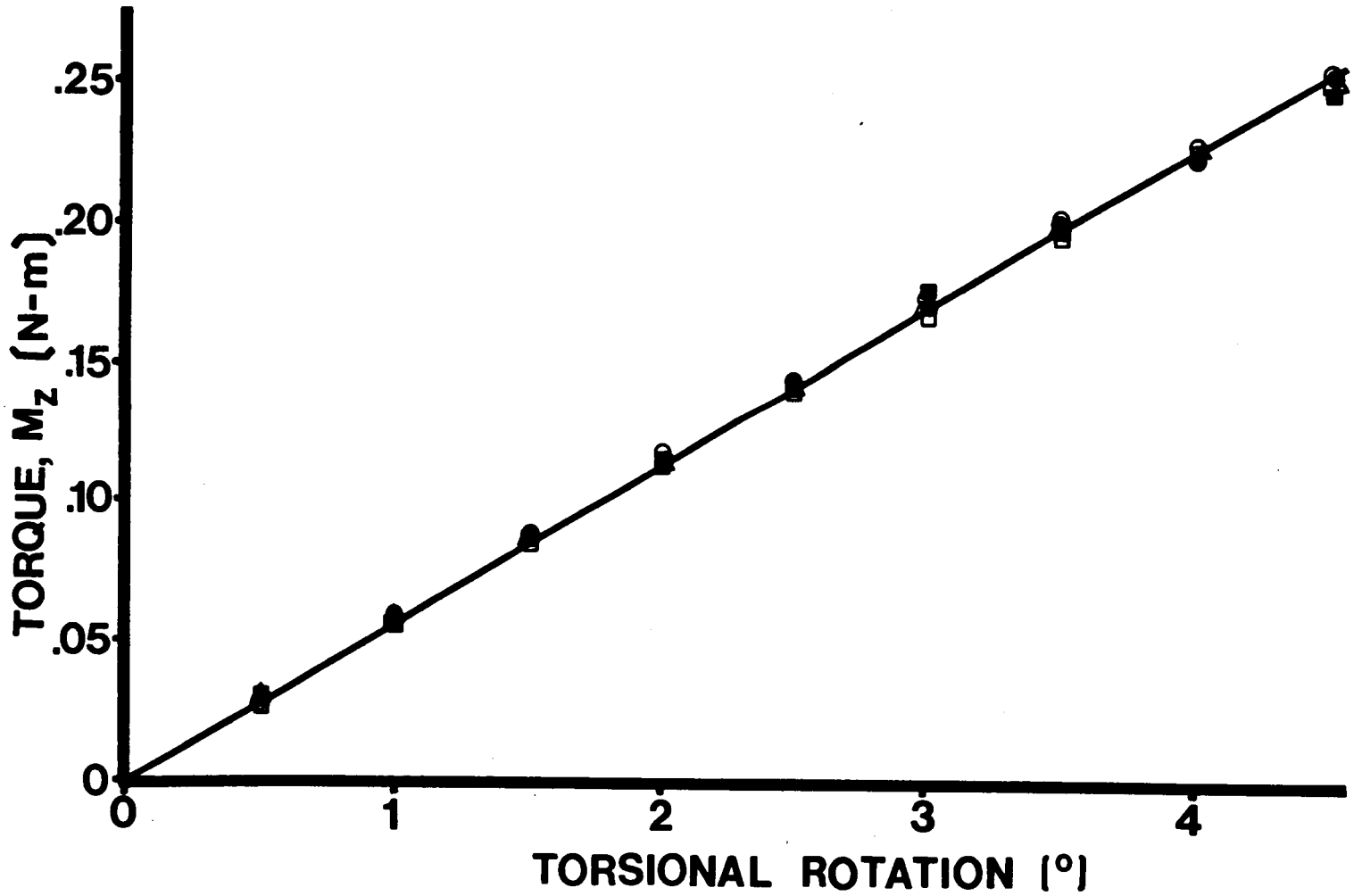

Figure 12. Torsion Characteristics in the Presence of an Orthogonal Torque of a Silicone Rubber Ring: RTV-615, 25.4 mm O.D., 12.7 mm I.D., 6.4 mm thick. M_z: 0 (□), 0.17 N-m (○), 0.34 N-m (●), 0.51 N-m (■), 0.68 N-m (△).

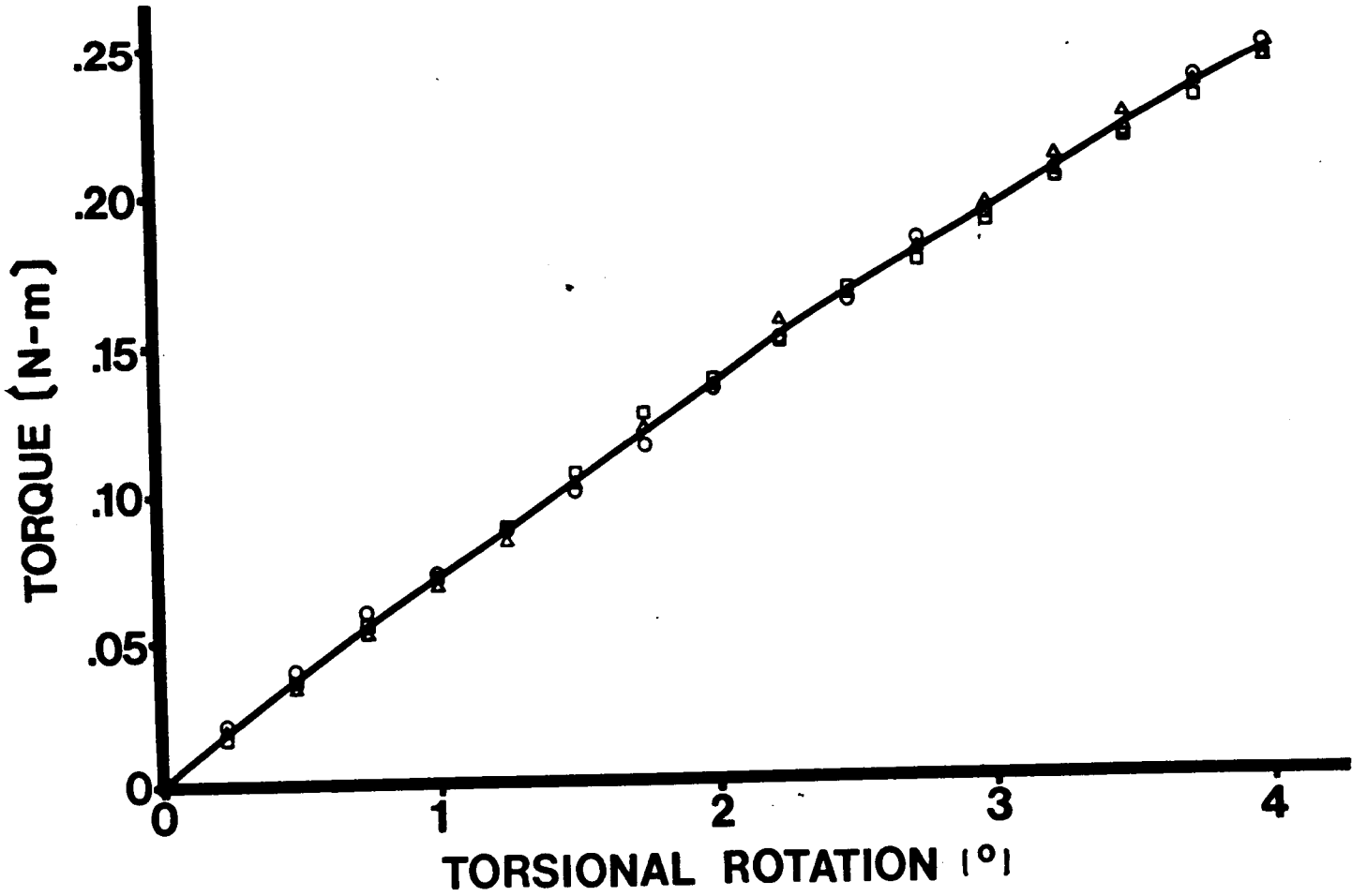

Figure 13. Torsion Characteristics (M_z) in the Presence of Shear Force (F_x) of a Silicone Rubber Ring: RTV-615, 25.4 mm O.D., 12.7 mm I.D., 6.4 mm thick. F_x: 0 (△), 4.45 N (□), 8.90 N (○).

constant) of the force-displacement characteristic. Previous experiments with interfering force-torque components showed that the silicone rubbers used were isotropic materials (over the range of deformations used). Therefore, time dependent effects such as hysteresis, creep, etc. should not depend upon elastomer orientation. Consequently, dynamic testing was almost entirely limited to cyclic compression of the rubber specimens. One measurement was made with cyclic shearing of the rubber with results not materially different from those of the compression tests, thereby partially justifying limiting the tests to compression. Also, no tests were conducted using cyclic torque loads. It was felt that these would provide no new information since torques M_x and M_y apply compression-tension forces to the rubber and, therefore, would produce the same results as compression loading. Similarly, M_z shears the rubber sample circumferentially so that the results would be the same as those for linear shear loading.

A small horizontal milling machine was used as the test bed for the dynamic elastomer characterization studies. The arbor was fitted with a ball bearing assembly mounted off-center that pressed against a metal plate covering the rubber sample. The eccentricity of the bearing could be changed to give different displacements. A second, larger eccentric was also mounted on the arbor and used to drive a spring-loaded linear potentiometer to provide an electrical signal proportional to displacement. This signal was applied to the x-axis channel of an oscilloscope. A second metal plate was placed beneath the rubber sample and on top of the 445 N load cell which was mounted on the mill table directly underneath the bearing. In this fashion, the cyclic compression force on the sample was measured by the load cell and displayed on the y-axis of the oscilloscope. The milling machine was operated at three different speeds to cover a range of loading rates. These were 61 RPM (1.02 RPS), 101 RPM (1.68 RPS), and 166 RPM (2.77 RPS).

All the rubber samples were ring-shaped (25.4 mm O.D. x 12.7 mm I.D. x 6.4 mm thick) having a cross sectional area of 3.8 cm^2 except the R-45 natural rubber sample which was a 9.5 mm x 40 mm x 6.4 mm thick rectangle of the same cross sectional area. Not enough R-45

rubber was available to fabricate a ring. The first series of tests cyclically displaced the rubber sample 1.27 mm (0.050 in.). In each case the minimum force was 111 N (25 lbs.). That is, in the hysteresis loop the lowest point on the curve corresponds to a force of 111 N. The test results are given in Figues 14, 15, 16, 17 and 18. In these Figures the vertical axis corresponds to the compressive force with each centimeter being 44.5 N (10 lbs). The horizontal extent of the loop is 1.27 mm (0.050 in.). The loop is made in a clockwise direction with the upper curve being for increasing force and the lower curve being for decreasing force. Figure 14 is for RTV-615 silicone rubber; Figure 15 is for RTV-J silicone rubber; Figures 16, 17 and 18 show the results for natural rubbers A, B, and R-45, respectively.
The three different curves in each Figure correspond to the three rates as indicated. Table 4 summarizes the photographic information. There was no measurable difference between curves taken at the three different rates. The entries in the fourth column of Table 4 are the maximum time change in force for the curve taken at 166 RPM, assuming the force varies sinusoidally. The hysteresis would be a maximum at the highest rate. The per cent hysteresis entries are ratios between the hysteresis values and force excursion, expressed as a percentage.

This series of experiments was repeated with the same rubber samples under the same test conditions except that each sample was only displaced by 0.090 mm (0.0035 in). The results are shown in Figures 19 through 23. In this test the minimum force was 8.9 N (2.0 lb.) and the vertical deflection corresponds to 22 N (5 lb.) per centimeter. Table 5 summarizes the results. The last entry in Table 5 is for an RTV-615 silicone rubber ring that was cyclically sheared (in the plane of the ring as happens when F_x and F_y forces are applied) 2.7 mm (0.11 in). Figure 24 shows the hysteresis loops for this sheared sample taken, from top to bottom, at 61, 101 and 166 RPM. The offset force 8.9 N (2.0 lb) and vertical sensitivity, 22.2 N (5.0 lb) per large division, is the same as the previous five Figures. Again, in both the low displacement compression curves and the shear curve, there is no significant effect of cycle time (i.e. loading/unloading rate).

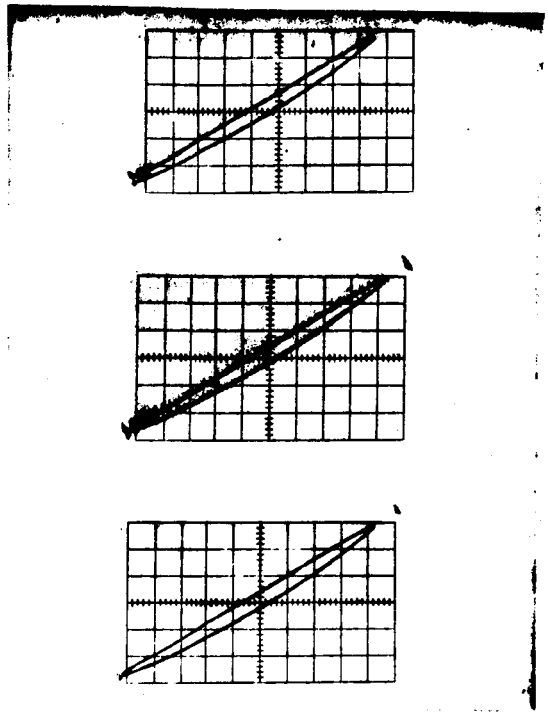

Figure 14. Large displacement hysteresis loops for Silicone Rubber RTV-615 at 61, 101, and 166 rpm (top to bottom).

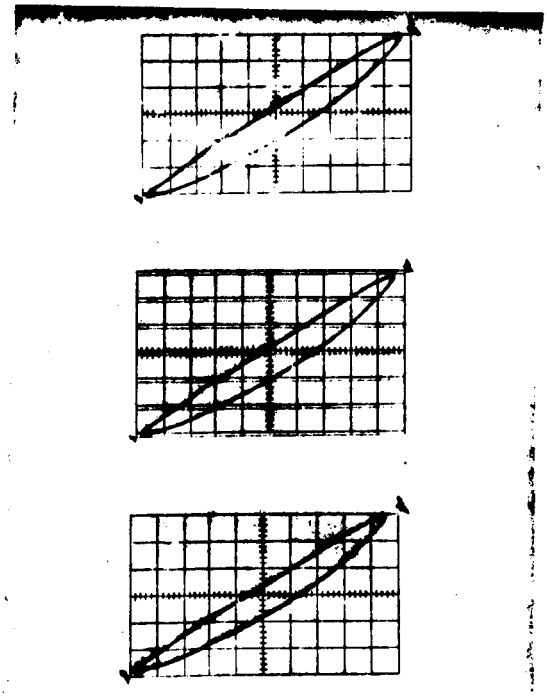

Figure 15. Large displacement hysteresis loops for Silicone Rubber RTV-J at 61, 101, and 166 rpm (top to bottom).

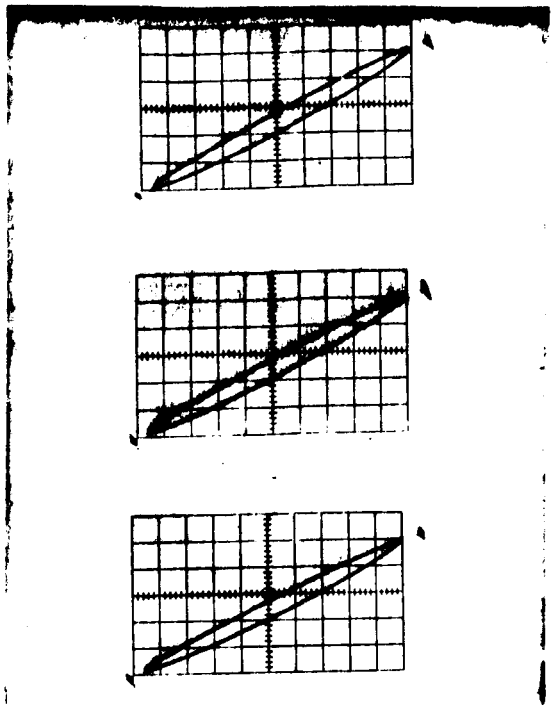

Figure 16. Large displacement hysteresis loops for Natural Rubber A at 61, 101, and 166 rpm (top to bottom).

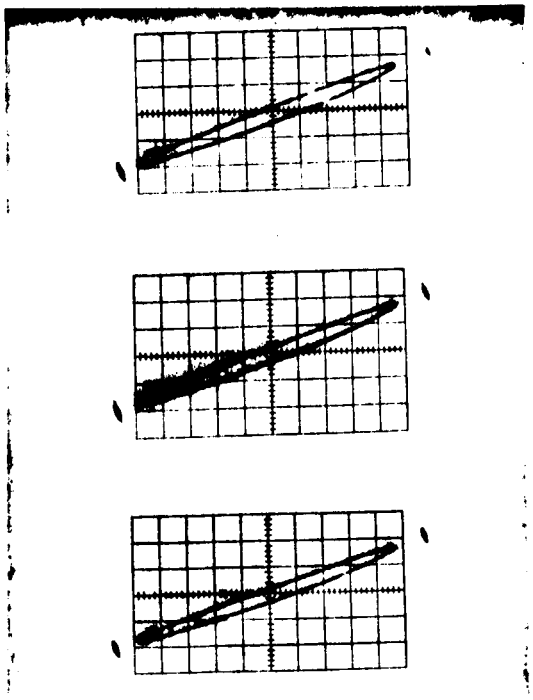

Figure 17. Large displacement hysteresis loops for Natural Rubber B at 61, 101, and 166 rpm (top to bottom).

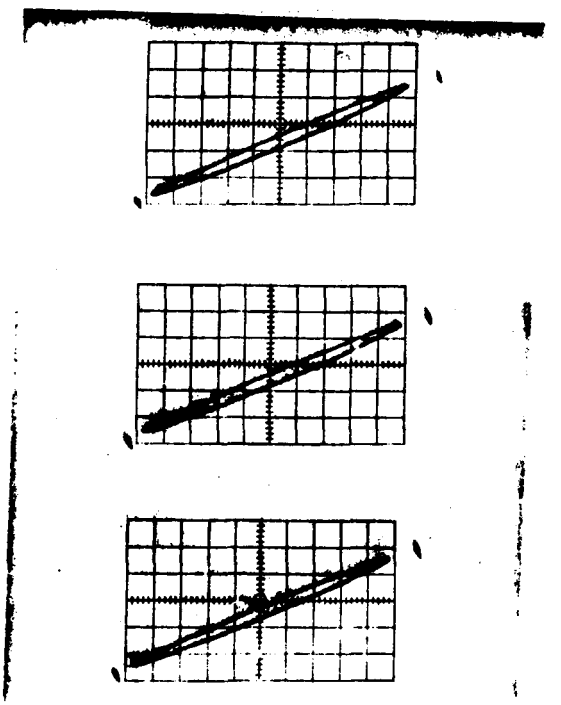

Figure 18. Large displacement hysteresis loops for Natural Rubber R-45 at 61, 101, and 166 rpm (top to bottom).

TABLE 4

HYSTERESIS RESULTS - LARGE DISPLACEMENT

SAMPLE	FORCE EXCURSION		HYSTERESIS		MAXIMUM RATE OR FORCE APPLICATION		% HYSTERESIS
	N	LB	N	LB	N/S	LB/S	
RTV-615	250	55	27	6	2100	480	11%
RTV-J	260	58	53	12	2200	500	21%
N.R. A	210	48	36	8	1900	420	17%
N.R. B	150	34	22	5	1300	300	15%
N.R. R-45	180	40	18	4	1500	350	10%

RTV-615 Silicone Rubber, General Electric Co.
RTV-J Silicone Rubber, Dow Dorning Corp.
N.R. A Natural Rubber, Engineered Rubber Products, Inc.
N.R. B Natural Rubber, Engineered Rubber Products, Inc.
N.R. R-45 Natural Rubber, R.C. Musson Rubber Company

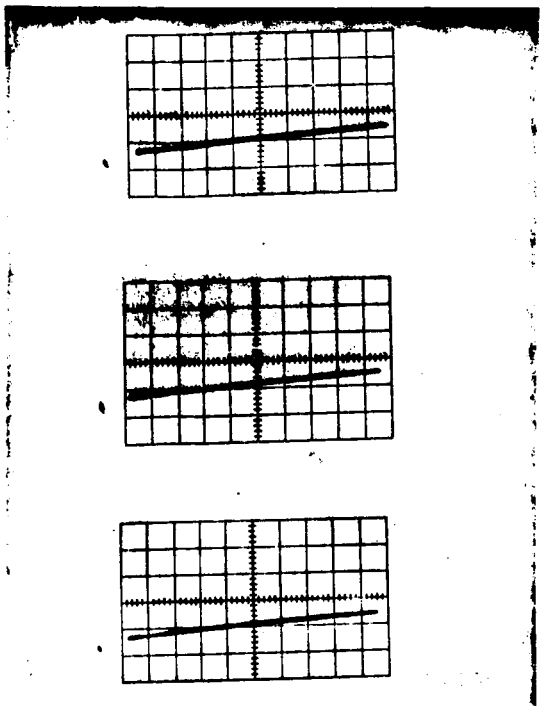

Figure 19. Low displacement hysteresis loops for Silicone Rubber RTV-615 at 61, 101, and 166 rpm (top to bottom).

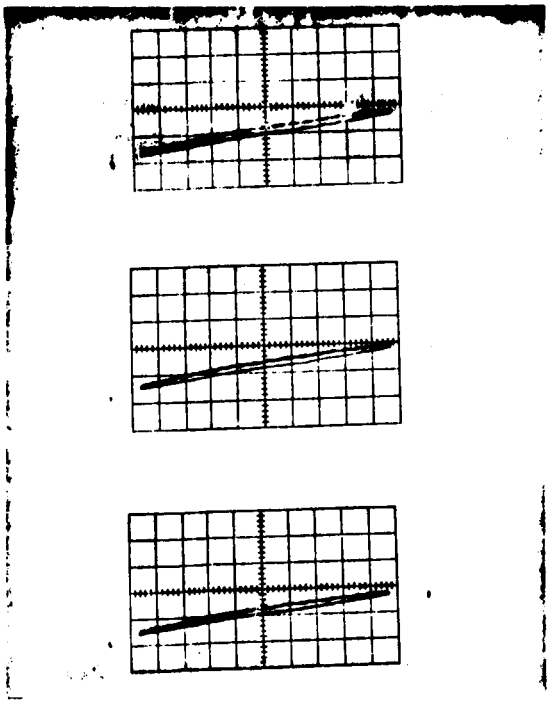

Figure 20. Low displacement hysteresis loops for Silicone Rubber RTV-J at 61, 101, and 166 rpm (top to bottom).

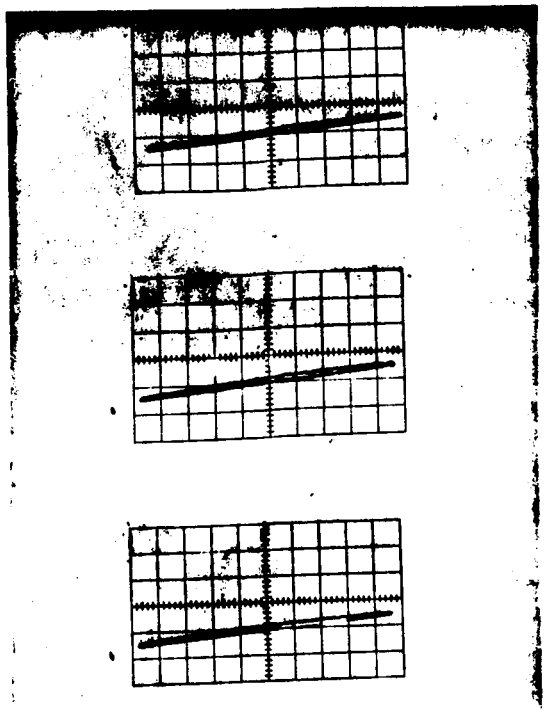

Figure 21. Low displacement hysteresis loops for Natural Rubber A at 61, 101, and 166 rpm (top to bottom).

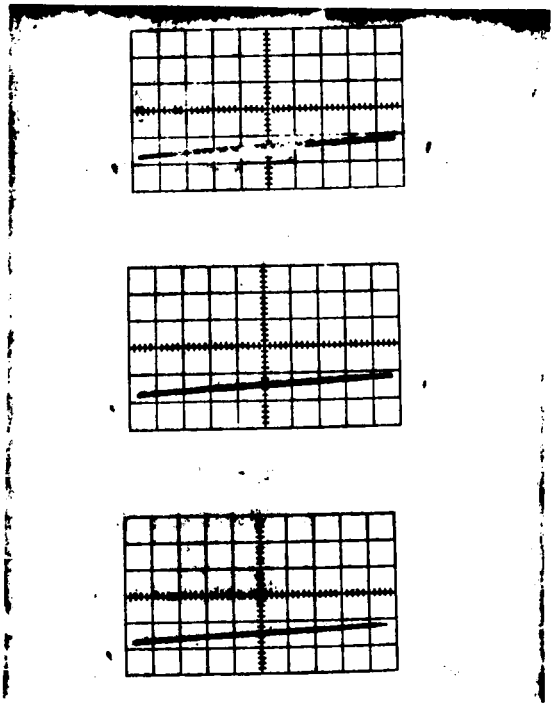

Figure 22. Low displacement hysteresis loops for Natural Rubber B at 61, 101, and 166 rpm (top to bottom).

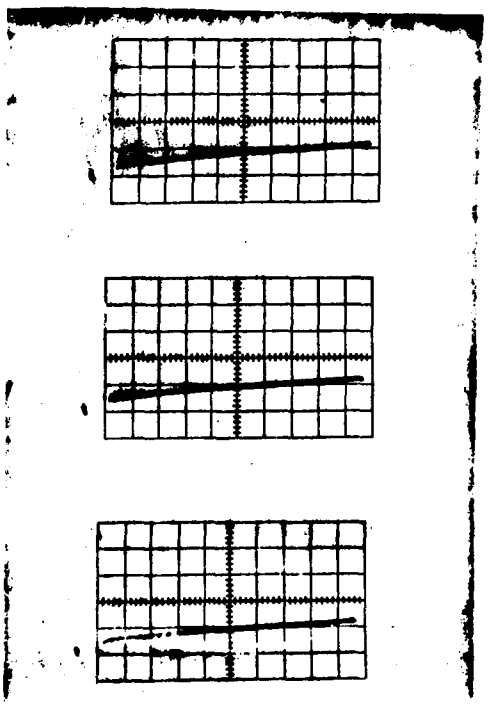

Figure 23. Low displacement hysteresis loops for Natural Rubber R-45 at 61, 101, and 166 rpm (top to bottom).

TABLE 5

HYSTERESIS RESULTS - LOW DISPLACEMENT

SAMPLE	FORCE EXCURSION		HYSTERESIS		MAXIMUM RATE OR FORCE APPLICATION		% HYSTERESIS
	N	LB	N	LB	N/S	LB/S	
RTV-615	18	4	2.2	0.5	160	35	12%
RTV-J	27	6	4.5	1.0	230	52	17%
N.R. A	22	5	4.5	1.0	200	44	20%
N.R. B	13	3	2.2	0.5	120	26	17%
N.R. R-45	18	4	2.2	0.5	160	35	12%
*RTV-615	58	13	**------		490	110	----

* This sample sheared 2.7 mm (0.11 in)

** Not measurable (less than 2.2 N (0.5 lb))

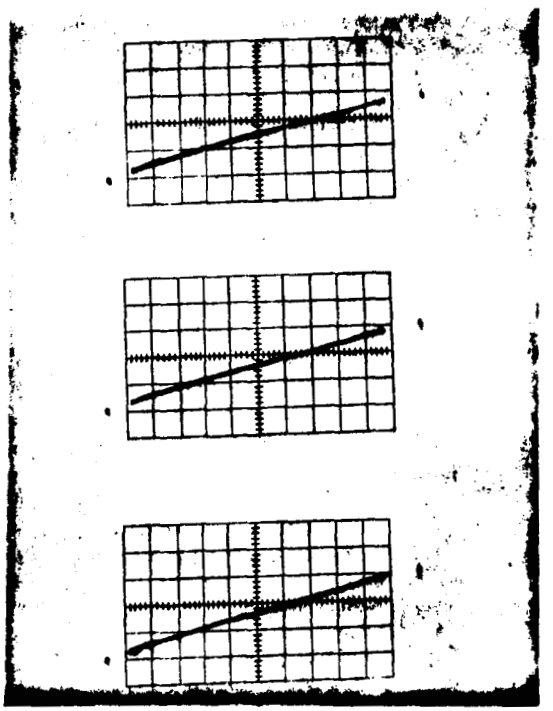

Figure 24. Hysteresis loops for a sheared RTV-615 silicone rubber ring at 61, 101, and 166 rpm (top to bottom).

The test results of the dynamic elastomer characterization experiments were both surprising and most encouraging. They were surprising in that previous measurements made on RTV-615 silicone rubber showed very large hysteresis (similar to that for RTV-700 shown in Figure 2). As can be seen in Tables 4 and 5 the hysteresis for RTV-615 under the above test conditions is comparable to that of the best natural rubber (R-45). At least a partial explanation for this result lies in the test conditions and elastomer geometry. Previous measurements were made on 38 mm x 25 mm x 6.4 mm thick rectangular pieces of rubber. These were compressed in an Instron to 60% of their original thickness (2.6 mm), resulting in a force of about 900 N (200 lb). This large of a compression on a solid block of rubber produces very large internal forces that can cause the material to creep with resultant force relaxation. With only 20% compression, the maximum used for the Table 4 results, and with a ring geometry these forces are much less and can be relieved by lateral expansion of the ring inward as well as outward.

We found no significant change in the shape of the hysteresis curves with rates up to 2.8 Hz corresponding to force application rates from 1300 to 2200 N/s, depending upon the stiffness of the rubber sample. Higher rates were not used because of limitations in the experimental set-up. The slope of the curves did not change so that, over the range tested, the material spring constant is invariant (although two different constants would have to be used for high hysteresis materials - one for increasing and one for decreasing force). The small offsets among the three curves in each Figure are due to drift in the instrumentation and not changes in material characteristics with time. The hysteresis seen ranged from 10 to 21% in the compression tests, depending upon the elastomer type. Surprisingly, RTV-615 silicone rubber had a hysteresis component comparable to the best natural rubber, R-45 (11-12% versus 10-12%). In the shear experiment, even at force application rates up to 490 N/s there was no measurable hysteresis as well as no changes among the three rates used.

Prototype Sensor Evaluation

Evaluation of the prototype sensor was not nearly as extensive as we suggested in the Phase I proposal. This was for two reasons. First, some of the proposed measurements would almost be redundant compared to those already obtained, adding little information while consuming a disproportionate amount of time. Second, some potentially interfering effects proved to be much smaller than we previously anticipated so that more sophisticated techniques would have been necessary for their quantitation than we envisioned.

Prototype Sensor Construction

Based upon the results of the elastomer characterization studies we chose RTV-615 silicone rubber for the elastomeric ring in the prototype sensor. This material was well documented under both static and dynamic conditions, having low hysteresis - comparable to the best natural rubber we have tested so far. Also, this particular silicone rubber compound is very easy to degas and cast, plus being clear it facilitates visual inspection during fabrication, assembly, and alignment.

The transducers used were 3.2 mm x 1.6 mm x 28 μm thick rectangles of PVDF bonded to hollow brass tubes. The four horizontal transducers were bonded to 2.4 mm square brass tubes having 0.4 mm wall thickness. These tubes were positioned and held by friction in crossed slots milled in a 6.4 mm thick aluminum plate (see Figure 25). The four post-mounted transducers were mounted on a 4.8 mm x 2.4 mm rectangular brass tube, also with a 0.4 mm wall thickness. This tube was mounted vertically at the intersection of the machined slots as shown in Figure 25. The two transducers on the wider surface of this post were offset as shown in Figures 25 and 5. The other pair was centered. A port was machined into the aluminum base plate to allow filling the central ring with a silicone oil acoustic couplant after the cover plate was attached. The cover plate was made from 1.6 mm thick brass plate with individual brass tabs mounted on it for vertical reflectors. The cover plate was bonded to the top surface of the elastomeric ring with Dapcotac #3300 adhesive.

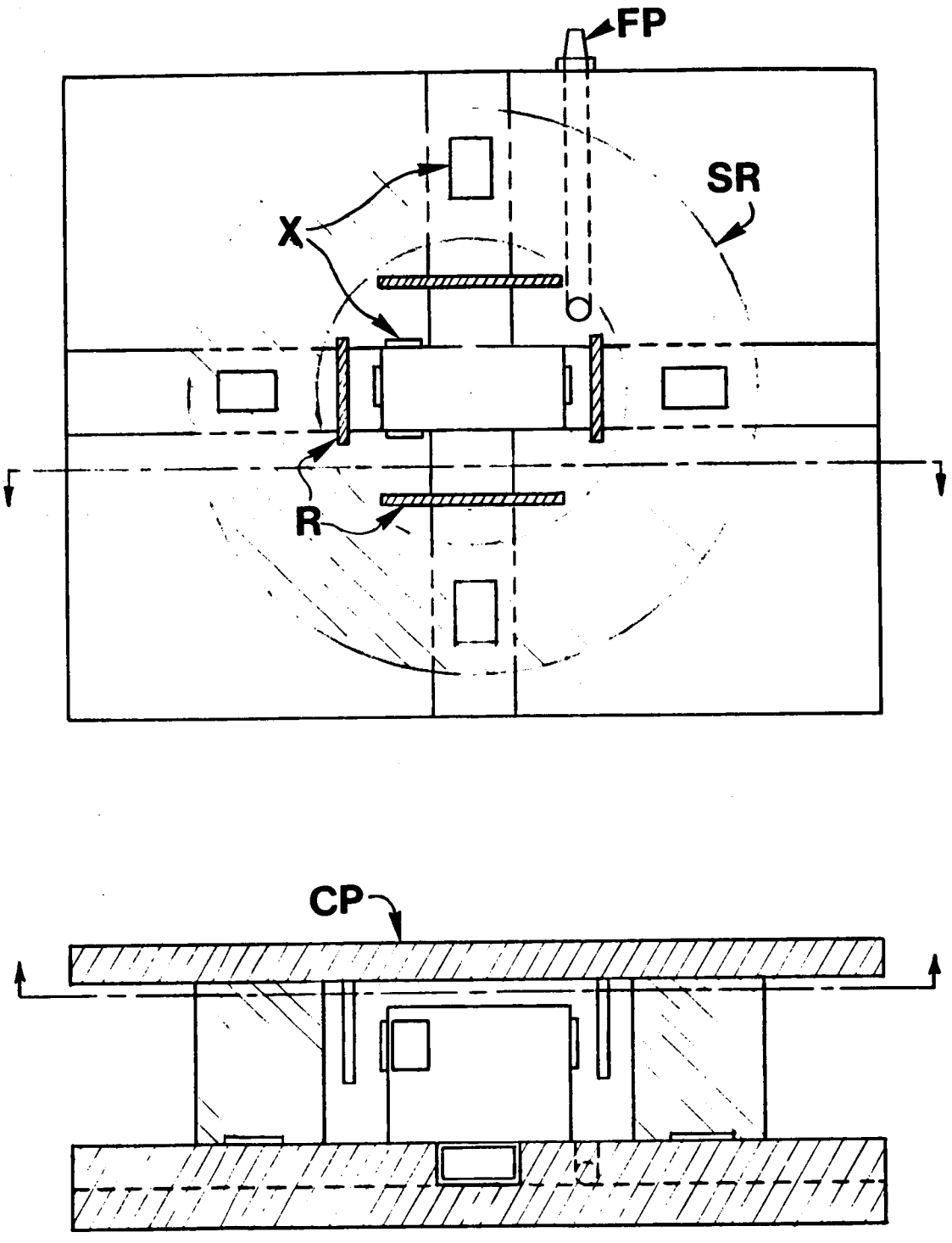

Figure 25. Prototype Force-Torque Sensor. X, brass tube mounted transducers; R, reflectors; SR, silicone rubber ring; FP, filling port; CP, cover plate.

Static Evaluation of Prototype Sensor

One of the first measurements made with the prototype sensor was ultrasonic echo strength with and without a ten-foot length of coaxial cable connected between the sensor and signal amplifier. The insertion of the cable reduced signal amplitude to 1/4 the value without the cable (i.e. 0.12 V versus 0.47 V). This reduced signal level was still adequate for time interval measurement by zero-crossing detection. However, with much smaller transducers such as 1.0 mm x 1.0 mm the signal would be about 1/5 as large and detection would probably be marginal at best. Consequently, for very small, gripper-mounted force-torque sensors either on-sensor circuitry or short cables to an arm-mounted amplifier module would be required. On-sensor circuitry would also minimize the number of wires exiting the sensor package.

In the Phase I proposal we stated that we would evaluate the prototype sensor by applying force and torque components individually and in combination while measuring the ultrasonic transit time for each sensor. These transit time measurements then were to be used with the previously measured spring constants and the equations in Table 2 to calculate the force and/or torque loadings and compare these values with the applied loading. This procedure would be time consuming and add little to determining the feasibility of the technique or to our understanding of its limitations. The proposed procedure would be a test of the workmanship used in the construction of the prototype sensor and the sophistication of the fixtures for applying the force-torque components, not of the underlying concepts.

All three force components (F_x, F_y, and F_z) applied alone or in combination produce only translation of the cover plate and, therefore, its reflecting surfaces. Consequently, the sensor's accuracy to force loading depends solely upon elastomer characteristics which were previously determined. The three torque components (M_x, M_y, and M_z) tend to rotate the reflecting surfaces out of alignment thereby altering the ultrasonic path length and therefore changing the transit time. We have shown in our reflector alignment studies that rotations up to $\pm 5^{o}$ can be tolerated before transit time, as measured by zero crossing, changes by more than $\pm$ 5 ns. Therefore, with the exception

of M_z, torque loading accuracy depends again primarily upon elastomer characteristics.

The relationship giving M_z in terms of changes in transit time is complex and nonlinear, owing to the geometry involved (Figure 5). Again, we have shown for small rotations ($\pm 5^o$), the difference in transit time varies linearly with cover plate rotation. An additional experiment was conducted to measure M_z versus change in transit time using the RTV-615 silicone rubber ring. The results of this experiment are shown in Figure 26. The results are quite linear over the $\pm 5^o$ measurement range.

A potentially complicating factor in the use of an elastomer as a multidimensional linear spring in our application is the change in thickness that occurs when the rubber is sheared (either linearly or angularly). An attempt was made to measure the change in thickness of the RTV-615 ring during the application of M_z. This was difficult and may be inaccurate since the cover plate is not perfectly free to move in the z-direction when M_z is applied. However, measurements obtained indicated a possible change in thickness of 0.009 mm per degree rotation of the cover plate. Consequently, without correction, an erroneous F_z indication of 1.3 N (0.3 lb) would occur for an M_z that rotates the cover plate by one degree. This effect has to be more accurately quantitated in Phase II and if necessary, correction algorithms developed.

We did not independently calibrate the prototype sensor based upon first principles and previously measured spring constants because we have found small variations in elastic properties between silicone rubber rings of the same compound. These differences are likely due to variation in mixture ratios for the two part silicone rubber system and to a lesser extent variations in the rubber-to-metal bond. Because of these variations and others introduced during sensor construction (e.g. transducer location, ring location, etc.) the only practical form of sensor calibration is by loading the sensor and recording its response.

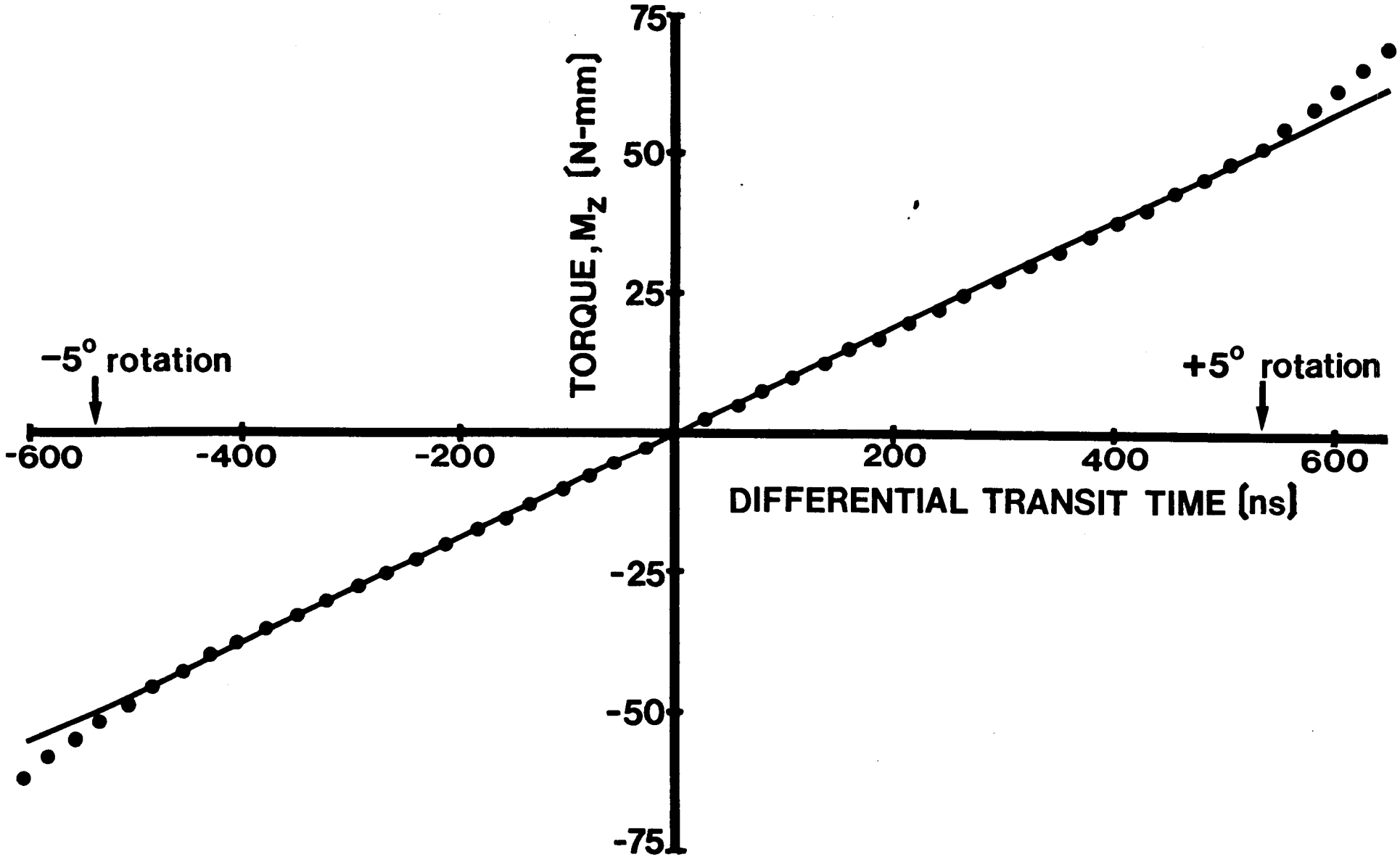

Figure 26. M_z Torque Versus Differential Transit Time of a Silicone Rubber Ring: RTV-615, 25.4 mm O.D., 12.7 mm I.D., 6.4 mm thick.

Dynamic Evaluation of Prototype Sensor

No dynamic evaluation was made of the prototype sensor for two reasons. First, we currently have no means of dynamically measuring ultrasonic transit time and displaying or recording it (this will be developed during Phase II of this project). Therefore, the sensor's reaction forces and torques could not be monitored. Second, these tests would probably reveal little or no new information over that which was already known from the dynamic elastomeric characterization studies.

Coupling Agent Evaluation

Prime candidates for acoustic coupling agents in the sensor cavity are silicone oil and gel. These materials have acceptably low acoustic attenuation and are inert and compatible with other sensor materials. We were previously concerned that these materials may significantly affect the mechanical properties of the sensor either by 1) augmenting the stiffness of the elastomer ring, or 2) excessively dampening cover plate motion by their viscosity. With the low viscosity silicone oil used (Dow Corning 200 Fluid, 5 cs viscosity) neither concern is founded. The silicone gel (Dow Corning 3-6527 Silicone Dielectric Gel) was not nearly as viscous as we anticipated and was very compliant (compared to RTV-615 silicone rubber). However, to test its mechanical effect we filled the sensor cavity with the gel and subjected the cover plate to cyclic displacement along the x-direction while measuring the resultant shear force and cover plate displacement. This experiment was the same as that performed for Figure 24 and the results were the same, indicating that the gel had no appreciable effects on mechanical properties of the sensor.

Pyramidal Reflector Post

One additional experiment was conducted. The purpose of this experiment was to determine the change in the ultrasonic echo signal produced by placing a 45^{o} metal reflecting surface in the ultrasonic path. This would test the validity of the concept presented in

Figure 3 of the Phase I proposal, and reproduced here in Figure 27, in which all ultrasonic transducers are mounted on the planar surface of the sensor substrate and an inverted pyramidal reflector post, having 45^{o} facets, reflects the ultrasonic pulses so that they travel horizontally through the coupling agent to the vertical reflectors and back again. If feasible, such a design would greatly simplify sensor construction and improve accuracy, by allowing all transducers to be mounted at once, in a fixed geometric relationship. Furthermore, by having the array metalization on the substrate rather than the PVDF sheet, no connections have to be made to the PVDF film.

A small, flat-bottomed chamber was fitted with a brass plate at one end oriented at 45^{o} so that a horizontal ray of ultrasound would be reflected downward by the brass plate and reflect from the chamber bottom back through the same path to the transducer. The chamber was filled with mineral oil and a 3.2 mm x 1.6 mm x 28 μm thick PVDF transducer was positioned vertically and aligned with the reflector. The transducer was pulsed and the echo signal was recorded. The experiment was repeated without the 45^{o} reflector over the same ultrasonic path length. The echo signal amplitude and shape were the same. Consequently, the scheme in Figure 27 appears to be feasible.

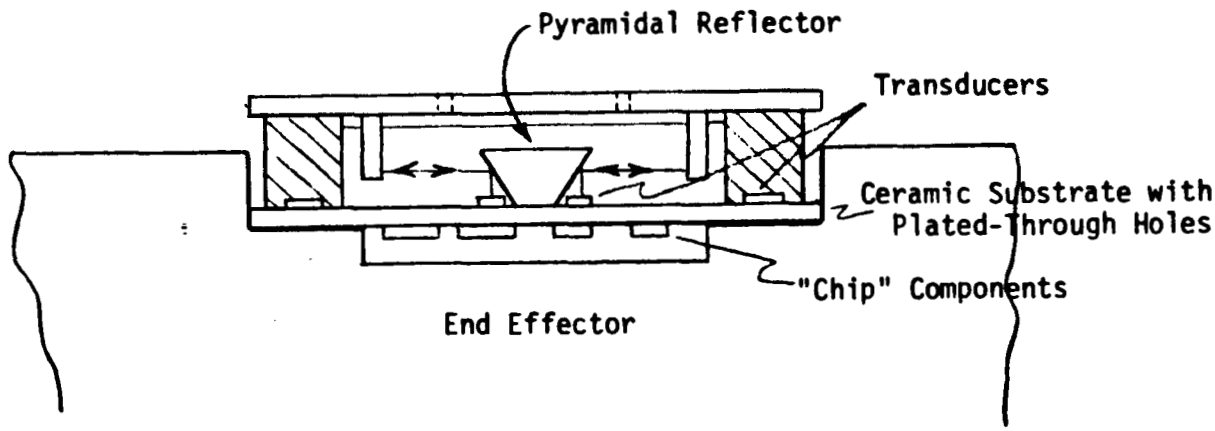

Figure 27. Sensor Design Using a Pyramidal Reflector Post to Allow All Transducers to be Mounted on a Plane Surface.

IMPLICATIONS OF THE RESULTS

We have successfully met our Phase I research objective. The six-component force-torque sensor can be made small enough (e.g. 10 mm diameter) to be placed on the gripping surface of a robotic end effector with ultrasonic echo signals still large enough for accurate time interval measurement. However, this may require on-sensor electronics for echo signal amplification and transducer element multiplexing. Simple planar reflectors coupled with zero-crossing detection of the ultrasonic echo signal allow reflectors to be rotated out of alignment by at least $\pm 5^{o}$ before significant time interval measurement errors occur, thus limiting angular displacement of the sensor cover plate, due to applied torques, to $\bullet\ 5^{o}$ or less. This small angular range is desirable in order to reduce object position errors due to sensor compliance. However, such errors are correctable since exact object location is still known.

We have developed a better method for measuring M_z, the z-axis torque, than originally proposed. M_z measurement was the weakest link in the proposed method for measuring sensor cover plate orientation. The revised technique uses one less transducer and gives accurate, linear results. The silicone rubber ring in the force-torque sensor has linear compression and shear characteristics so that spring constants can be derived to convert the ultrasonic distance measurements into force or torque values. Furthermore, over the range of loadings of interest, RTV-615 silicone rubber is an isotropic material. Consequently, its stiffness under compression is unaffected by the degree of shear present. This finding greatly increases the feasibility of the sensor design. The silicone rubber rings had much less hysteresis and force relaxation that we expected. RTV-615 was comparable to the best natural rubber we've tested to date, having about 10% hysteresis in compresssion under cyclic loading. Without compensation, some force torque values could be in error by 10% when that component is decreasing. However, we have no reason to believe that hysteresis can't be reduced further.

An interesting finding for the ring geometry used is the difference in force-torque component sensitivity. F_x and F_y force sensitivity is about ten times higher than that for F_z. Similarly, M_z torque measurement

is about ten times more sensitive than M_x or M_y. This difference can be advantageous. For example, with a screw-driver-type device in the gripper, the more sensitive F_x, F_y, and M_z measurements could give information on tip position relative to the fastener while the M_x or M_y measurement (being less sensitive and, therefore, having a wider range) would give the torque on the fastener, and F_z (also having a wider range) would give the clamping or holding force on the tool.

Acoustically, either silicone oil or silicone gel are acceptable coupling agents for the sensor cavity. At this point the gel is preferable since it is easier to contain.

Second order complicating effects have been smaller than we anticipated and therefore, more difficult to measure. These include such things as changes in elastomeric ring thickness due to shear and changes in M_z sensing geometry with sensor cover plate translation. Quantitation of these effects will be made in Phase II of this project. Compensation for these effects can be made, in principle, in sensor software. But being small effects, they may not be significant.

Interposing 45^0 reflecting surfaces in the ultrasonic path length does not materially change the echo pulse. Consequently, force-torque sensing schemes can be used with <u>all</u> transducers mounted on the same planar substrate, thus greatly simplifying sensor construction.

Finally, the force-torque sensor, especially with all transducers mounted on a planar substrate, is highly compatible with our tactile sensors. Both sensors could share a common substrate to give an integrated sensing package significantly smaller and more reliable than two separate sensors.

TECHNICAL FEASIBILITY CONCLUSIONS

On the basis of the Phase I feasibility study and our past experience in the development of tactile sensors using PVDF ultrasonic transducers and elastomeric pads, we conclude that our six-component robotic force-torque sensor is entirely feasible. More work is needed to quantify certain second order effects and to extensively evaluate the sensor under realistic operating conditions in order to fully determine its capability.

It is important to remember that the main features of the force-torque sensor are potential small size, low cost, moderate accuracy, and high compliance. Therefore, it cannot be viewed as a replacement for current strain gauge cross devices, with their high accuracy and low compliance, in all applications. However, in many applications, such as small parts assembly, compliance can be an advantage and high accuracy is usually unneccessary. Being of small size the sensor can be mounted on the gripping surface of the end effector without significant loss in robot payload.

REFERENCES

Benjamin, H. L., The Development of a Production Robot Tactile Position Sensor, Proceedings of the 13th International Symposium on Industrial Robots and Robot 7, pp. 18-57 - 18-76, 1983.

Bejczy, A. K., Sensors, Controls, and Man-Machine Interface for Advanced Teleoperation, Science, v. 208, 20 June 1980.

DeReggi, A. S., and G. R. Harris, Polymer Hydrophone Probes, Proceedings of the 1980 IEEE Ultrasonics Symposium.

Gaillet, A., and C. Reboulet, A (sic) Isostatic Six Component Force and Torque Sensor, Proceedings of the 13th International Symposium on Industrial Robots and Robots 7, pp. 18-102 - 18-111, 1983.

Seltzer, D. S., Tactile Sensory Feedback for Difficult Robot Tasks, Proceedings of the 12th International Symposium on Industrial Robots and Robots 6, 1982.

Sussner, H., The Piezoelectric Polymer PVF_2 and its Applications, Proceedings of the 1979 IEEE Ultrasonics Symposium, pp. 491-498.

PHASE II TECHNICAL OBJECTIVES

In Phase I we proved the feasibility of our force-torque sensor concept by demonstrating the feasibility of the various aspects of the technology. In Phase II we will continue the research in the areas of sensor design and fabrication, and associated electronics and elastomer evaluation and selection. This will enable us to construct and evaluate laboratory prototype force/torque sensor systems. It is anticipated that these sensors will have no more than four electrical leads exiting the sensor package and will have the pyramidal reflector configuration shown in Figure 27 to allow all eight ultrasonic transducers to be on the sensor substrate thus simplifying construction and increasing consistancy.

It is the intention of Bonneville Scientific during Phase II to keep pertinent NASA technical personnel apprised of sensor development progress and to send to NASA prototype force/torque sensors that may be redundant or no longer needed for evaluation. This would allow NASA personnel to become familiar with the sensor and facilitate its incorportion into NASA systems. Laboratory prototype force/torque sensors will be constructed in differenct sizes having elastomer rings of different dimensions, durometer, and elastomer type in order to measure forces and torques over a wide range as well as to better define the applicability and limitations of this technology. We anticipate communications with NASA personnel to better focus sensor development in order to meet mission needs.

A major thrust in Phase II will be devoted to the integration of the force/torque sensor with a dedicated microprocessor. The microprocessor will control sensor ultrasonic transducer operation, accept the transducer echo time data, compute the value of the six force/torque components, format the data for graphic display, and set control lines so that the robot can take appropriate action. This dedicated microprocessor approach:

1. Frees the robot controller from coping with the "raw" transit time data;

2. Results in a "stand-alone: force/torque sensor system, under hierarchical control of the robotic controller, capable of interfacing with existing robotic controllers;

3. Allows the same hardware to be used with a variety of force/torque sensors; and

4. Offers flexibility in data processing and control signal generation.

The overall goal of the Phase II research is the design, fabrication, and evaluation of a prototype force/torque sensor system. The design and construction of this system will be based upon the results of this Phase II project. In order to meet this goal it will be necessary to fulfill the following objectives:

Objective 1 - To further force/torque sensor component research and development

Objective 2 - To design, construct, and test associated sensor electronics

Objective 3 - To further elastomer research and selection

Objective 4 - To construct laboratory prototype force/torque sensors

Objective 5 - To integrate the force/torque sensor with a microprocessor

Objective 6 - To evaluate the force/torque sensor system

CONSULTANTS AND COLLABORATIVE ARRANGEMENTS

The research which will be necessary to complete the objectives of Phase Two will cover several technical disciplines and industrial applications. Therefore, we have recruited a number of individuals with specific areas of expertise to form a well-rounded research team. We believe that this approach will both accelerate and improve the quality of the research and will assure development of application-oriented technology. The individuals and organizations which will consult with us are listed below:

Kent F. Smith, Ph.D., Associate Professor of Computer Science, Research Assoc, Prof., Electrical Engineering, University of Utah, Salt Lake Cify, Utah. Dr. Smith is responsible for the computer-aided design and production of the photolithographic masks for the ultrasonic array fabrication. His extensive experience in microcircuit design and manufacture and access to his university facilities will aid our development of array fabrication techniques and design of the supporting electronic circuitry.

Kenneth L. DeVries, Ph.D., Professor, Mechanical and Industrial Engineering, University of Utah, Salt Lake City, Utah. Dr. DeVries is an expert in elastomeric materials science. He will advise us on the choice of elastomer materials and will provide laboratory facilities for the fabrication (rubber mill, etc.) and evaluation (Instron Materials Testing Apparatus) of these materials.

Curt Woods, Monsanto, Rubber Chemicals Division, Akron, Ohio. Mr. Woods has expressed a willingness to help us in the selection of elastomeric materials. He will provide samples of materials available from his laboratory.

James Dillhoeffer, Vice President, Engineered Rubber Products, Akron, Ohio. Mr. Dillhoeffer will also provide natural and synthetic rubber samples for evaluation. His experience in design and fabrication of specialty rubber products will be valuable in selecting formulations which perform well mechanically and which possess desirable resistance to environmental conditions.

Victor Scheinman, Vice President, Advance Systems, Automatix, Billerica, Mass. Mr. Scheinmen is our principal contact at Automatix.

They have expressed a strong desire to work with us in coupling the sensor to their robot controler and algorithms for sensory feedback robotic control.

Rick Casler, Manager, New Product Development, Unimation, Danbury, Conn. Mr. Casler will act as an advisor on applications and functions needed for integrated sensor machine functions. He has also indicated that they would assist in evaluation of the prototype sensor system, and will place a Puma 560 robot with us for sensor evaluation.

Gary Rutledge, Manager, Machine Preception Department, GMF Robotics, Troy, MI. Mr. Rutledge has indicated a strong interest in force-torque sensing to be utilized in conjunction with their current vision aided control systesm. He has indicated that General Motors will work with us in developing interfaces and robot-sensor control loops.

Dr. Smith and Dr. DeVries will act as paid consultants for Bonneville Scientific. Curriculum vitae are included in Key Personnel. Mr. Woods and Mr. Dillhoeffer will offer services through their respective firms and may charge directly for specific elastomer fabrications. The robot firms will donate their services.

METHODS AND RESULTS

Objective 1 - To Further Force-Torque Sensor Component Research and Development

As stated in the Phase II proposal, a major goal of this objective was to design and develop a force-torque sensor having 1) a minimum number of electrical leads exiting the sensor package, 2) all ultrasonic transducers on one piece of PVDF mounted on a planar surface, and 3) the ultrasonic transducer electrode pattern on the sensor substrate rather than on the PVDF. A scale drawing of the proposed sensor configuration is shown in Figure 28. Figure 29 shows the originally proposed metallization pattern on the top surface of the sensor substrate. The central structure in Figure 28 is a four-facet reflector post that converts the vertical ultrasonic beam from the four centrally located transducers to horizontal beams, thereby allowing all eight transducers to be mounted on the sensor substrate surface. This pyramidal reflector post is shown in Figure 30.

The rationale for consideration one (minimizing the number of leads) is the need for a cable whose size, stiffness, routing, etc. does not impede robot/end-effector performance rather than absolutely minimizing the number of leads brought out of the sensor package. Obviously, whether or not a particular cable is appropriate would depend upon both robot/end-effector morphology and the task to be performed. The trade-off we have is whether to bring out of the sensor four leads (plus a shielding ground lead), carrying low-level signals, that can only be several

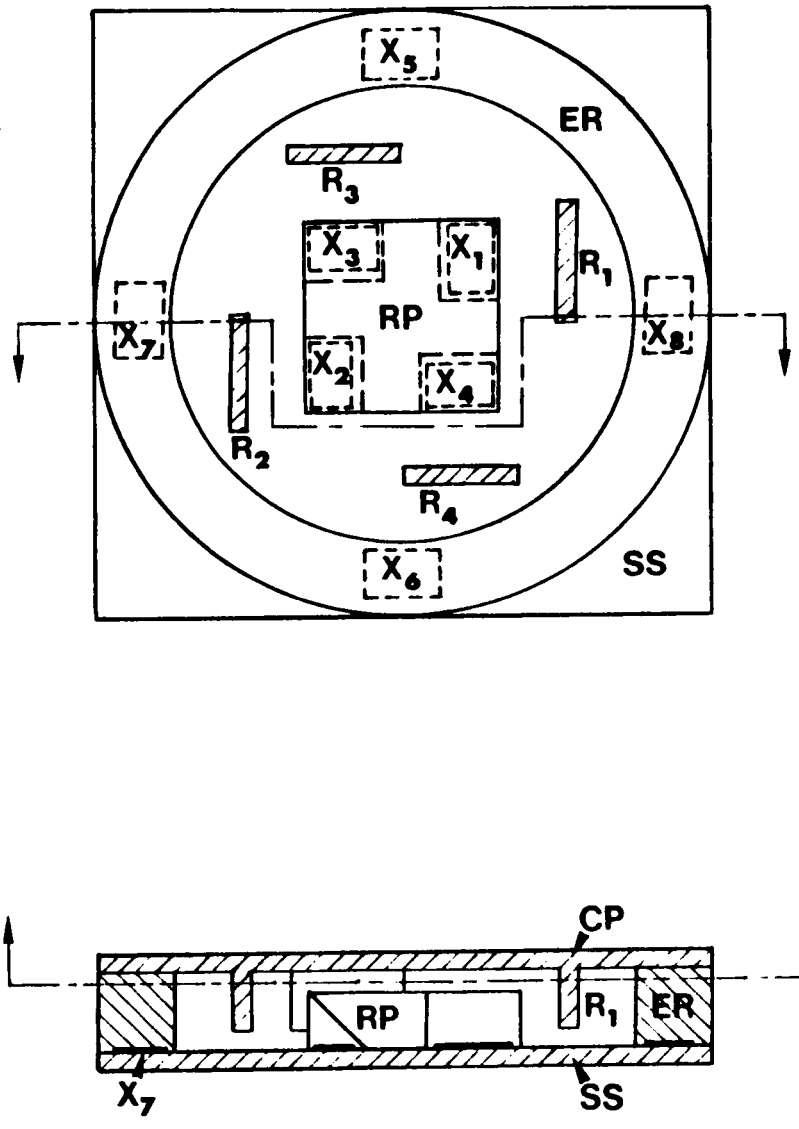

Figure 28. Proposed Phase II prototype force/torque sensor. X_1 - X_8 = ultrasonic transducers; RP = reflector post; R_1 - R_4 = reflectors attached to cover plate; ER = elastomeric ring; SS = sensor substrate; CP = coverplate

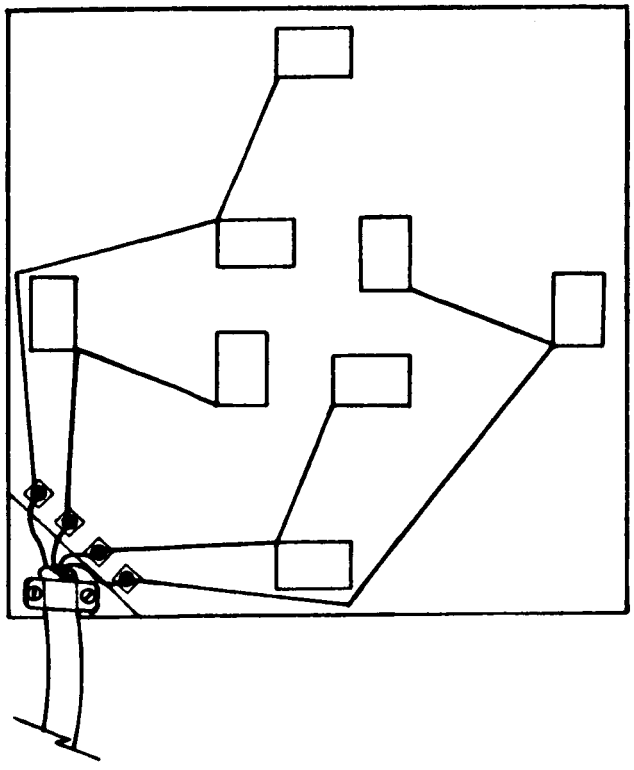

Figure 29. Proposed Phase II substrate metalization pattern.

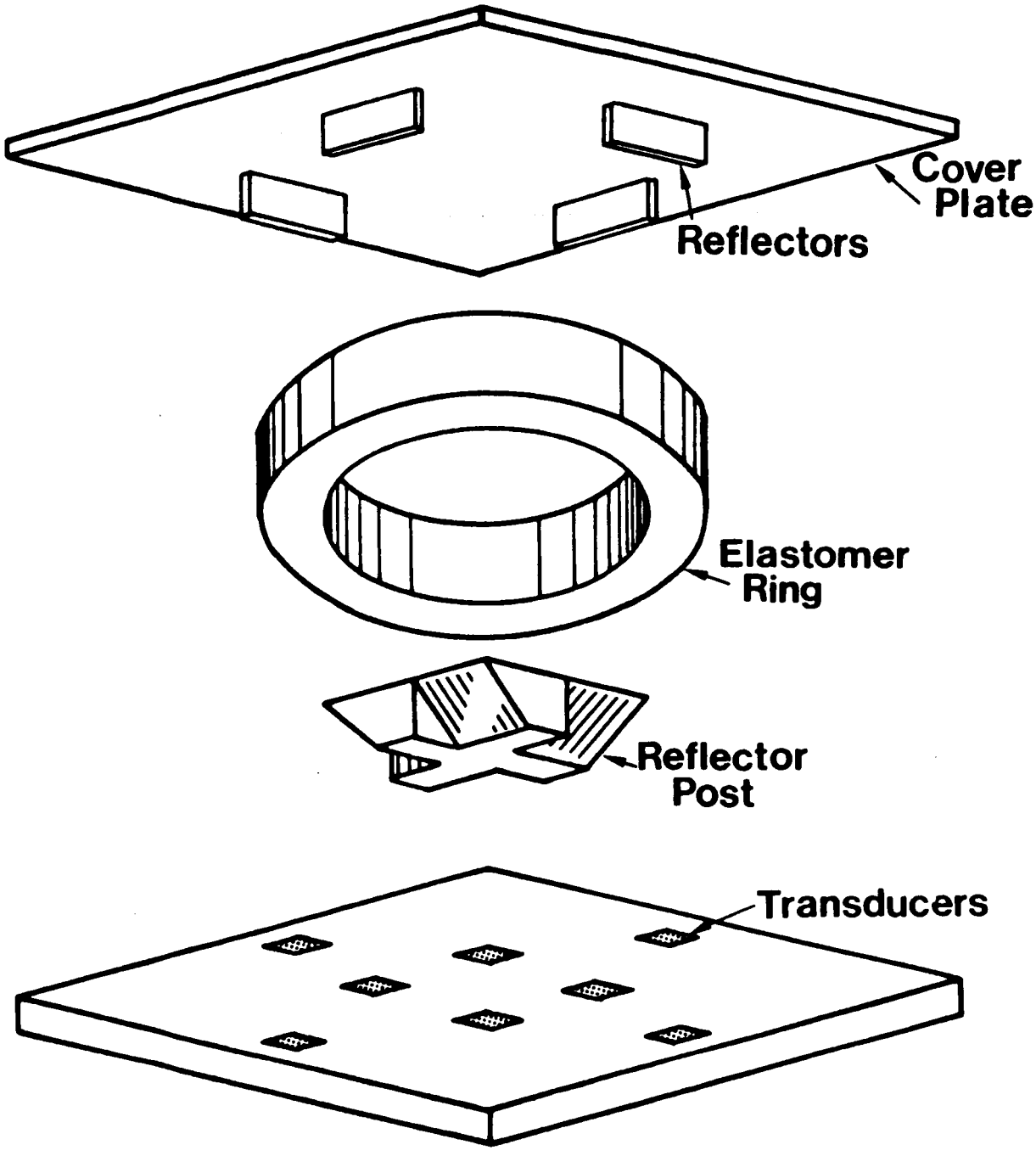

FORCE-TORQUE SENSOR

FIGURE 30

inches long before terminating in an electronics module that provides signal amplification and switching; or to have on-sensor electronics which would require more leads in the cable but the cable could be long enough to terminate at or near the robot controller. We have both options available to us.

Referring to Figure 28, the ultrasonic pathlength for transducers X_1 through X_4 has been made sufficiently greater than the pathlength for transducers X_5 through X_8 so that echoes for each set of transducers will not have overlapping time ranges under all allowed force/torque loadings of the sensor. Consequently, each central transducer can be connected electrically to each peripheral transducer to reduce the required number of electrical leads to four while being able to distinguish which echo belongs to which transducer by the time window in which it appears. Figure 31 shows the four pairs of echoes obtained in this way. Echoes from transducers one through four are to the right of the larger, centrally-located echoes (from transducers five through eight). The echoes occurring later in time are smaller because the coverplate is not properly aligned. The sensor wiring pattern actually used for this configuration is shown in Figure 32. A disadvantage of this method is that the electrical charge produced by the ultrasonic echo is divided between the two transducers so that the resultant signal voltage is approximately one-half as large as it would be for separate transducers. Experiments were conducted that showed that echoes can still be reliably detected with this configuration.

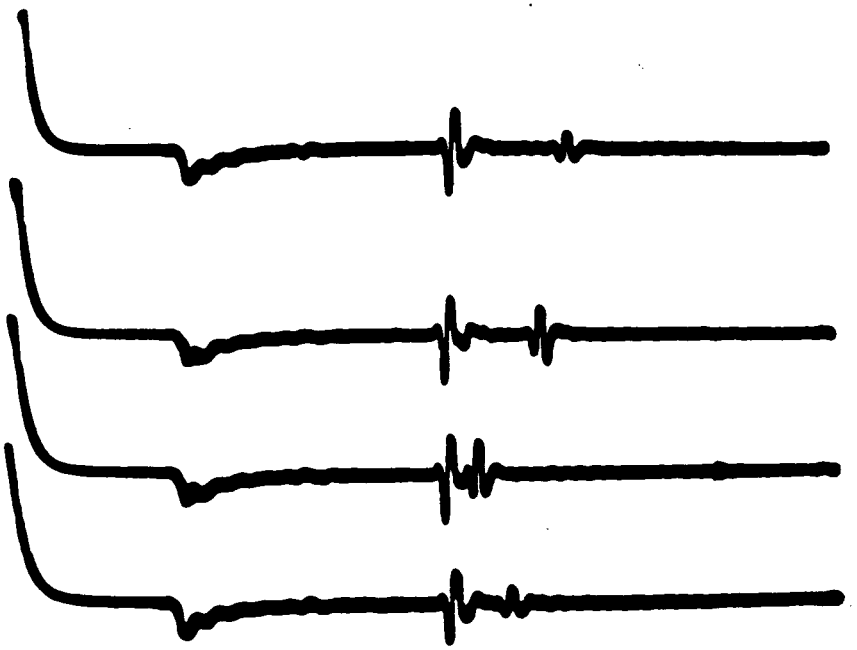

FIGURE 31. Oscilloscope Traces of Each of the Four Pairs of Transducers.

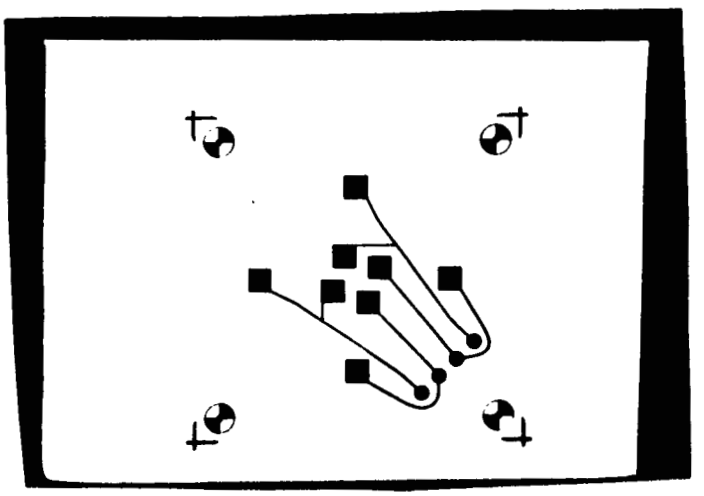

FIGURE 32. Photomask of Four-Lead Electrode Arrangement.

By having all transducers on one planar surface of the sensor only one piece of PVDF needs to be bonded to the sensor substrate thereby greatly simplifying sensor construction. This makes possible putting the transducer electrode and lead pattern on the sensor substrate rather than directly on the PVDF. The advantages of this are 1) the ceramic substrate is potentially easier to pattern than the PVDF, 2) lead attachment (except for ground connection) to the thin metal coating on the PVDF is eliminated, and 3) alignment of the PVDF relative to the substrate is not critical.

Although putting the transducer electrode and wiring pattern on the sensor substrate is advantageous, it does place additional demands upon the PVDF-to-substrate bond. This bond must be achieved with an adhesive layer no more than about 1 μm thick. Appreciably thicker layers will significantly reduce the voltage appearing across the PVDF film both when it is pulsed and when it receives an echo due to the capacitance voltage divider effect of the glue layer. The bond layer must also be of relatively uniform thickness across the substrate so that the individual transducer sensitivity does not vary grossly.

During the Phase II effort we made excellent progress in both photolithography of, and lead attachment to, the PVDF metallization. This progress is best illustrated by our achievements in tactile sensor fabrication. We are now able to pattern both sides of the PVDF metallization to produce 1024-element tactile sensors having 1/4 mm^2 elements with 6 mil wide

interconnects. The active area of the sensor occupies 0.8 $in.^2$. This sensor, for experimental reasons, had 128 copper-foil leads attached to the sensor rows and columns with conductive epoxy. Having this capability, we have not pursued putting the electrode pattern on the substrate and producing extremely thin, uniform glue layers.

In the past we have almost exclusively used 28 μm thick PVDF film since it is not so thick as to be difficult to cut accurately or so thin as to be difficult to handle. However, as the transducer elements become smaller their capacitance (about 10 pF for a 4 mm^2 transducer) becomes comparable to the input capacitance of the receiving amplifier or multiplexer. Therefore, the echo signal amplitude can be significantly reduced by the capacitance voltage divider effect. By using 9 or 6 μm thick film the transducer capacitance is increased by about three to five times to offset this anticipated loss. To determine the magnitude of this loss single-element transducers were constructed from 9, 28, 52, and 110 μm thick PVDF. These transducers all had an active area of 56 mm^2. Sensitivity measurements were somewhat inconsistent (probably due to our rather primitive fabrication technique at the time). Ultrasonic echo strengths were about 1, 5, 4, and 6 volts for the 9, 28, 52, and 110 μm thick films, respectively. Consequently, the effects of transducer signal loading by the associated electronics was not a significant problem so that there was no compelling reason

to change film thickness from the most-convenient-to-use 28 μm size.

We have found in previous work that thin plates of beryllium oxide ceramic work extremely well as a highly reflective acoustic backing for PVDF. We expected cheaper alumina plates to be about as good because of the high acoustic impedance of these materials. Experiments were conducted to compare the acoustic performance of each ceramic. 28 m-thick PVDF was bonded to 1.0 mm-thick alumina and beryllia plates. The active area of each sensor was 56 mm^2. Leads were attached and a 1/4"-thick layer of silicone rubber was bonded to each transducer. When excited, the echo signals were approximately of equal amplitude (within 3%). Although these transducers were crudely constructed relative to current standards, so that it is impossible to say which material performs better the implication of the result is clear. Since the same size alumina substrate is about one-twenty-fifth the cost of a beryllia unit, alumina is preferable in most applications.

Since there is a wealth of information available on producing metallic patterns on the surface of either of these ceramics (either by vacuum deposition or chemical etching) for hybrid circuitry, we anticipated no insurmountable problems in producing the transducer and lead patterns on these materials. As previously explained, we did not pursue putting the lead patterns on the ceramic but we did try placing the force-torque sensor multiplexer electronics on the metallized alumina sensor

substrate. A local vendor produced a thin electroless metallic plating on the substrate surfaces and in holes through the substrate to provide interconnections from the sensor elements to the multiplexer switches. Bonneville Scientific electrolytically built up this initial plating and patterned it for the sensor elements and the multiplexing components. Surface-mount components were soldered to the metallization on one side of the substrate and the force-torque sensor components mounted on the opposite side. This sensor configuration worked thus proving the feasibility of this approach. However, this concept was not pursued further because it was more time-consuming than using conventional circuit board materials for the electronics and the electroless plating had poor adhesion to the ceramic. This latter problem was likely due to insufficient cleaning of the ceramic by the vendor before plating.

Original plans were to use the University of Utah's Computer Science Department's CAD/CAE computer system to produce emulsion-on-glass photomasks for the force-torque sensor electrode and lead wire pattern. However, we developed an in-house technique for photomask fabrication using 35 mm slide photographs of large-scale taped patterns. These photomasks have worked well, are disposable, and easily replicated at low cost. Moreover, this technique allows us to easily and quickly produce new masks to try modifications.

In order to photolithographically process the PVDF metallization it must be covered with a thin, uniform coating of

photoresist. For this we have been using a semiconductor wafer spinner. However, in order to support and hold the PVDF film a number of custom vacuum chucks and fixtures were made to allow both sides of the PVDF to be coated sequentially. The method we ended up with uses a rigid (plastic) backing plate to support the film and, for rectangular pieces of PVDF, four small pieces of double-sided tape to secure each corner of the PVDF to the support plate.

Design and fabrication of the sensor's reflecting post (Figure 30) is straight-forward. A special fixture was used that allowed bar stock to be precisely rotated at 90° increments with the stock horizontal, vertical, or at 45°. Once the fixture is aligned and positioned on the milling machine table, only two table-feed positions are required for machining the 45° reflecting facets. After the facets are machined, the post is cut to length on a lathe using a parting tool. Fabrication time is about ten minutes. Both brass and aluminum posts were made.

Fabrication of the sensor coverplate is more time-consuming, but then, little effort was spent to optimize the procedure. One-thirty-second-inch thick brass plate was mounted on an arbor and then turned down to a circle of the desired diameter on a lathe. The arbor, with brass plate attached, was then placed in the same indexing fixture used in post fabrication and four narrow slots were machined into the plate 90° apart. Brass shim-stock is inserted into each slot and soldered in place. Shim-stock protruding from the top of the coverplate is machined flush

while the stock below the cover plate is milled to the desired depth and width, thus forming the four vertical reflectors. In order to protect the force-torque sensor from overload damage the coverplate would differ slightly. Tabs would protrude along the top of the coverplate that would fit into corresponding recesses in the end-effector structure to prevent distortion of the elastomer ring beyond safe limits.

We have been able to find excellent adhesives for both bonding the coverplate to the elastomer ring as well as the ring to the PVDF metallization. Suitable adhesives have been found for specific formulations of silicone, urethane, and natural rubbers. Silicone rubbers are the most difficult to bond to and are the weakest (more readily cut or torn).

We have not tried to increase the coefficient of friction of the top (i.e. loading) surface of the coverplate with polymer coatings. We would anticipate using thin (e.g. 5 mil) high-durometer urethane since this material bonds well to the coverplate and is quite abrasion resistant.

The central cavity (surrounding the reflector post and bounded by the inner wall of the elastomer ring) of the force-torque sensor needs to be filled with a material capable of efficiently conducting the ultrasound. This material also must not impede motion of the cover-plate-mounted reflectors or the elastomer ring. In Phase I we made preliminary experiments with silicone gel and found that this material worked quite well. This was also used in Phase II. Acoustic attenuation in the gel

was less than that in the silicone rubber ring even though the path length was greater.

Research results concerning the elastomer ring are given under Objective 3.

Objective 2 - To Design, Construct, and Test Associated Sensor Electronics

The force-torque sensor electronics consists of three subsystems. A system block diagram is shown in Figure 33. One subsystem consists of the transducer multiplexer, echo signal amplifier, and transducer excitation circuitry. The excitation circuitry could be mounted remotely, however, the other two components need to be mounted close to the sensor in order to minimize signal loss and electrical interference. The option of mounting these electronics on the sensor (either on the back of the sensor substrate or on the top surface of an extended substrate) or near the sensor depends upon the configuration of the end-effector. It is interesting to note that on-sensor electronics would probably require more electrical leads exiting the sensor package than our four-lead sensor design previously explained. However, the advantage of on-sensor electronics would be greater signal levels and, perhaps, a smaller diameter cable.

The second subsystem consists of the echo signal zero-crossing detector, the time-of-flight (TOF) detector (that measures the echo time interval and converts it into a binary word compatible with the microcomputer), and the controller.

The third subsystem is the microcomputer. This subsystem is discussed under Objective 5.

Figure 34 shows a simplified schematic for the first subsystem. A T-bar multiplexer integrated circuit (available with up to 16 channels) connects the desired transducer to the

FIGURE 33

ULTRASONIC FORCE-TORQUE OR TACTILE SENSOR

BLOCK DIAGRAM

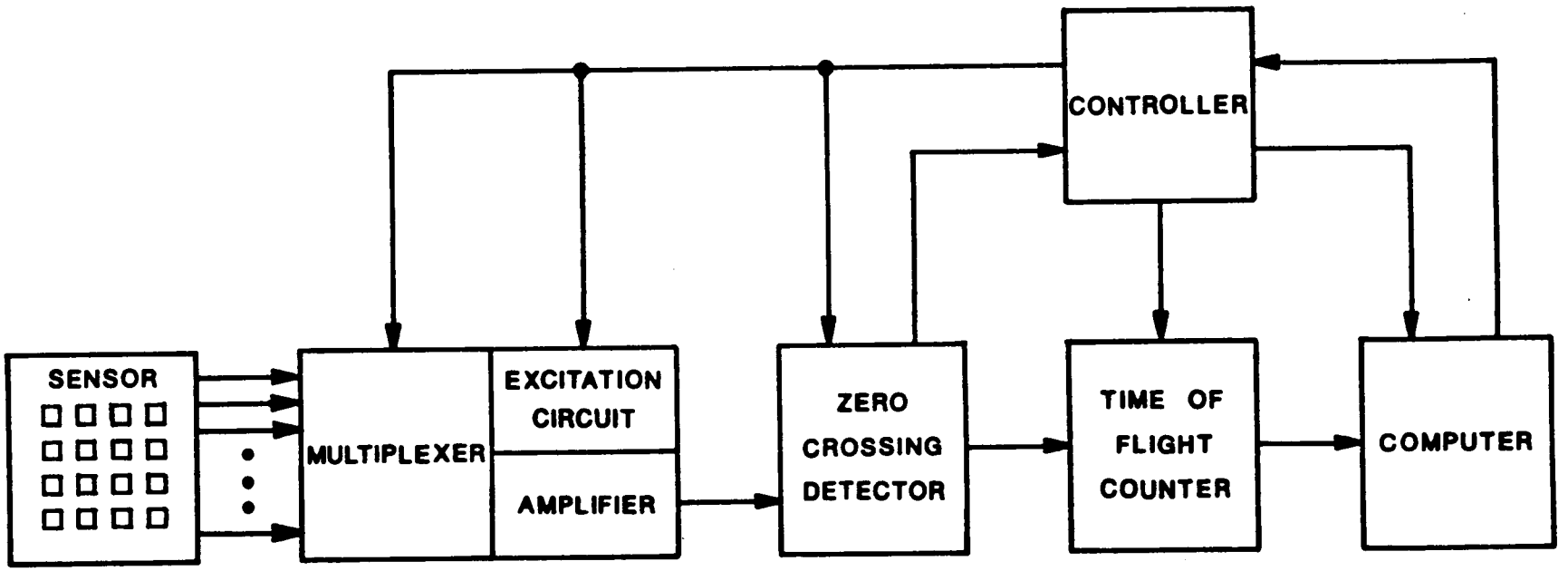

FIGURE 34

FORCE TORQUE OR TACTILE SENSOR

MULTIPLEXER, EXCITATION AND AMPLIFIER CIRCUIT

(SIMPLIFIED SCHEMATIC)

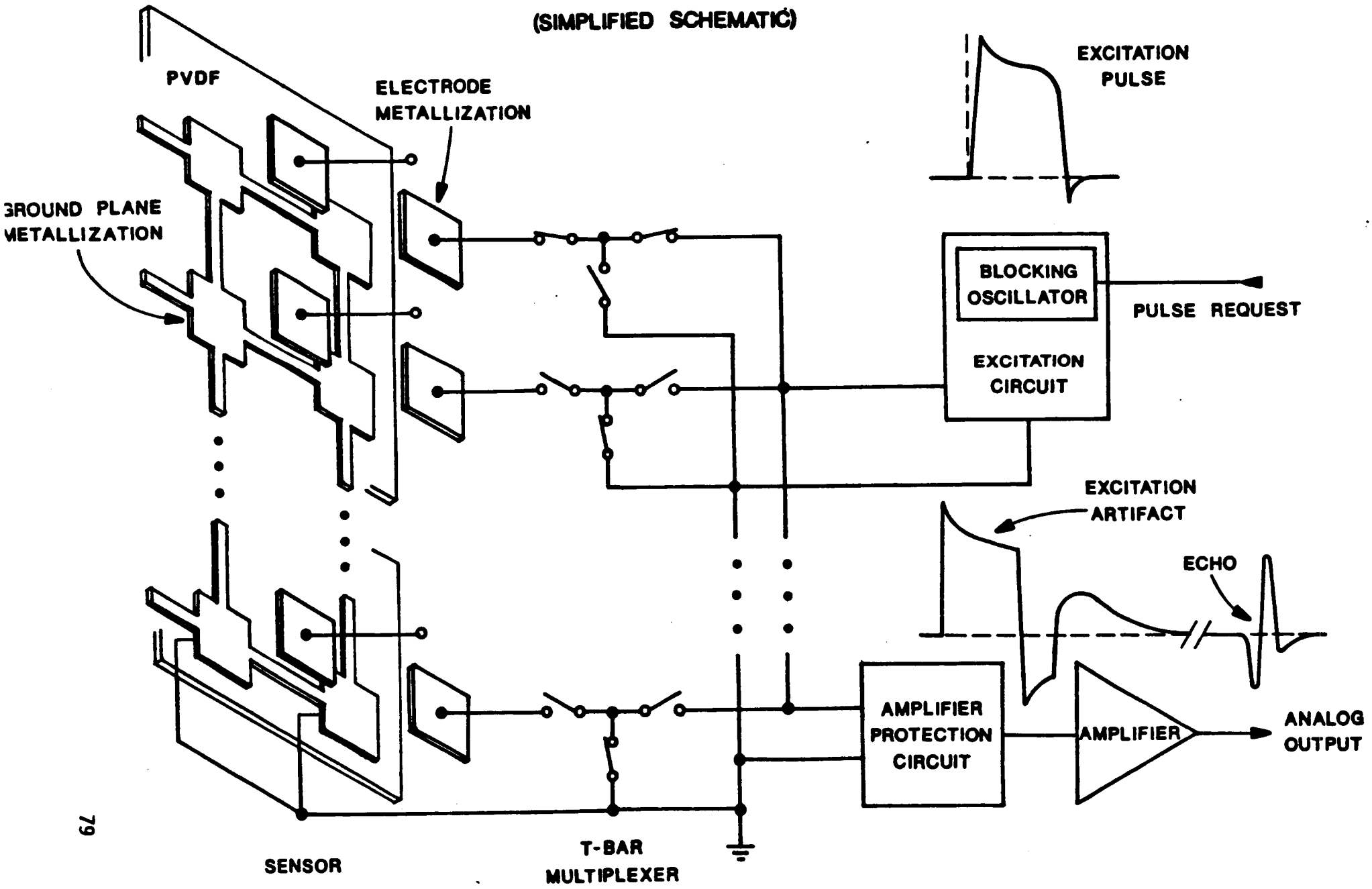

excitation and amplifying circuitry. This multiplexer has a built-in latch for storing the sensor element address. The excitation circuitry consists of a three-transistor blocking oscillator with a custom-made surface-mount transformer. This oscillator supplies a 10-15 volt pulse of approximately 100 ns width, independent of moderate changes in trigger pulse parameters. In order to prevent overload and the ensuing prolonged recovery of the echo pulse amplifier due to the excitation pulse, a simple diode protection circuit is used at the input to the amplifier. This consists of two anti-parallel shunting diodes across the amplifier input with a series resistance to reduce loading on the blocking oscillator. The echo amplifier circuitry consists of two cascaded video amplifiers providing an overall gain and bandwidth of about 900 and 50 MHz respectively, with an input impedance of 10k ohms in parallel with 47 pF. Figure 35 shows the amplified echo pulse. The top trace shows the excitation pulse artifact at the far left with the echo pulse toward the right. The bottom trace is the echo pulse expanded in time (10:1) showing the zero-crossing region.

Figure 36 shows a simplified schematic for the second electronics subsystem. The first component of this subsystem is the zero-crossing detector. Arrival time of the echo pulse is defined to be the time interval from the leading edge of the excitation pulse to the first zero-crossing of the approximately single sinewave-cycle echo pulse. Because of the electrical noise, baseline irregularities due to the excitation pulse, and

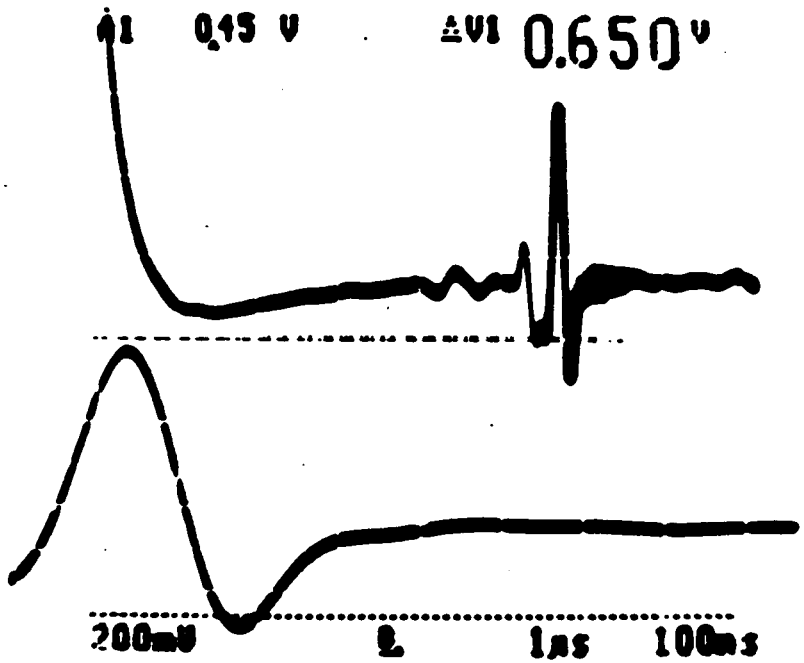

FIGURE 35. Top-Excitation Artifact and Ultrasonic Echo Bottom-Echo Pulse Expanded in Time (10:1)

FIGURE 36

FORCE TORQUE OR TACTILE SENSOR
ZERO CROSSING CIRCUIT
(SIMPLIFIED SCHEMATIC)

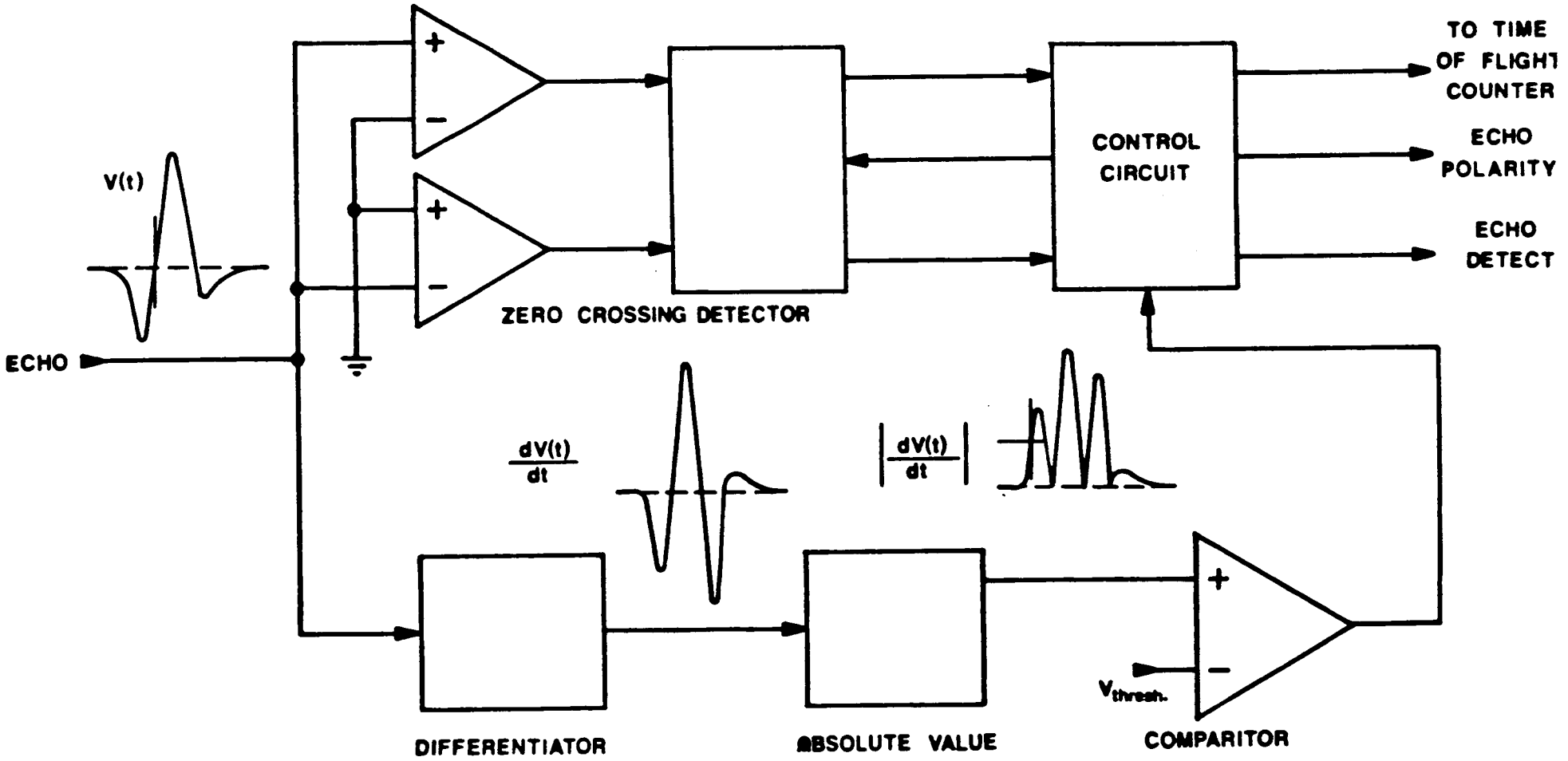

the variable amplitude of the echo pulse, timing windows, filters, and nonlinear analog signal processing functions (differentiation and absolute value) are used to enable a precision, high-frequency zero-crossing detector. With this configuration we can discriminate against detection errors. The zero-crossing detector generates digital data corresponding to zero-crossing time and polarity (used with tactile sensors where echo polarity depends upon the relative acoustic impedance of the grasped object) of the echo signal and also generates an error signal in the event of false or no detection.

Components of the first subsystem and the zero-crossing detector were tested with a force-torque sensor and we found that amplifier recovery, gain, impedance, and bandwidth were sufficient. Neither multiplexer on-resistance nor spurious capacitive loading of the array element was objectionable.

The next component of this subsystem is the time-of-flight (TOF) detector shown in Figure 37. The TOF detector measures the time interval between excitation and echo zero-crossing detection. A gated counter was used for this function that employs a 50 MHz time base that gives about 40 m resolution of elastomeric ring displacement. Concurrent with the development of this detector was a small design effort to implement a custom CMOS VLSI TOF detector having 10 ns or 20 m resolution. Working integrated circuits were fabricated but we have not pursued use of these circuits. First, tests need to be conducted with the

FIGURE 37

FORCE TORQUE OR TACTILE SENSOR
TIME OF FLIGHT CIRCUIT
(SIMPLIFIED SCHEMATIC)

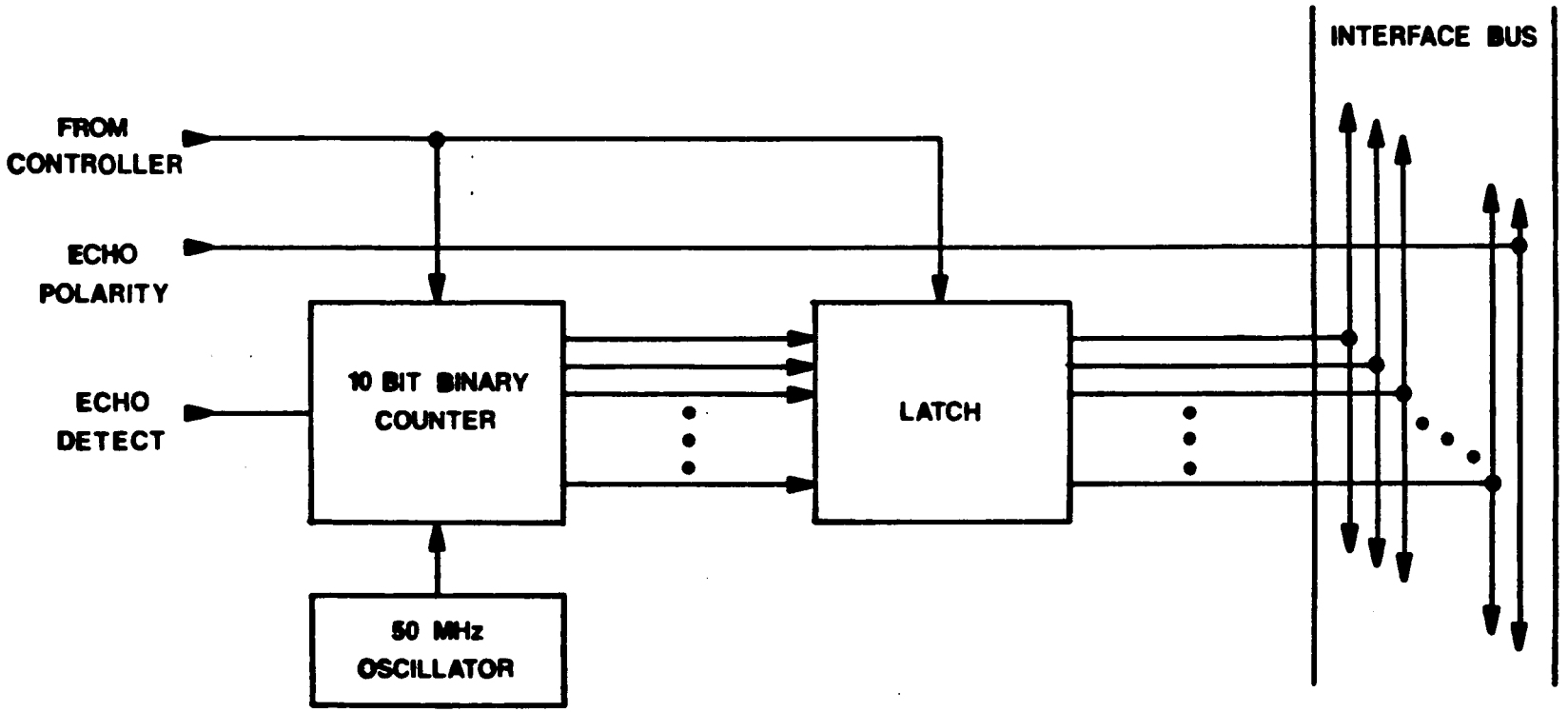

force-torque sensor to determine what time/displacement resolution is required.

The last subsystem component is the control circuitry and the interface to the 68000 microcomputer subsystem. The force-torque-sensor-to-68000 interface is a parallel interface which uses a finite-element state machine for control and a parallel interface integrated circuit (PI/T) for address and data transfer. Output signals from the microcomputer which initialize the sensor and state machine, pass through the PI/T. The state machine then controls timing, handshaking and data flow allowing the sensor to send its data through the PI/T to the microcomputer.

The heart of the interface is the finite-element state machine. Eight separate states are used for a complete cycle. These include: latching sensor element address, sending a start pulse to the sensor, latching the sensor data, and then transferring these data to the microcomputer for processing. The state machine operates at 20 MHz and interlocks the sensor and microcomputer allowing data transfer at the proper times.

Sensor element address and data are transferred via the Motorola 68230 PI/T integrated circuit. At the start of a cycle the microcomputer sends a sensor element address to the PI/T. The PI/T stores the information in one of its two 8-bit ports until the proper handshake signals are received from the state machine. The address is then sent to the sensor for element selection. As the sensor electronics processes the analog

signals, the PI/T and state machine wait for valid data to be sent from the sensor. These data are then latched into the PI/T where it waits for access to the VME buss and the 68000 microprocessor. When transferring large address words or large data words (greater than 8 bits) the two 8-bit ports can be combined into one 16-bit port.

A test mode was incorporated into the design to allow quick testing of the interface hardware and microcomputer software. This test mode, called loop back, electronically connects the interface input to its own output, disabling all connections to the sensor. Loop back was incorporated to allow quick troubleshooting of the complete system (i.e. microcomputer, interface, and sensor). When loop back is enabled, the microcomputer outputs data and immediately sees the same data on its inputs. The software then processes these data as if they had been sent from the sensor.

An emulator was constructed to copy the function of an actual sensor. With the emulator each time-of-flight (TOF) value for the eight force-torque sensor transducers can be varied independently. This allows software to be developed and the system to be checked out without connection of an actual sensor. The emulator connects directly to the interface exactly as the sensor would. Operation of the emulator is provided by a small finite-element state machine and an 8-bit, 8-channel A/D converter. The emulator state machine controls all handshaking with the interface and also controls the A/D converter. Eight

potentiometers, one for each TOF value, are connected to the A/D converter.

The interface was designed and built with ease of operation in mind. The additional circuits, loop back and the emulator were incorporated to enhance software development as well as giving a person, unfamiliar with the circuit design, the ability to check out the entire system. Once the system has been checked with the emulator and found to be operating correctly, remaining faults lie with the sensor itself or the associated sensor electronics.

Objective 3 - To Further Elastomer Research and Selection

The primary requirement of the elastomer ring in the force-torque sensor is its behavior as a linear, multidimensional spring. For this the force/deformation characteristics of the material must be precisely determined. The stiffness or durometer of the material must be chosen to give the desired force-torque sensitivity and dynamic range which also depends upon linearity of the material characteristics. Because elastomeric materials exhibit stress relaxation, there is some dependence of force on the speed of compression. Therefore, the force/deformation characteristics must be determined dynamically as well as statically. Hysteresis, which is directly related to stress relaxation, is also undesirable because decreasing forces or torques may require different calibration factors. Another undesirable characteristic of some elastomers is creep or compression set. This is evident when the material does not return to its original shape after it is severely compressed or stretched for long periods of time. We must select elastomers that will satisfy the desired operating parameters and minimize undesirable characteristics.

Natural rubber has several unique properties for our application. It has the greatest resilience of any elastomer and is the most suitable for applications requiring a combination of high resilience, strength, fatigue resistance, and low hysteresis. It is available in a wide range of hardnesses and resists fatigue by crack propagation because of strain-induced cry-

stallization at the apex of the crack. Its major disadvantages are lower resistance to solvents, oil, oxidation and extreme temperatures along with limited bonding options. New accelerated efficient vulcanization systems of different vulcanizing agents such as urethane reagents or peroxides can improve some of these deficits. Further improvement in environmental resistance with, perhaps, some sacrifice in mechanical properties can be obtained with alternative materials. These include neoprene for oil resistance; various chlorinated polymers for good chemical, oil, solvent, oxidation, or temperature range, oxidation resistance and very low compression set; or fluorosilicones with increased fluid and heat resistance. Urethanes are more rugged than natural rubbers and recently have become available in low modulus (durometer) formulations with low hysteresis.

We have evaluated the compression characteristics of several different formulations of natural and synthetic rubbers. Our selection of materials was based upon our experience and the recommendations of Dr. Kenneth L. DeVries of the University of Utah and Mr. James Dillhoeffer, Vice President, Engineered Rubber Products, Akron, Ohio.

Initial screening of the elastomers was on a Chatillion Tension-Compression Tester at Bonneville Scientific. This machine can be programmed to apply or remove forces until a preset upper or lower limit is reached; or to compress or stretch a specimen at a constant rate until preset limits are reached. Our standard screening test consisted of compressing the elas-

tomeric compound at a constant rate (usually 0.2 in/min) until 20% or 40% compression was reached. This deflection was held for 2.0 minutes so that material stress relaxation could be measured and then the material was decompressed at the same rate as compression. During this test cycle loading force and elastomer deflection were recorded by an x-y recorder. Deflection output of the tester did not have sufficient resolution (0.001 in.) for this test. Consequently, a linearly variable differential transformer (LVDT) transducer was installed for deflection measurement. This transducer improved deflection resolution by about two orders of magnitude. We had proposed using ultrasonic pulse-echo ranging to measure elastomer deflection during this test in order to achieve the required resolution. This was not implemented because the LVDT method was simpler and more direct (e.g. immune to environmental temperature changes that would affect the speed of sound in the elastomer).

Figures 38, 39, 40, 41, 42, 43, 44, 45, and 46 show typical results of this test for several types of elastomers. Figures 38 and 39 show the results for two silicone rubbers having the lowest hysteresis we have found to date. The 184 compound is more easily bonded to than the 615. Figure 40 is another silicone formulation having low hysteresis and very low durometer. In each figure the upper curve is the rubber response for increasing force; the vertical drop at maximum deflection is due to the stress relaxation (over a two-minute period); and the lower curve results from decreasing force. An ideal material

FIGURE 38

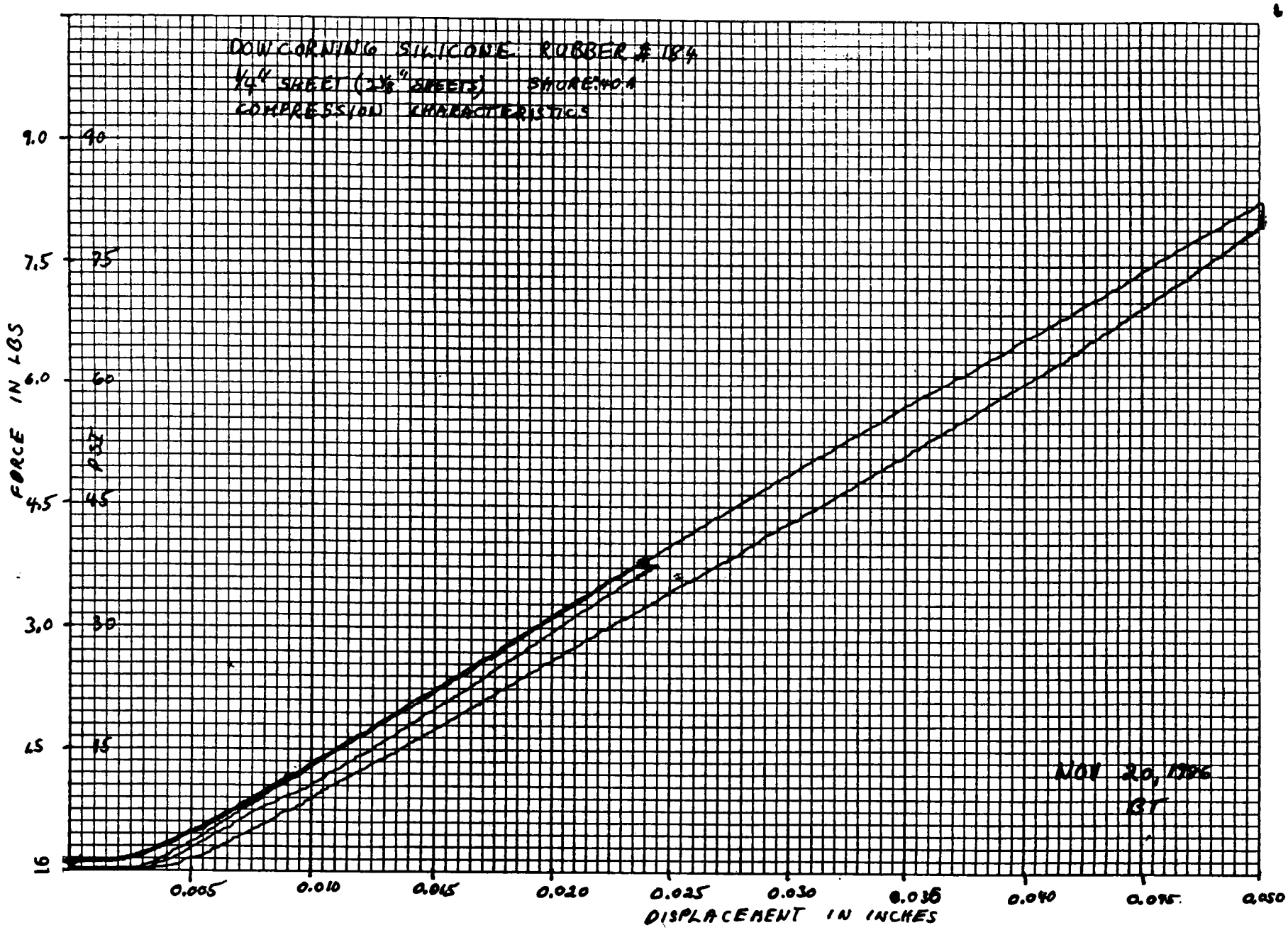

FIGURE 39

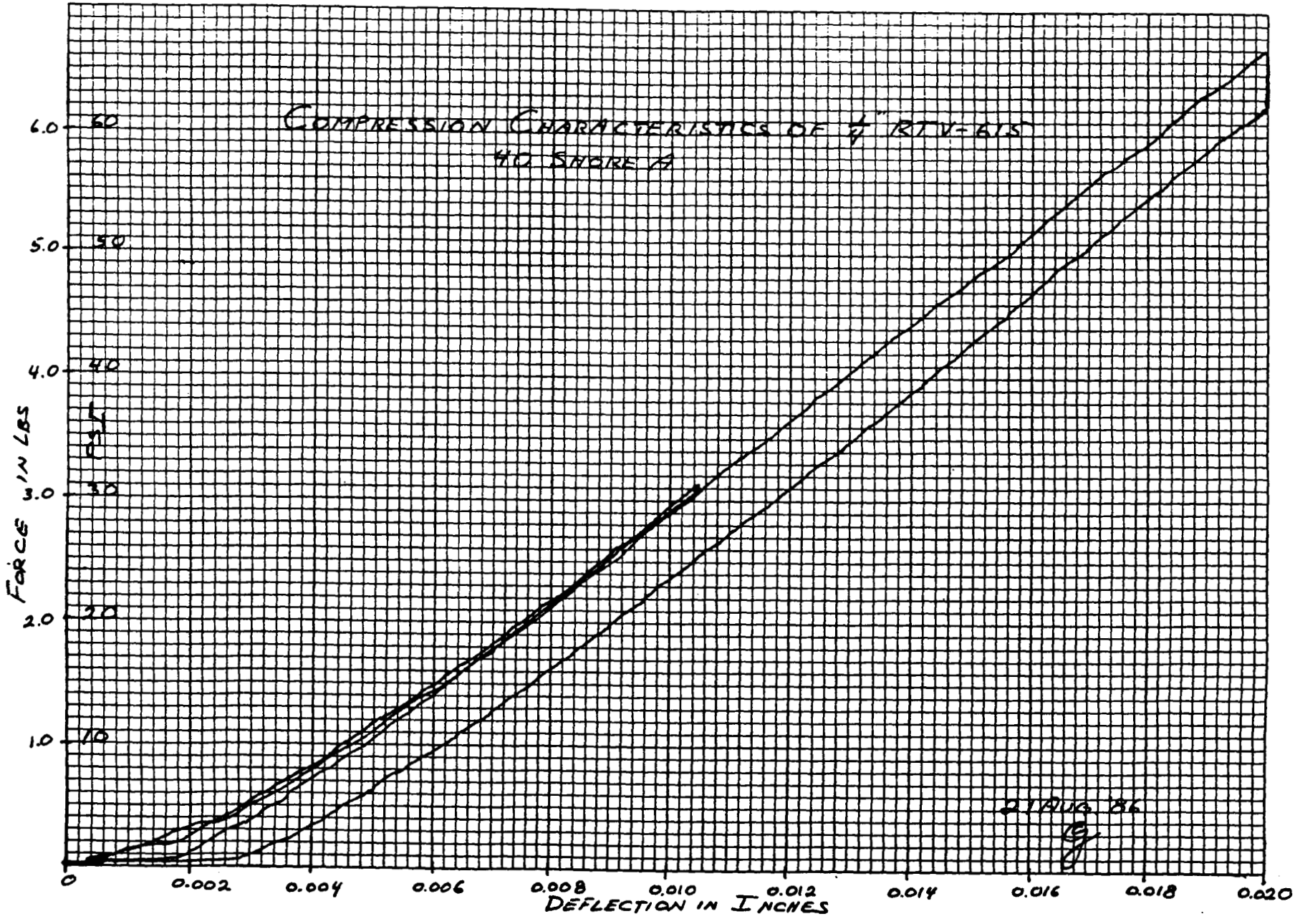

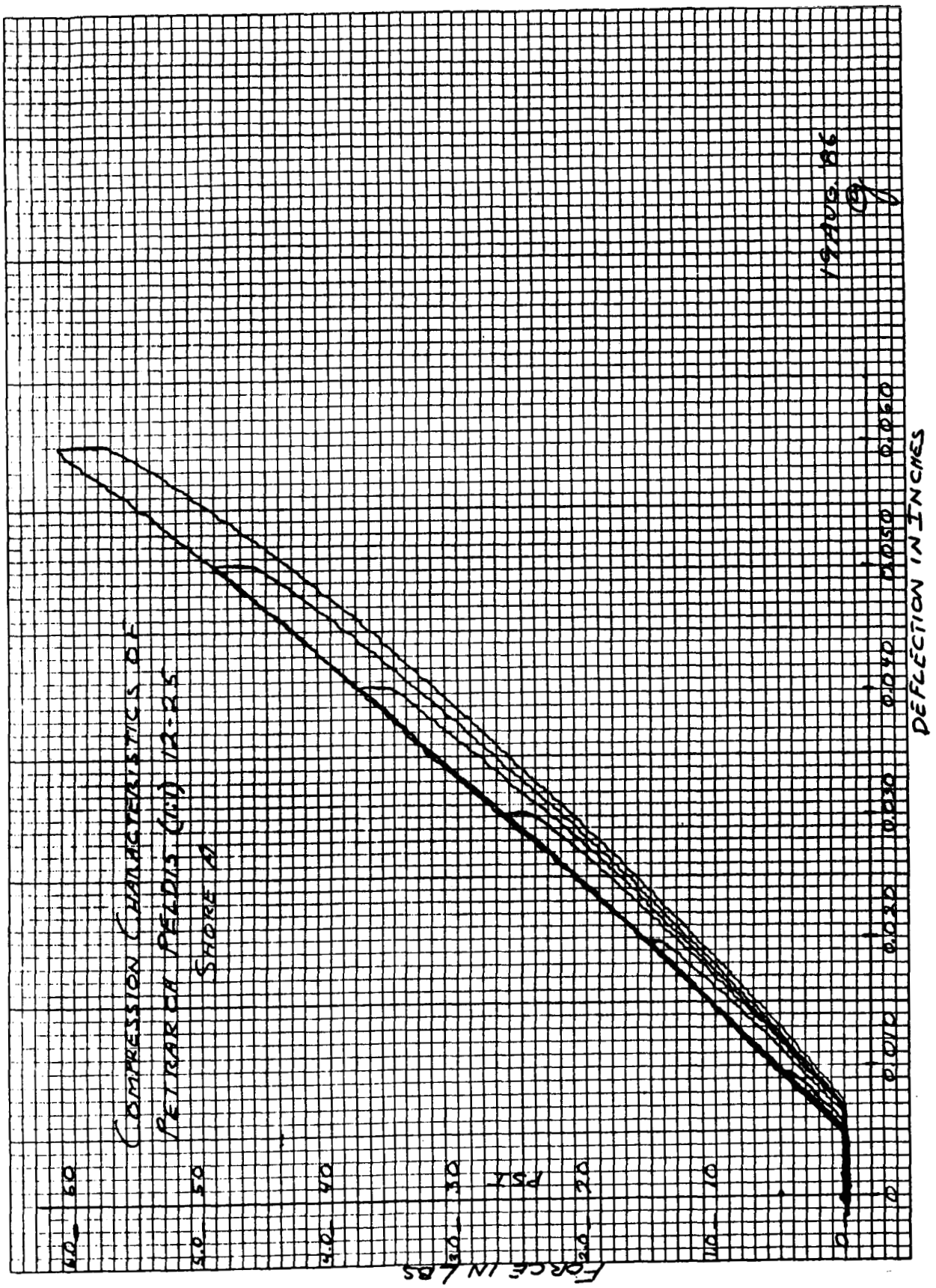

FIGURE 40

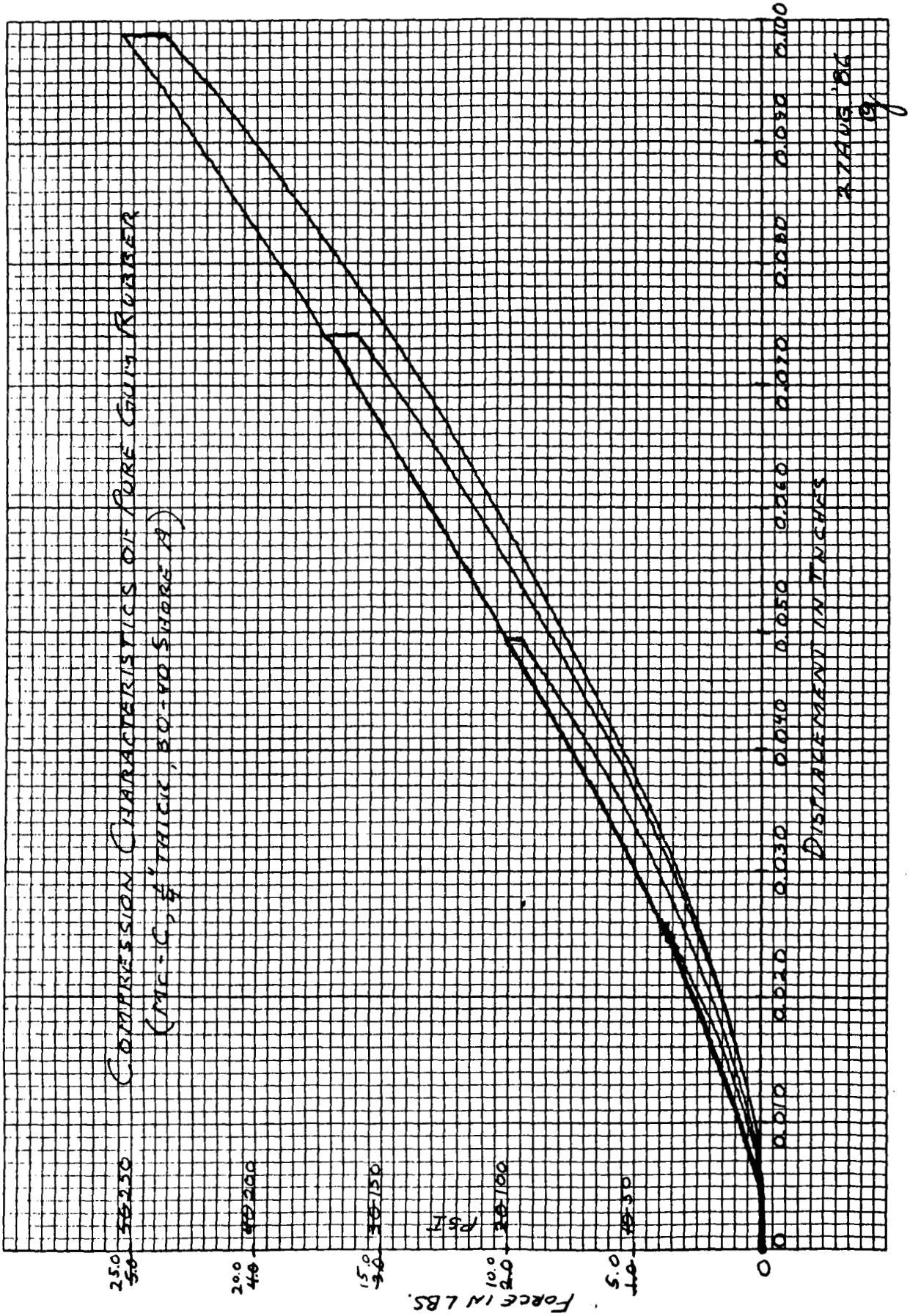

FIGURE 41

C-2

FIGURE 42

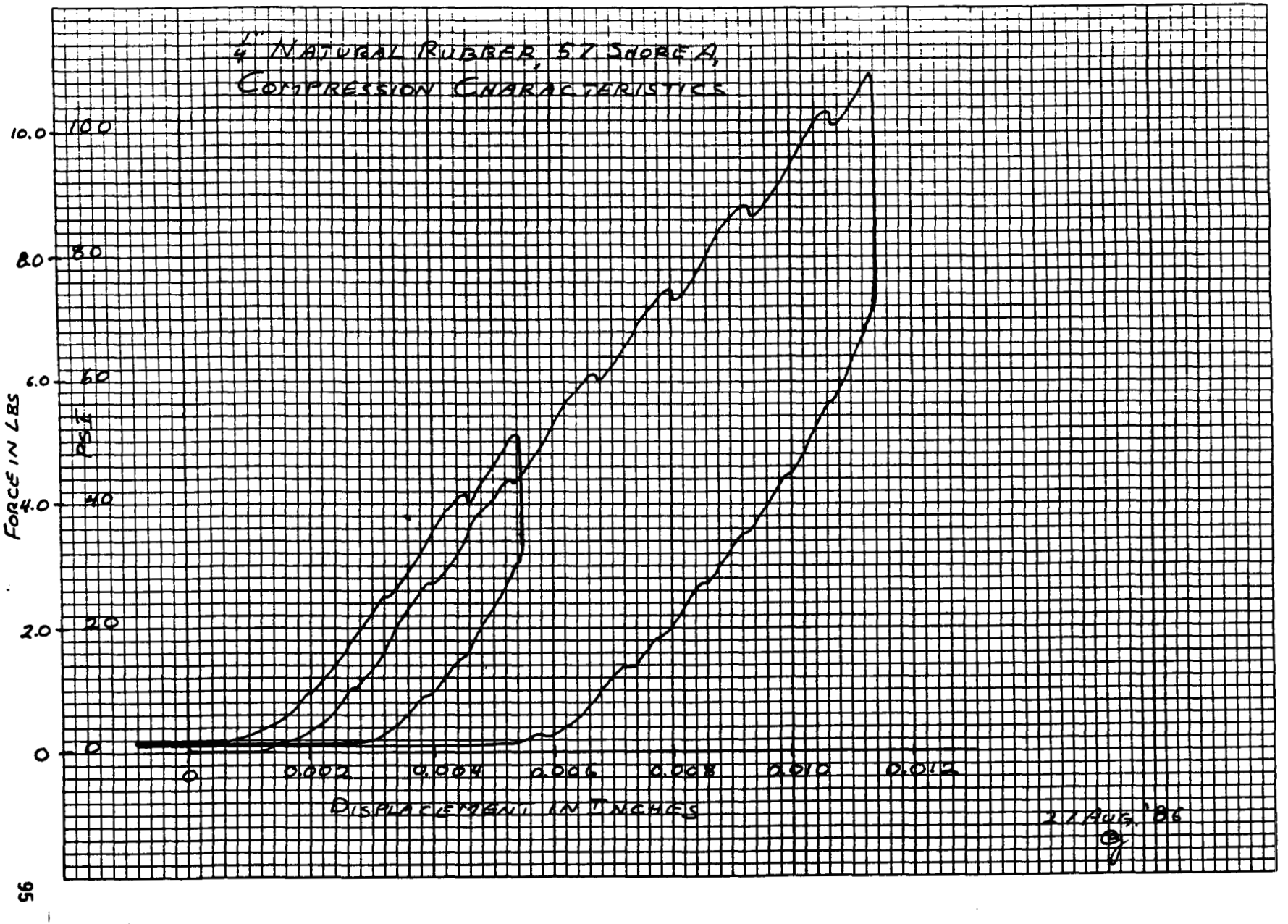

FIGURE 43

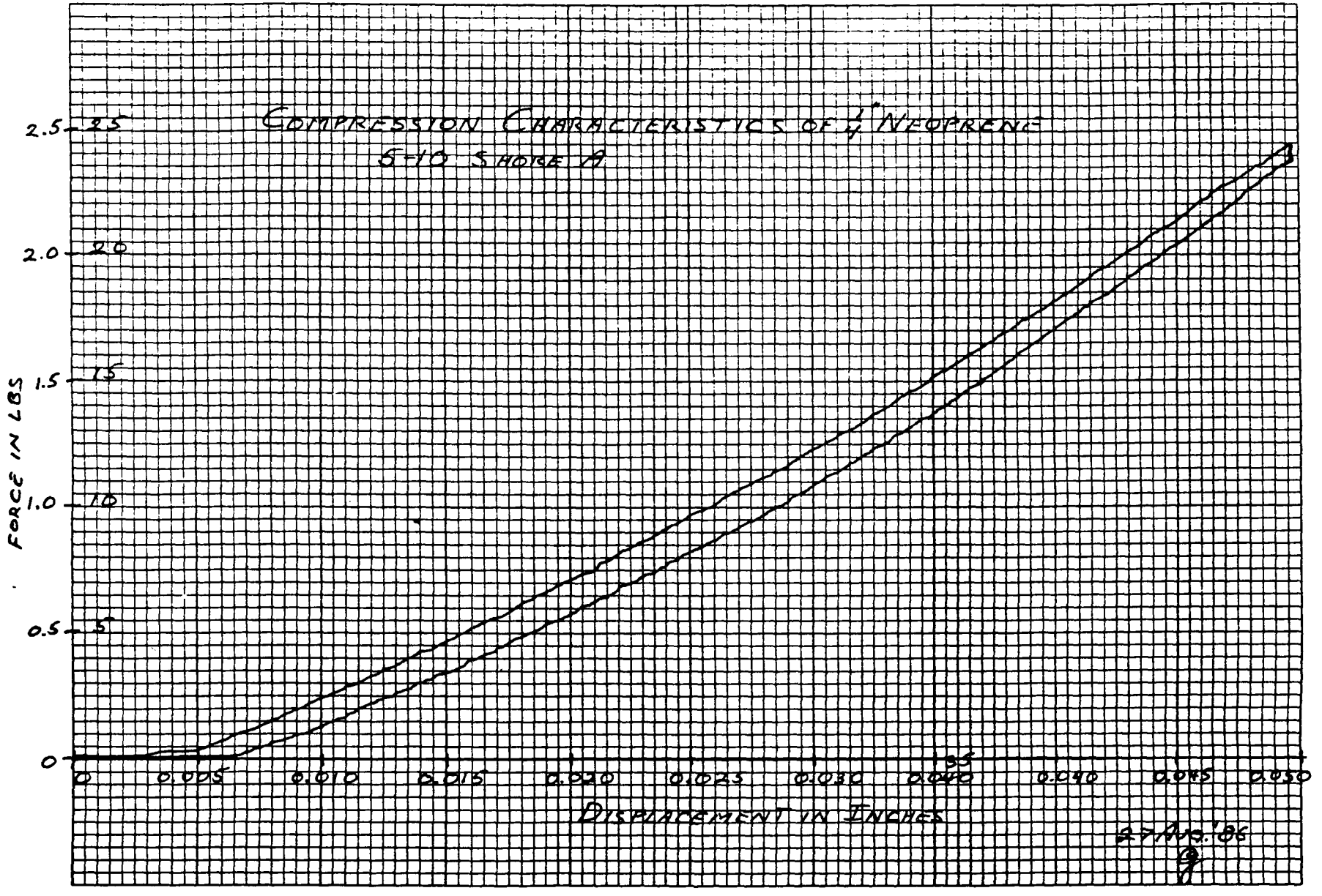
COMPRESSION CHARACTERISTICS OF ¼" NEOPRENE
5-10 SHORE A
FORCE IN LBS
2.5
2.0
1.5
1.0
0.5
0
25
20
15
10
5
0
0.005
0.010
0.015
0.020
0.025
0.030
0.035
0.040
0.045
0.050
DISPLACEMENT IN INCHES
27 Aug. '06

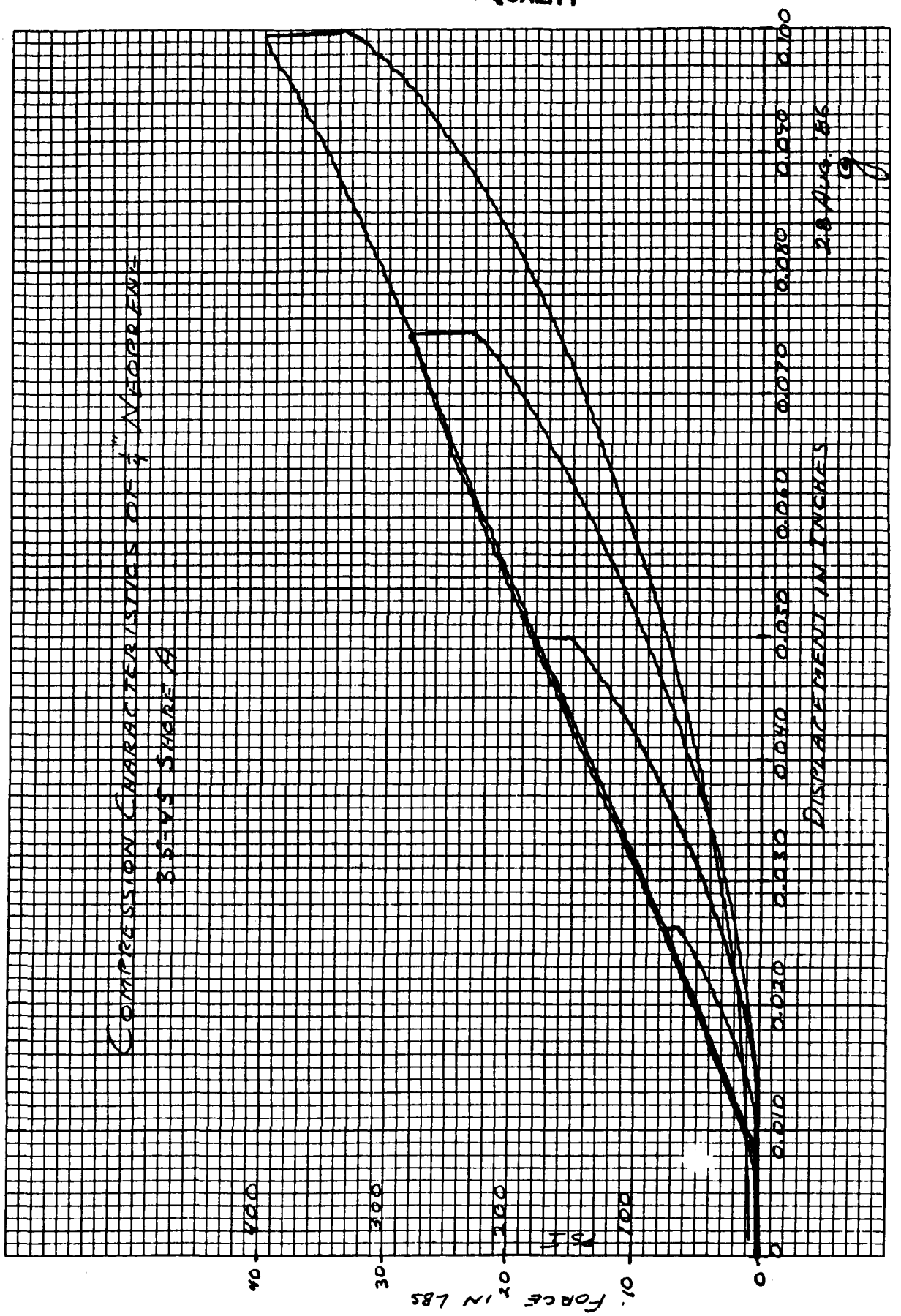

FIGURE 44

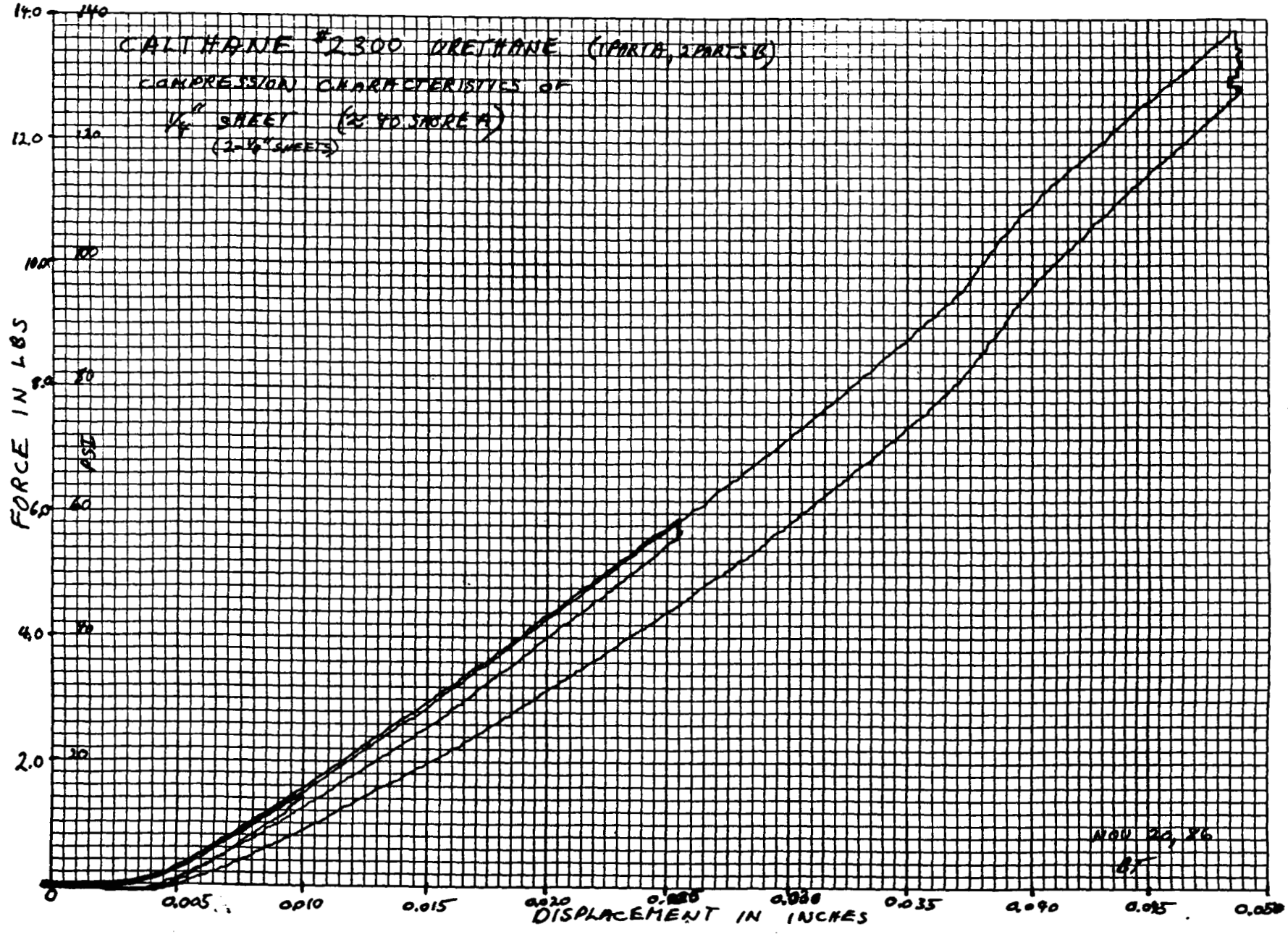

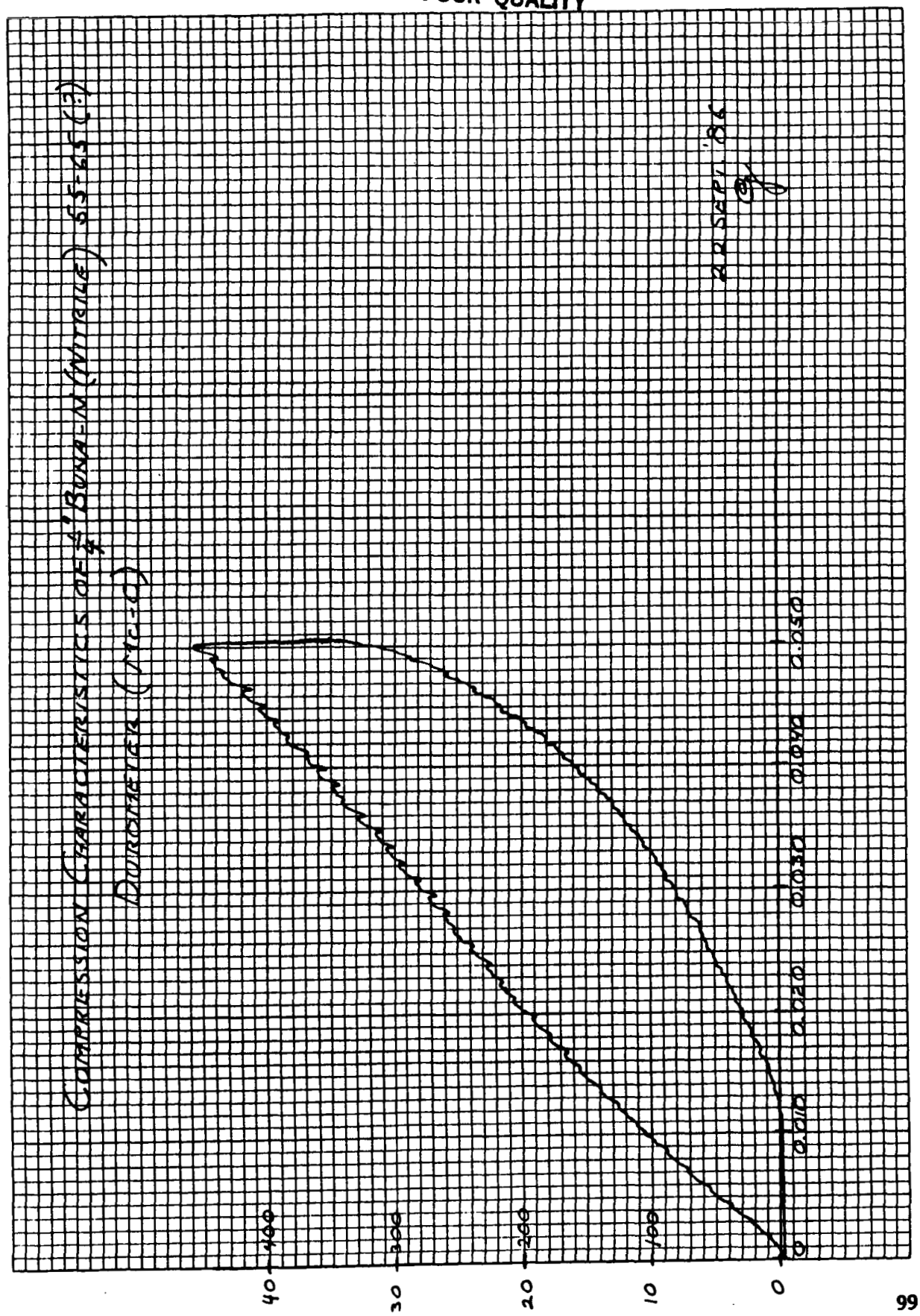

FIGURE 46

46 0702

K·E 10 X 10 TO THE INCH • 7 X 10 INCHES
KEUFFEL & ESSER CO. MADE IN U.S.A.

(i.e. spring) would produce a single straight line, the slope of which would give the material spring constant (force per unit compression). Therefore, our material selection criterion is to have the force-deflection characteristic as close to a single straight line as is possible (this also implies the least separation between the upper and lower curves). Figures 41, 43, and 45 show the deflection characteristics for natural rubber, neoprene, and urethane, respectively, for formulations having low hysteresis. We conclude that these formulations (Figures 38, 39, 40, 41, 43, and 45) are all candidates for use in the force-torque sensor. Figures 42, 44, and 46 are illustrative of materials with unacceptable-large amounts of hysteresis.

Figures 47, 48, and 49 show the time course of stress relaxation in silicone, natural, and neoprene rubbers. These curves show that for small compressions, especially with natural rubber and neoprene, stress relaxation occurs mainly within the first minute of load application so that the two-minute waiting period used in the first set of figures for stress relaxation to occur is valid.

The presented force-deflection characteristics determine the force-torque sensor's response to the normal compressive force F_z. Figures 50, 51, and 52 give the rubber characteristics for the other five load components. As one can see for the tangential or shear force components, F_x and F_y, the characteristics are quite linear with little hysteresis. An artifact caused by the fixturing appears as a nonlinearity at low force. The

FIGURE 47

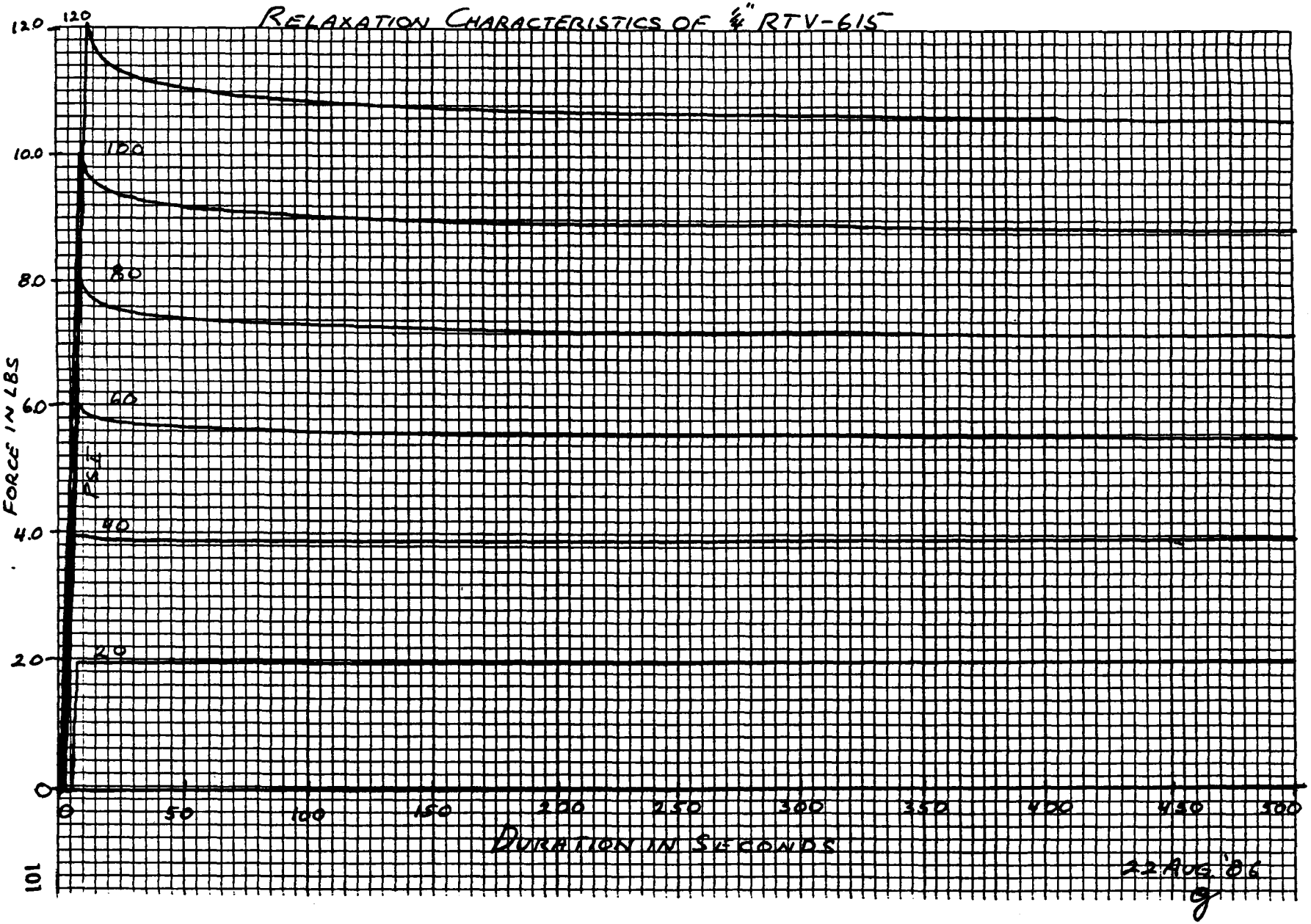

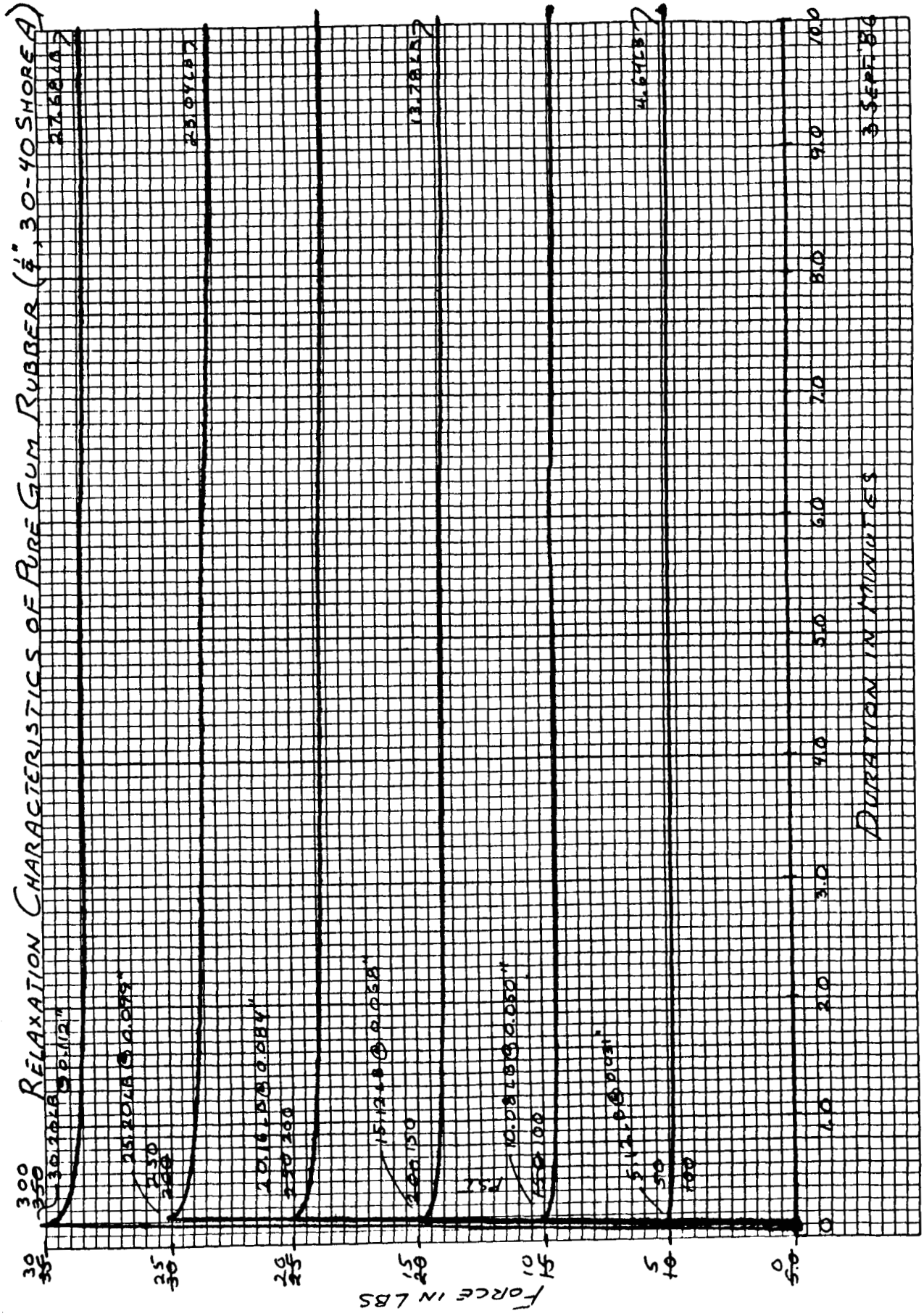

FIGURE 48

46 0702

102

ORIGINAL PAGE IS
OF POOR QUALITY

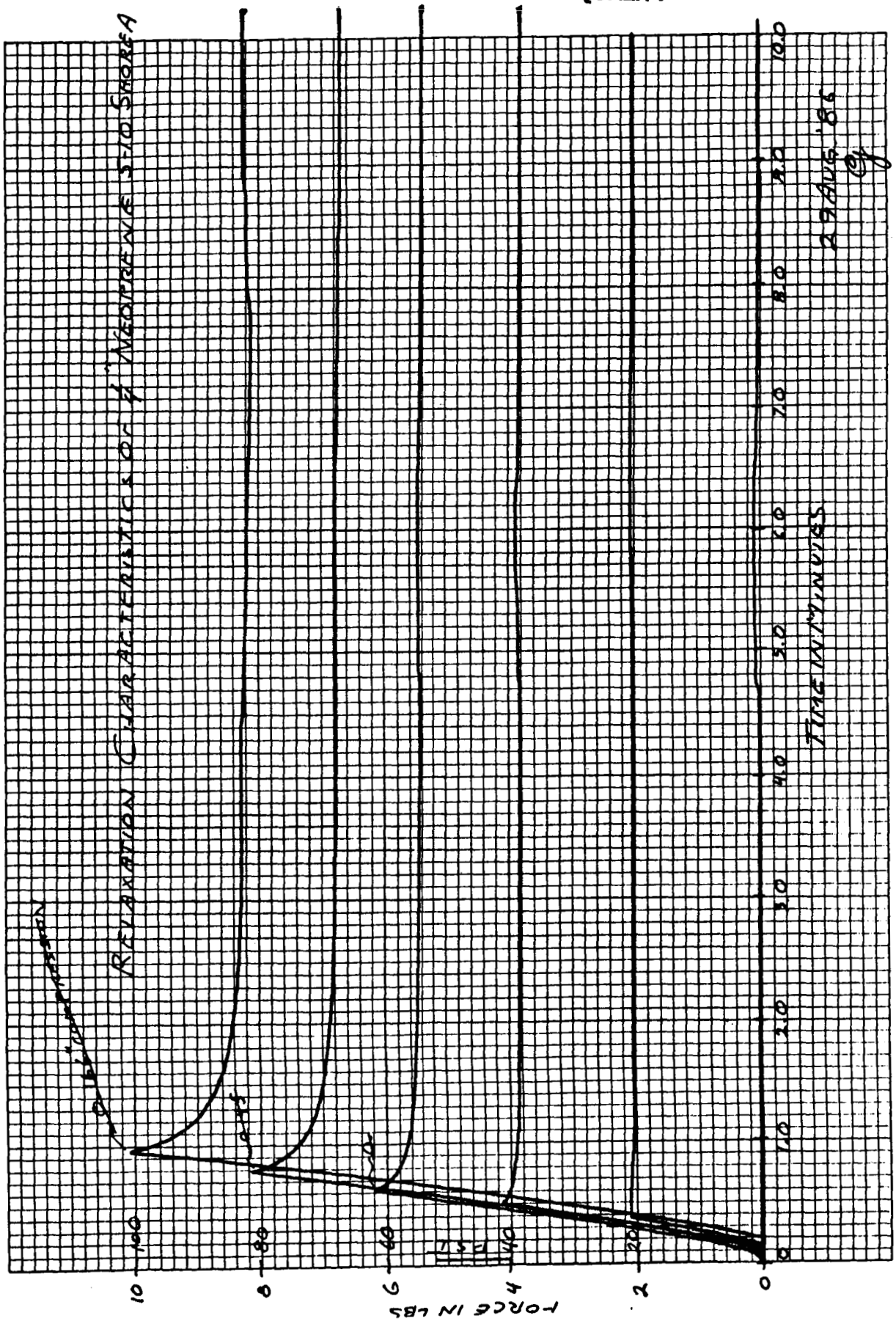

FIGURE 49

FIGURE 50

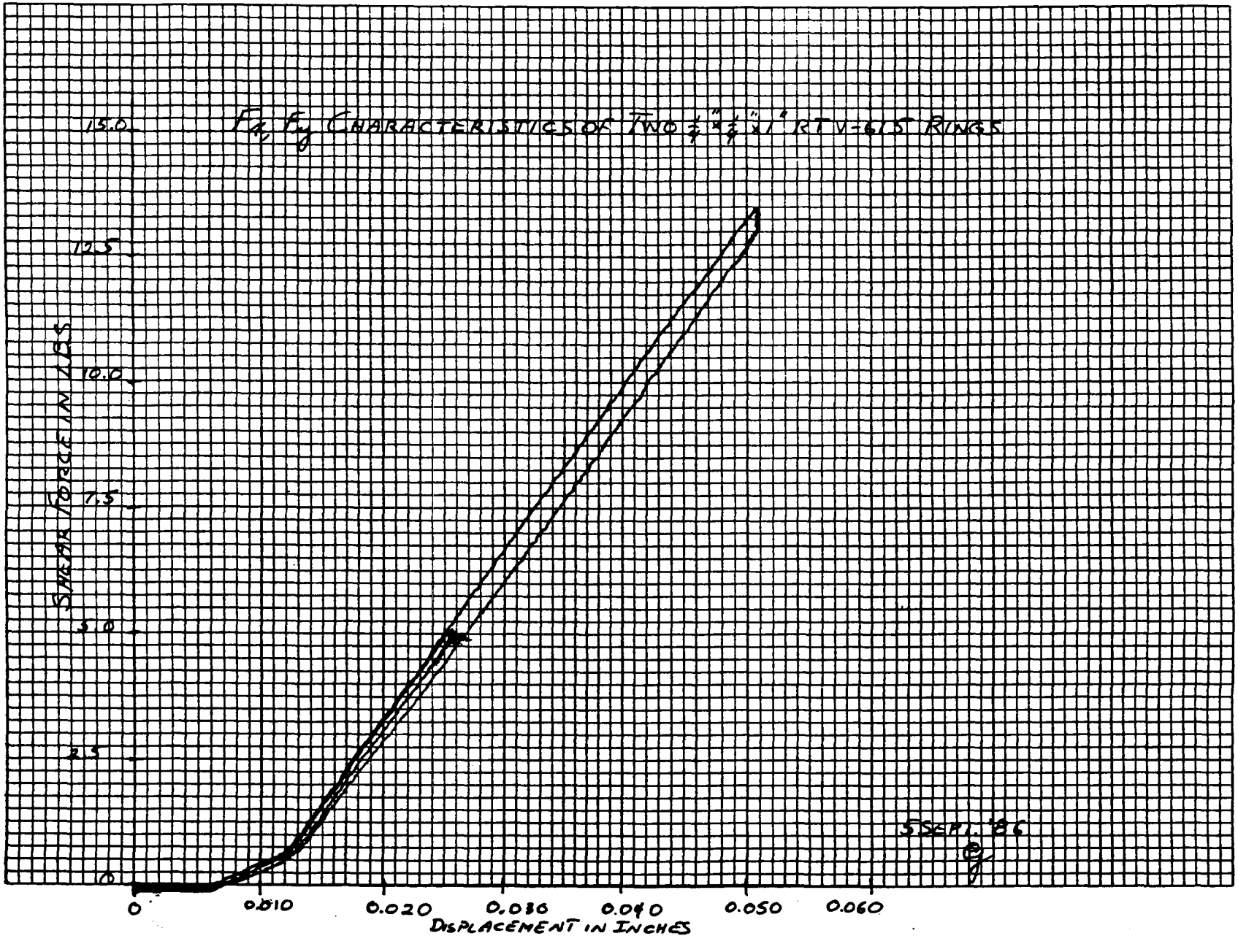

FIGURE 51

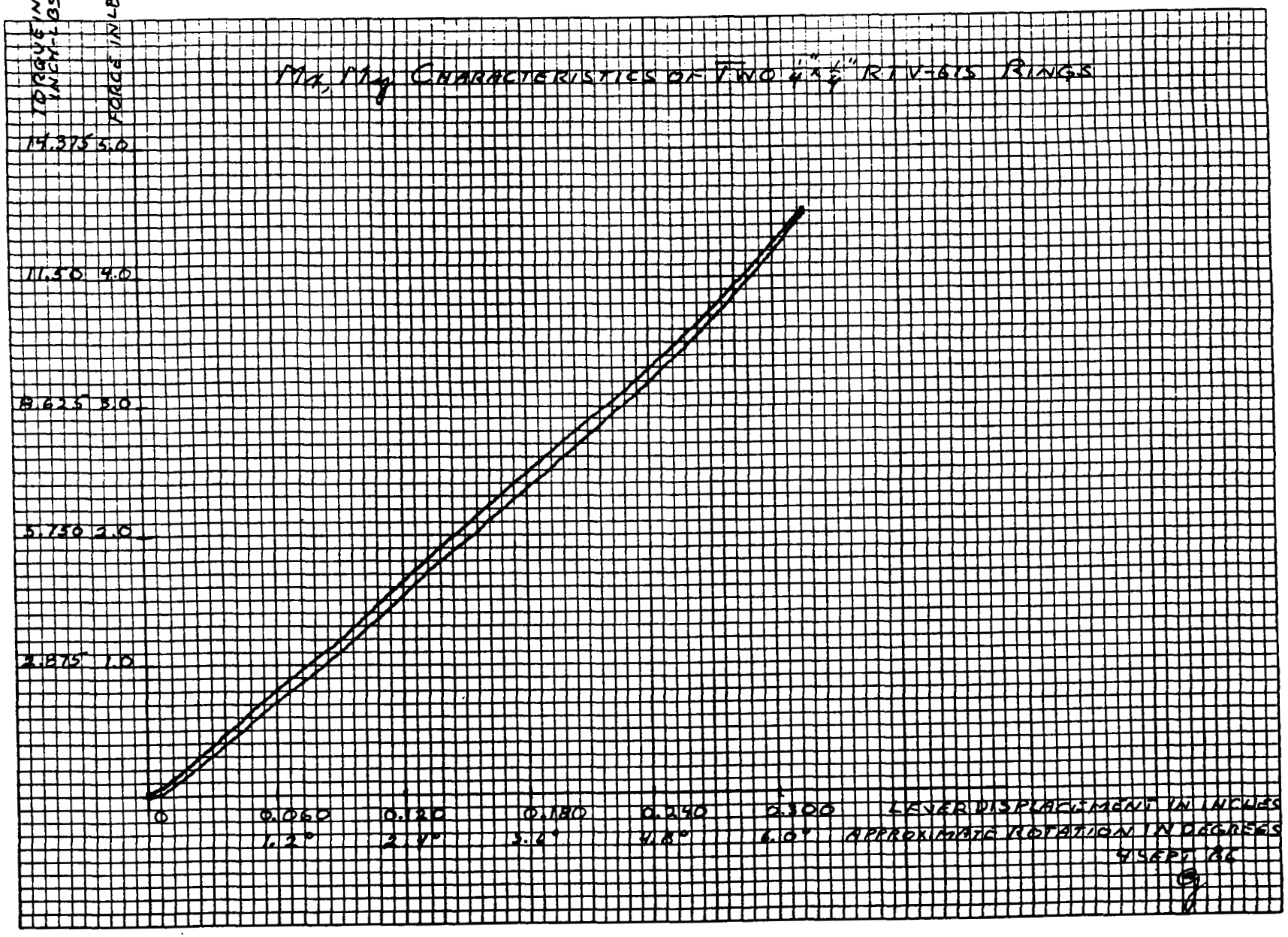

FIGURE 52

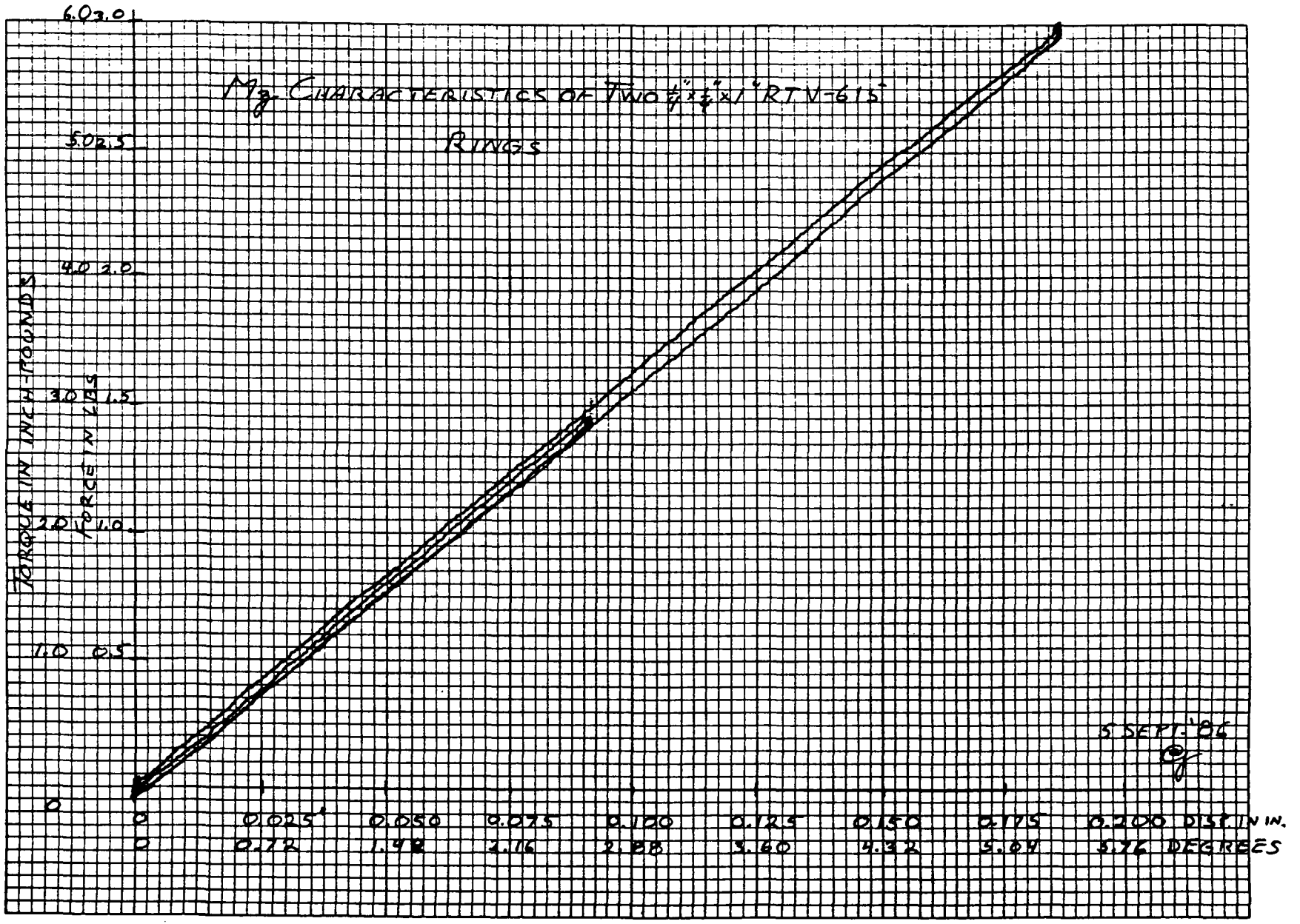

rocking torque components, M_X and M_Y, also have approximately linear characteristics with little hysteresis. The remaining torsion component, M_Z, (Figure 52) also is quite linear with very little hysteresis.

We proposed measuring compression set of candidate elastomers at room temperature for initial screening at then elevated temperatures for the final material selection. Instead, we relied upon the manufacturer's published values. For example, for one of the urethanes compression set was from 1.8 to 3.2% (depending upon the amount of plasticizer used) after being compressed for seven days at 25° C. Measurements are typically made at large compressions (e.g. 50%) where compression set can be expected to be large. The 1.8 to 3.2% range means that the material returned to within 0.9 to 1.6% (1.8-3.2% x 50%) of its prestressed state. For silicone rubbers compression set is typically 20% after 22 hours at 177° C. This temperature is extreme and beyond the survival temperature of the force-torque sensor. At lower temperatures compression set is much less. The practical consequences of compression set are minor. The force-torque sensor readings would be periodically zeroed when the sensor was unloaded. This would compensate for changes in elastomer ring dimensions due to both compression set as well as temperature.

Durability of a representative elastomer was measured from life-test results. For this test apparatus was fabricated so that a metal plate driven by a cam compressed the material in a

cycle similar to that expected with an operating robot. The duty cycle passed through a zero stress point to simulate robotic manipulations and because fatigue life of rubbers is much shorter if the material passes through a relaxing phase in the cycle. Immediately after cyclic compression the force/compression slope was determined to see if there had been any alteration of the mechanics of the material which would indicate the need for recalibration following extended use.

A 1/4"-thick piece of Sylgard 186 silicone rubber was life-tested by cyclic compression (0.10" or 40%) at a rate of about one per second for 16 million cycles. After testing, the force-displacement characteristics of this piece and a control sample from the same batch were measured (see Figure 53). There was no significant difference between the characteristics indicating that life testing did not affect this mechanical characteristic.

From the results of the preceding tests we conclude that specific formulations of silicone, urethane, natural, and neoprene are all well-suited for use in the force-torque sensor. However, we have concentrated on the use of the silicones and urethanes because with simple laboratory procedures and apparatus they can be fabricated with different durometers and easily cast in different shapes. Consequently, we have conducted limited studies on the effects of temperature on these materials and sensor performance. One series of tests was to determine how the compression characteristics of these elastomers change with temperature. Measurements were made from room temperature up to

FIGURE 53

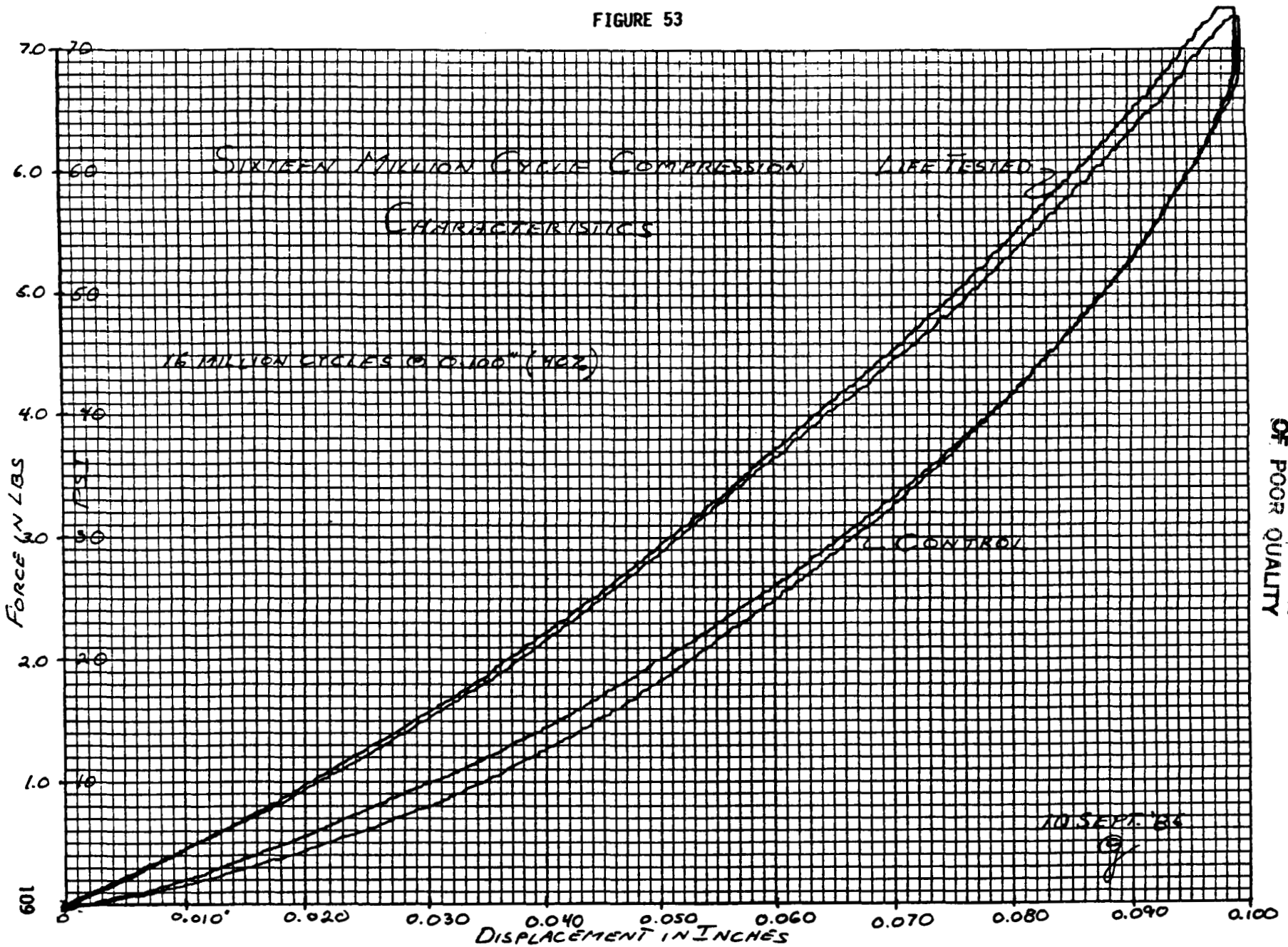

95° C for silicone and 70° C for urethane. The results showed that there was no change in the slope or the amount of hysteresis of the compression-deflection curves so that one constant (i.e. the spring constant) can be used over a range in temperature. However, there was an offset in the curves due to the expansion of the rubber with increasing temperature. The second series of tests was to measure the ultrasonic propagation time of pulses in silicone and urethane elastomers at different temperatures. This transit time depends upon both the thickness of the elastomer and the speed of sound in the elastomer (both of which are functions of temperature). These measurements are shown plotted in Figure 54 for temperatures ranging from about 20 to 60° C. The slopes of the lines, normalized to unit thickness of elastomer are 6.5 ns/mm-°C for silicone rubber and 3.4 ns/mm-°C for urethane. The smaller effect in urethane is primarily due to the smaller linear coefficient of thermal expansion of urethane (1.1×10^{-4}/°C) versus silicone (3×10^{-4}/°C). Based upon these values the speed-of-sound change with temperature was calculated and is presented in Figure 55. The change is linear over the temperature range investigated and the slopes of the lines are negative. Since the pulse transit time is the quotient of distance (i.e. material thickness) and sonic velocity, the negative slope serves to increase transit time with temperature increase. However, the main temperature effect is material expansion with temperature.

At this point in our research it appears that the effects of changing temperature on the force-torque sensor data can be

FIGURE 54

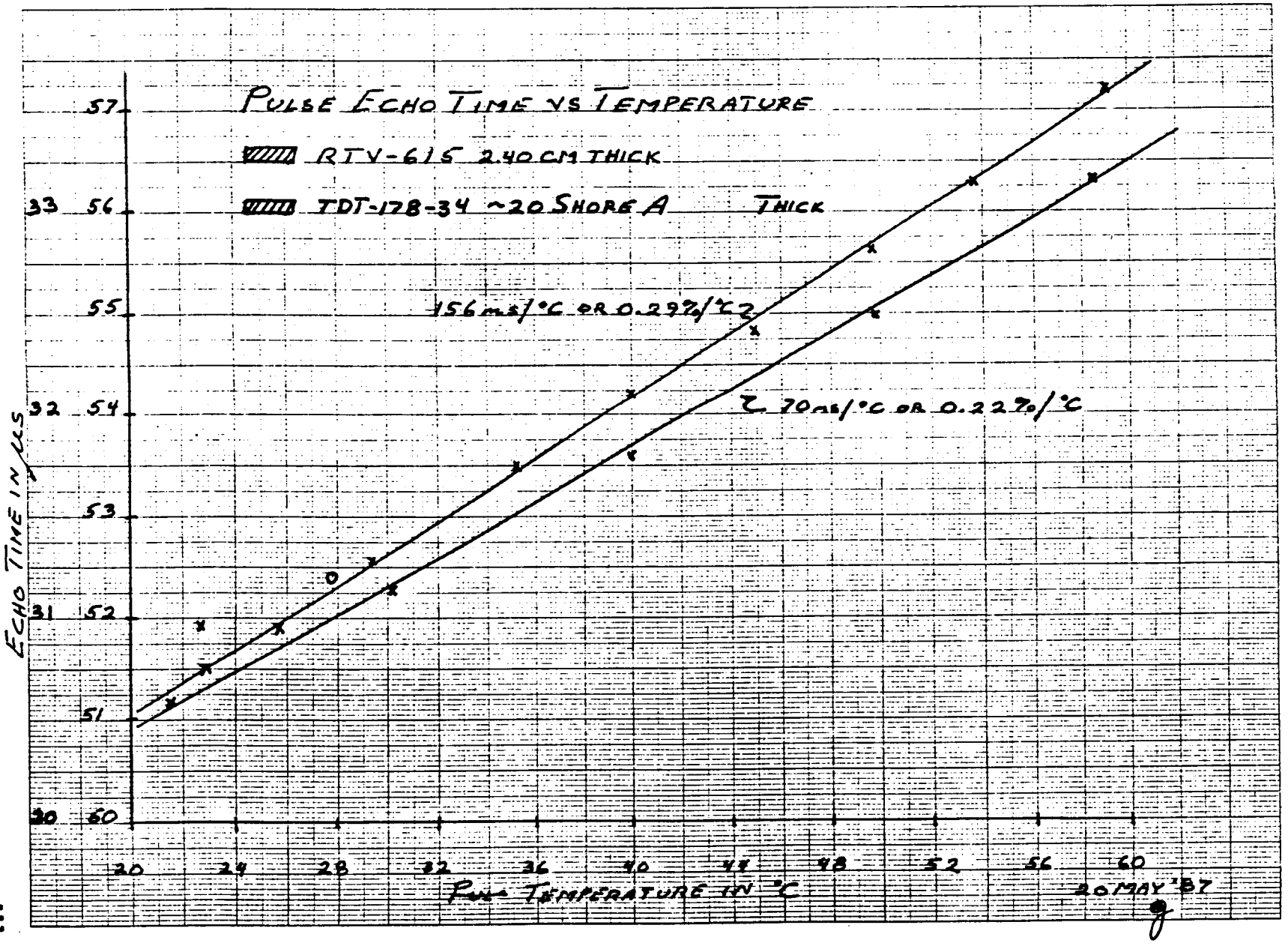

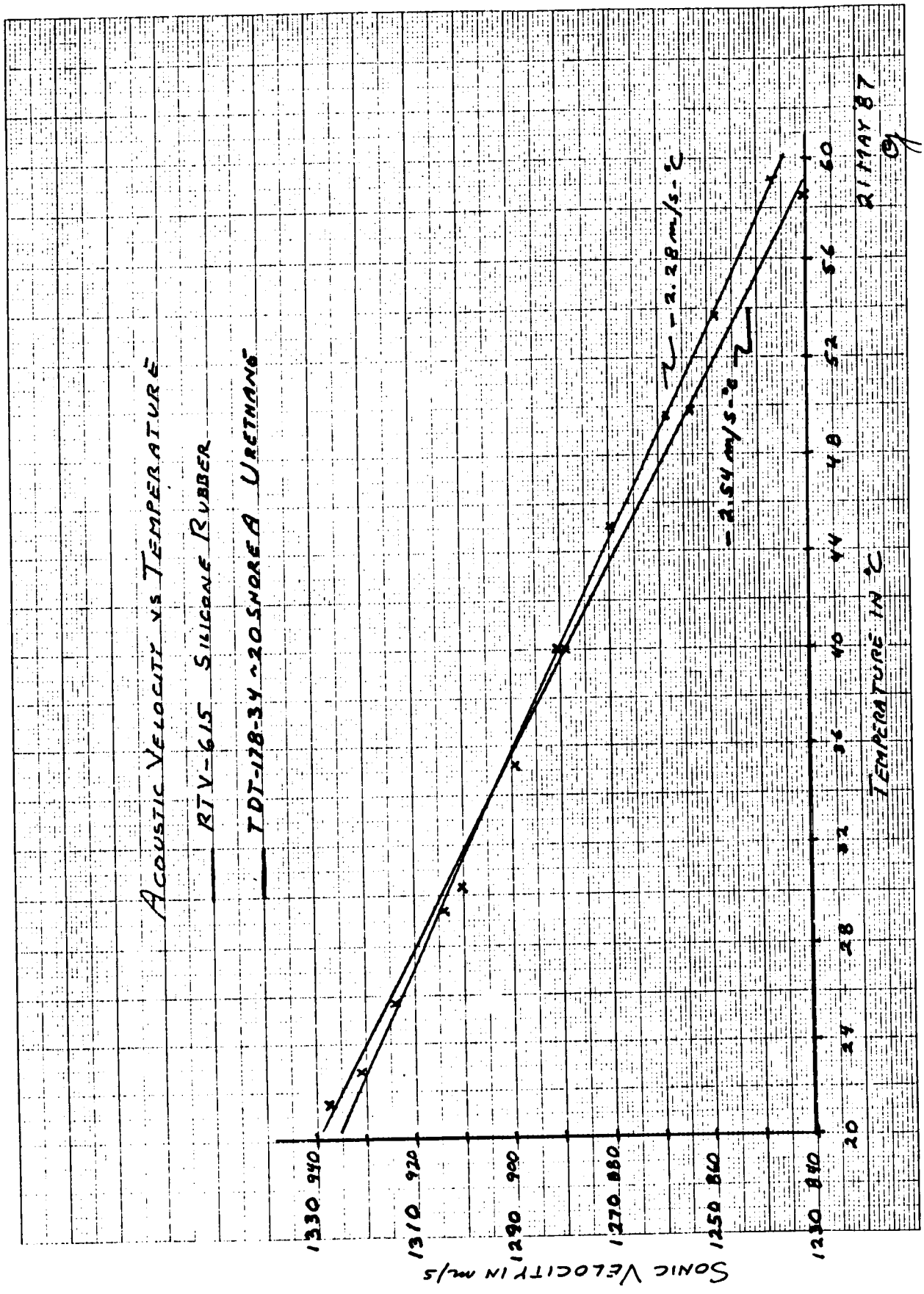

FIGURE 55

compensated by zeroing the sensor periodically when it is unloaded. Zeroing is achieved by recording the TOF values for each of the eight transducers when the sensor is unloaded. Ensuing force-torque measurement are based upon only the change in transit time with loading so that these offsets would be cancelled.

No significant effect of adhesives on the force-torque characteristics of the elastomer were observed. The date taken for Figures 50, 51, and 52 involved elastomeric rings that were bonded to metal plates.

Objective 4 - To Construct Laboratory Prototype Force-Torque Sensors

The key aspects of this objective are the proper alignment of the elastomer ring, reflector post, and coverplate; and the bonding of the elastomer ring to the coverplate and metallized surface of the PVDF, and the bonding of the reflector post to the sensor substrate. Towards this end, a number of laboratory prototype force-torque sensors were fabricated.

The elastomer ring must be centered over the four peripheral ultrasonic transducers that transmit through the ring. This is complicated by the fact that the transducer and lead pattern is on the bottom surface of the PVDF next to the substrate and, therefore, cannot be seen. A similar problem exists in centering the reflector post. These problems have been solved by placing alignment marks on the top metallized surface (i.e. the ground plane) of the PVDF. Figure 56 shows the pattern of these marks on the photomask for the ground plane (the concentric dashed circles), and the reflector post (dashed perpendicular lines and small central medallion). During fabrication adhesive is applied to the bottom surface of the elastomeric ring, and it is carefully positioned within the boundaries of the circular patterns. For mounting the center post a small hole is drilled through the central medallion and ceramic substrate. This hole allows the reflector post to be bolted to the substrate. Before tightening the bolt the interior lateral walls of the 45^{o} facets are aligned

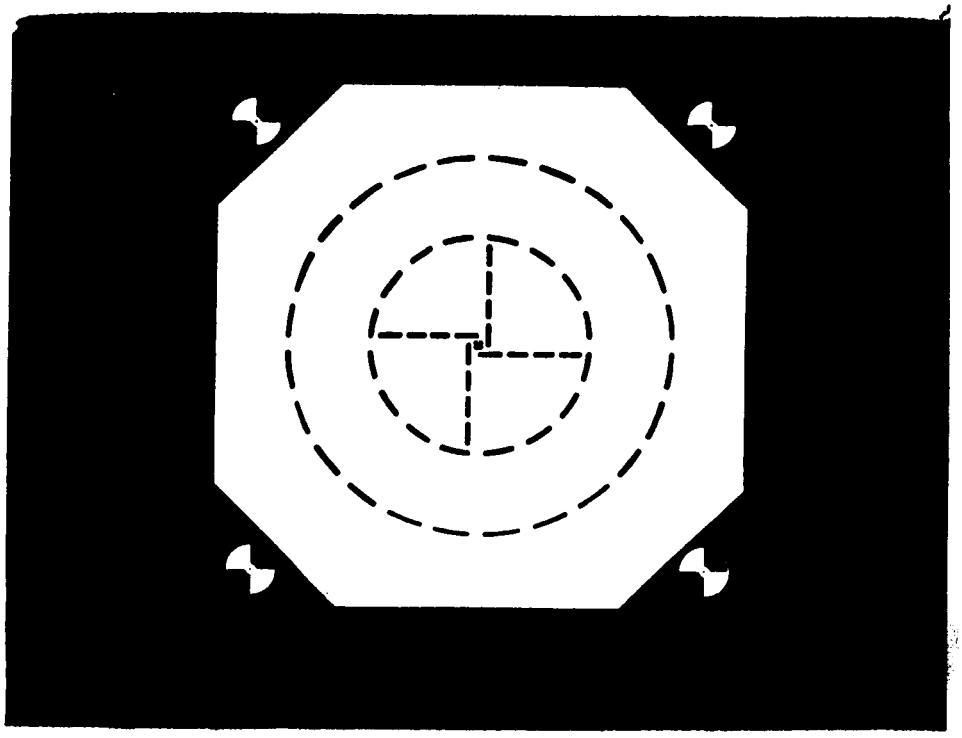

FIGURE 56. Photomask for PVDF Ground Plane Showing Alignment Marks (2 X Magnification).

with the dashed perpendicular lines. This procedure is simple and it works well.

Coverplate alignment is done by the method presented in the Phase II Proposal. That is, transducers X_1, X_2, X_3, and X_4 (Figure 31) are sequentially energized while the coverplate is translated until all four echoes occur at the same time when viewed on an oscilloscope, indicating that the four vertical reflectors on the coverplate are equidistant from their respective transducer. The final step is to rotate the coverplate until all four echoes are a maximum amplitude, indicating that the reflectors are now perpendicular to the ultrasonic beam. In practice, this procedure was almost impossible to perform by hand. Just small motions of the coverplate (25 microns) will produce large time-excursions (100 ns) of the echo pulses. Consequently, an X-Y-0 table should be used for coverplate alignment. This fixture can also be used to prevent motion of the coverplate during curing of the bonding agent that attaches the coverplate to the elastomer ring.

The force-torque sensor is comprised of several layers of various materials all of which must be securely bonded together. Consequently, choice of the proper adhesive for each bond is vital to the survival of the sensor. The least demanding bond in the sensor is between the PVDF layer and the ceramic substrate. Since the bonded surface area is so much greater than that of the other areas, the bond strength can be less. For this bond we use a general purpose, low viscosity epoxy adhesive. This is cured

at 65° C for three hours. The more critical bonds are between the PVDF metallization and the elastomer ring, and the ring and coverplate. The type of adhesive used here depends upon the elastomer family used. In general cyanoacrylate adhesives work very well with neoprene and natural rubbers. During destructive testing the rubber typically fails rather than the adhesive. For urethane elastomers polyurethane adhesives work well, although for very-low durometer formulations the additional plasticizer required may impede bonding. The most difficult compound to bond to is silicone rubber. Initial experiments with a two-component silicone-rubber-based adhesive gave good results when used in thick layers (the uniformity of which is difficult to control) but the material failed to cure when used in thin layers. We thought that this problem was due to the poisoning of the adhesive by the sulphur or tin ions in the silicone rubber catalyst. However, switching to a platinum-based catalyst did not solve the problem. The elastomer vendor suggested that atmospheric oxygen might be poisoning the adhesive--a difficult problem to solve. We eventually ended up with a single-component silicone rubber adhesive/sealant used in conjunction with a primer. This is cured at room temperature and results in strong bonds.

In Phase I we constructed a crude prototype force-torque sensor having an elastomeric ring with a one-inch outside diameter. This sensor size seemed reasonable and was the size stated in the Phase II proposal. However, when complete proto-

type sensors were constructed we went to a 1 1/4 in. diameter ring to make fabrication easier. After several sensors of this size were constructed and we gained confidence in the fabrication procedure, we explored how small the sensor could be made before the current procedure failed. We didn't reach this point, but we did fabricate a miniature force-torque sensor having a ring 3/8 in. in diameter with a reflecting post 0.080 in. across. Ultrasonic echoes from the approximately 1 mm^2 elements were detectable. However, we don't yet know whether a sensor this small will be practical. Being scaled down in size by about a factor of three, the time resolution of the TOF detector must be increased by three. This will be more costly.

Objective 5 - To Integrate the Force-Torque Sensor with a Microprocessor

A major goal of Phase II was the integration of the six-component force-torque sensor with a dedicated microprocessor. The ensuing sensor system is a laboratory research tool that can serve as a test bed for continuing sensor research and development, data acquisition and analysis, and algorithm development rather than a market-ready product. The microcomputer system consists of a VME CPU board, VME card cage and power supply. The CPU board contains an 8 MHz 68000 microprocessor, 128 Kbyte DRAM (upgradable to 512 Kbyte) 32 Kbyte of EPROM space, two RS-232C SIO channels, one 16 bit bidirectional channel, programmable timer, real-time clock, and battery support. Several expansion slots are available in the card cage that could be used in augmenting microprocessor memory and I/O capability.

The software support for this system includes an I/O library that directly supports the high-level language "C". The development software aids in program and EPROM generation for maximum portability of "C" code. Any application written in "C" can be ported to this system with minimal effort. The "C" code can be placed in read-only-memory allowing the entire low-level system to be contained on the CPU board.

The system has been configured and programmed to demonstrate the functioning of a force/torque sensor in real time. In this configuration, the 68000 board is attached to three other devices. One of these is the sensor interface board, which links

the sensor to the 68000 via the VME bus. Another is a standard CRT monitor. This provides the user's interface to the microcomputer.

This terminal is connected to one of the serial ports. Finally, a second serial port is used to communicate with an Apollo DN3000 workstation. This is a more powerful computer with a color monitor and bit-mapped color graphics capability. This capability is exploited in displaying the force/torque data in a visually meaningful format.

The next two sections describe in greater detail the tasks performed by the 68000 microcomputer board and the Apollo workstation, and the software which has been developed to achieve these goals.

As discussed above, the 68000 processor is the central controller of the system, and as such it is responsible for collecting, interpreting, and routing the force-torque data. A single datum, or reading, from a sensor is defined as the TOF value of each of the sensor's eight transducers at a given instant. The processor takes such a reading by polling each of the elements in turn. At the software level, this is accomplished by writing a control word to a register of the memory-mapped parallel port on the sensor interface board, and then waiting for the port to indicate that it has received data from the sensor. The control word includes the address of the element being polled, and the data returned is the eight-bit TOF value from that element. This is done eight times with eight

different transducer addresses to input a complete sensor reading.

Once raw TOF data have been input to the processor, the next step is to perform the conversion from this form to values of force and torque. Since force and torque are each vectors in three-space, a total of six values are computed from a single sensor reading. The mathematics of this conversion are determined by the geometry of the sensor and are given in Table 2. It is a simple linear mapping in which each component of force or torque depends on either two or four of the eight time-of-flight values, and each TOF value affects exactly one force and one torque component. Thus the six conversion functions are quite decoupled. It might appear that in converting eight values to six, some information is being lost; however, this is not the case, since the eight TOF values are not independent of each other due to the constraints imposed by the physical sensor. In fact, they have only six degrees of freedom. The constants in the linear equations which define the mapping to force and torque depend on the sensor, and are determined empirically. To aid in calculating these conversion constants, a calibration facility is provided in the microprocessor's software which directs the user to apply various loads to the sensor and takes readings of the sensor under these loads. These readings, along with the inverse conversion relations, uniquely determine the correct constants to use.

If this facility is not invoked, a set of default constants is used. These defaults assume that each of the sensor's transducers can produce values in the full 8-bit range of 0 - 255 (which is not necessarily true of a real sensor). When appropriate (calibrated) conversion constants are used, the conversion functions as implemented in 68000 software yield integer values which range in [0,255], where 0 indicates the minimum (most negative) value of force or torque which the sensor can produce, 255 corresponds to maximum value, and 128 maps to zero. This eight-bit format was chosen because it simplifies data transmission on serial lines, and because resolution is currently limited to 8 bits by the TOF detector.

The final task of the microprocessor, having collected and interpreted a datum from the sensor, is to have it displayed. Data can be displayed on either the monitor's screen, the Apollo workstation's screen, or both. In order to transmit force-torque data to the Apollo, a format was devised in which each single component of force or torque is encoded as two ASCII characters, which together denote the data value in hexadecimal. Each of the six values is thus encoded in two bytes, and an implicit ordering of these byte-pairs determines which of them corresponds to which force-torque component. For synchronization, a non-hex ASCII character is transmitted between each reading.

Altogether, then, a single sensor reading formatted for transmission comprises 13 bytes. These are sent over a serial

(RS-232) line at 9600 baud, achieving a data rate of over 80 sensor readings per second.

All of these features of the microprocessor's software are tied together in a single menu-driven system. The menu allows a user to specify the number of consecutive readings to be made and the destination of the data. If the destination includes the terminal screen, the user can also choose among different data formats, such as raw TOF values, force-torque values in hex or decimal, or a combination of these. The implementation of this menu system takes advantage of the escape sequences and graphics characters of the WYSE-50 standard monitor. The entire program resides in two programmable read-only memory chips, which plug into the microprocessor board.

The purpose of the graphics application programs developed on the Apollo workstation is to display force-torque data in real time in a meaningful way. Two different display concepts have been developed. One of these uses two-dimensional graphics to draw what is essentially an animated histogram of the six data components, and the other draws a three-dimensional object on the screen and manipulates it in response to incoming force-torque data. Both of these programs operate as slaves; that is, they wait for data to arrive on the serial link to the microprocessor board and display it in an endless loop.

The two-dimensional version paints on the screen six horizontal bars, each of which indicates the value of one component of either force or torque in the input data. The left

end of a given bar corresponds to the minimum value of that component, and the right end corresponds to maximum value. Points in between the two ends map linearly to the range of component values; in particular, the midpoint of the bar corresponds to a value of zero force or torque. Initially, each bar is drawn as a hollow rectangle with a vertical line crossing it at the zero point. Such a bar indicates zero force or torque. A non-zero force or torque value is indicated by a filled rectangle drawn inside the appropriate bar. This solid rectangle extends from the zero point on one side to the point indicating the value on the other.

When several consecutive data readings are input to this program, the effect is to "animate" the bars. That is, as a data component changes value, the solid rectangle drawn in the corresponding bar changes size. Several or all of the six components may change simultaneously, and this is reflected by several changing rectangles in appropriate bars. This display algorithm is simple enough and the graphics hardware of the Apollo DN3000 is fast enough that the screen is updated about 35 times per second, a rate which provides very smooth animation. However, the histogram-style display does not give a geometrically intuitive feel for the meaning of the force-torque data.

The three-dimensional version attempts to overcome this shortcoming. It maps forces and torques applied to a sensor onto translations and rotations, respectively, of an object on the screen. Several objects were tried; the one deemed best is a

simple wireframe cube with an arrow drawn on its front face to help disambiguate its orientation. Initially, the object appears in an upright position in the center of the display area. This view of the object corresponds to an unloaded sensor, i.e. zero force and zero torque. As shear forces in X or Y are applied, the object shifts similarly in X or Y on the screen. Thus a shear force in the positive X direction moves the object to the right, and so forth. Forces along the sensor's Z-axis (normal to the sensor's surface) cause the object to grow or shrink, creating the impression of movement along the display's Z-axis (normal to the screen). In the same way, torques applied to the sensor about its coordinate axes produce rotations of the object about its own corresponding axes. (The object is considered to be at the origin, hence it always rotates around its centroid.) The magnitude of rotation about any one axis ranges from -45^{o} for minimum torque to $+45^{o}$ for maximum.

The implementation of this algorithm on an Apollo DN3000 succeeded in creating the desired illusion, i.e. that of manipulating the object by applying appropriate forces and torques to the sensor. However, it was unable to run as fast as the two-dimension version, due to the extra computational requirements of three dimensional object modeling. Faster floating-point hardware would reduce this problem. A more fundamental drawback pertains to the algorithm itself. This is that the position and orientation of the object, as displayed on the screen, is not always enough to determine uniquely the corresponding forces

and torques. This is due to information lost in projecting the object onto the two dimensional screen. In particular, if there is more than one non-zero component of torque, the rotations become difficult to disambiguate. Taken together, these two display programs compensate for each other's drawbacks. Unfortunately, due to display hardware limitations, it was not possible for us to integrate them in a single display. Nevertheless, they provide a good demonstration of the response characteristics of a force-torque sensor.

The whole system was tested and debugged using the sensor emulator previously described. The emulator uses the same interface at the hardware level as do real sensors, that is, it communicates with the sensor interface board with the same signal protocol. The simulated TOF data, too, take the same 8-bit format. Thus the box connects directly to the sensor interface and the rest of the system sees no difference from an actual sensor.

Objective 6 - To Evaluate the Force-Torque Sensor System

Unfortunately, time ran out before we were able to integrate the force-torque sensor with the controlling microprocessor in order to evaluate sensor performance. Part of this objective was to explore sensor calibration issues. The following presents our thoughts on the subject without the benefit of experimental results. One possibility would be to calibrate the sensor once by the individual application of each of the six force-torque components and assume this calibration remains valid until proven otherwise. At that point the sensor could be considered to have failed and therefore replacement is required. This approach is probably not realistic since the sensor will likely need periodic recalibration to maintain its specified accuracy and the user will require proof that the sensor is operating properly. The question then becomes do all six force-torque components have to be applied for calibration? The answer is no for a perfectly constructed sensor that has sustained no damage. This is true because components F_x, F_y and M_x, M_y are symmetrical so that only one from each pair needs to be applied. Furthermore, three components (F_z, M_x, and M_y) compress the elastomer while the other three (F_x, F_y, M_z) shear it. Therefore, in principle, only one component from each parenthetical groups needs to be applied since the sensor's response to the other four components can be predicted from its response to the two initial components. In practice, though, sensors will not be perfectly constructed and will age or receive minor damage that will affect calibration.

Therefore, a simple method to apply each of the six components is needed.

If the robot with its sensorized end-effector were to pick up an object in a macro-gravity environment at the object's centroid, then appropriate motion of the end-effector would produce the three force components, all of which would be equal to object weight. No torque components could be produced by this method since grasp is at the centroid. If instead the object is grasped a known distance along the x-axis from the centroid, F_x, M_y, and M_z would be individually produced (analogously for a displacement along the y-axis, F_y, M_x, and M_z would be produced). F_z could not be produced directly in this way, but probably could be accurately inferred form the M_x and M_y responses. Assuring that this calibration object is gripped repeatibly at the desired location could be achieved by having suitably formed indentations in the sides of the calibration object that would produce self-centering and self-aligning forces when grasped at the indented regions.

After many delays a PUMA 560 six-degree-of-freedom robot was lent to us by Unimation to aid us in our tactile and force-torque sensor development. This robot is operational and programs have been developed to move the wrist along different paths. Being supplied without an end-effector, we were fortunate in that a servo-operated, parallel-jaw gripper was lent to use by NASA Langley Research Center. This gripper was made for the PUMA but was supplied without a controller. A modest effort was applied

to interfacing this gripper to the robot, but our main thrust was to concentrate on completing the force-torque sensor system.

CONCLUSIONS

We have developed a technology for ultrasonically-based force-torque sensors capable of being mounted on the gripping surfaces of parallel-jaw end-effectors. The current prototype is about one-inch in diameter; however, a miniaturized sensor 3/8-inch in diameter has been constructed and indications are that this small size will be feasible. Further size reduction is possible but has not been attempted.

A unique feature of this technology is that the spring member (i.e. rubber ring) can be chosen to suit the application without affecting sensor design. In fact, sensors could be assembled (and tested) to the stage where the ring would be bonded to the PVDF and placed in inventory. Then, when an order is received for a sensor with a specific sensitivity, force-torque range, and environmental exposure, the ring having the appropriate rubber type and formulation can be selected and sensor fabrication completed.

The on- or near-sensor electronics is complete. The large, constant-shape echoes (compared to signals from the tactile sensor) are relatively noise-free and easily detected. Consequently, the existing circuitry can be simplified, with a concomitant reduction in cost. The currently used schemes for time-of-flight measurement (clock-pulse counting) provide rather coarse time resolution and, therefore, limit force-torque resolution. Alternative schemes are being reviewed.

1. Report No.	2. Government Accession No.	3. Recipient's Catalog No.
NASA CR-178347		

4. Title and Subtitle	5. Report Date
Six Component Robotic Force-Torque Sensor	August 1987
	6. Performing Organization Code

7. Author(s)	8. Performing Organization Report No.
Allen R. Grahn, Brad L. Hutchings, David R. Johnston, David C. Parsons, and Roland F. Wyatt	
	10. Work Unit No. 324-02-00-01

9. Performing Organization Name and Address	11. Contract or Grant No.
Bonneville Scientific, Inc. 918 East 900 South Salt Lake City, UT 84105	NAS1-17997
	13. Type of Report and Period Covered Contractor Report

12. Sponsoring Agency Name and Address	14. Sponsoring Agency Code
National Aeronautics and Space Administration Langley Research Center Hampton, VA 23665-5225	

15. Supplementary Notes

Langley Technical Monitor: A. J. Meintel
SBIR Phase II Final Report

16. Abstract

This report describes the results of a two-phase contract studying the feasibility of a miniaturized six-component force-torque sensor and development of a working laboratory system. The principle of operation is based upon using ultrasonic pulse-echo ranging to determine the position of ultrasonic reflectors attached to a metal or ceramic cover plate. Because of the small size of the sensor, this technology may have application in robotics, to sense forces and torques at the finger tip of a robotic end effector.

Descriptions are included of laboratory experiments evaluating materials and techniques for sensor fabrication and of the development of support electronics for data acquisition, computer interface and operator display.

17. Key Words (Suggested by Author(s))	18. Distribution Statement
Sensors, Robotics, Automation	Unclassified - Unlimited Subject Category 35

19. Security Classif. (of this report)	20. Security Classif. (of this page)	21. No. of Pages	22. Price
Unclassified	Unclassified	135	A07

For sale by the National Technical Information Service, Springfield, Virginia 22161

The 68000 microcomputer is ready and waiting for force-torque data from the sensor. Programs are in place for sensor control, data acceptance, solution of force-torque equations, and display of force-torque values. We are currently working on completing the electronic link from the sensor to the computer. Once this is established operational evaluation of the sensor can take place and key issues of sensor accuracy and useful resolution addressed.